

THE COMPUTER-AIDED OPTIMAL HEATING  
SCHEDULE OF FORGING INGOTS USING  
THE FINITE ELEMENT METHOD

CENTRE FOR NEWFOUNDLAND STUDIES

TOTAL OF 10 PAGES ONLY  
MAY BE XEROXED

(Without Author's Permission)

BHIMAVARAPU SUBBA REDDY







THE COMPUTER-AIDED OPTIMAL HEATING SCHEDULE OF FORGING INGOTS  
USING THE FINITE ELEMENT METHOD

by

Bhimavarapu Subba Reddy



A thesis submitted to the School of Graduate Studies  
in partial fulfillment of the  
requirements for the degree of  
Master of Engineering

Faculty of Engineering and Applied Science  
Memorial University of Newfoundland

July 1985

St. John's

Newfoundland

Canada

Permission has been granted to the National Library of Canada to microfilm this thesis and to lend or sell copies of the film.

The author (copyright owner) has reserved other publication rights, and neither the thesis nor extensive extracts from it may be printed or otherwise reproduced without his/her written permission.

L'autorisation a été accordée à la Bibliothèque nationale du Canada de microfilmer cette thèse et de prêter ou de vendre des exemplaires du film.

L'auteur (titulaire du droit d'auteur) se réserve les autres droits de publication; ni la thèse ni de longs extraits de celle-ci ne doivent être imprimés ou autrement reproduits sans son autorisation écrite.

ISBN 0-315-31026-X

ABSTRACT

This thesis presents the computer simulated thermal stress analysis of forging ingots during the heating and soaking periods. These results are then used to obtain the optimal heating schedule of these ingots.

The equations for the transient nonlinear temperature distribution within the ingot due to the convective and radiative heat flux are derived using the nonlinear finite element analysis. The nonlinearities due to the variation of material properties have been taken into account by calculating the temperature at different time steps first and then at each time step the elemental property matrices are recalculated. The nonlinear algebraic equations are solved using three techniques and then the best technique is selected from these three for further analysis.

The mathematical model for the thermal stress analysis has also been formulated using the finite element analysis. The temperatures obtained from the heat transfer analysis are used to calculate the force vector for the stress analysis. These finite element models are then used to calculate the effects of axial heat flux, the slenderness ratio of the ingot, and the linearization of the heat flux on the transient temperature and stress distributions within the ingot.

The optimal heating schedule has been obtained considering two types of constraints; the first type of the constraint is that the stresses developed should not exceed certain value established by some of the commonly known failure theories, and the second type is that the temperature in the ingot during the heating or soaking period does not exceed a specified value for a particular type of material. The method of optimization of the furnace heating schedule is selected after considering three alternate ways of carrying out the optimization.



ACKNOWLEDGEMENTS

The author is deeply indebted to his supervisor Dr. Anand M. Sharan for his continued guidance and encouragement during the course of this investigation. His contribution of time and technical expertise have helped me immensely.

I express my gratitude to the Memorial University for the award of a Graduate Fellowship.

The author appreciates the use of VAX.11/780 computing facilities of Memorial University. Finally, I thank Mrs. Levinia Vatcher for her care and patience in typing this thesis.

To My Mother

TABLE OF CONTENTS

	<u>Page</u>
ABSTRACT	ii
ACKNOWLEDGEMENTS	iv
TABLE OF CONTENTS	vi
LIST OF FIGURES	ix
LIST OF TABLES	xiv
NOMENCLATURE	xv

## CHAPTER 1

## INTRODUCTION AND LITERATURE SURVEY

1.1	The Forging of an Ingot	1
1.2	The Literature Survey	3
1.2.1	The Heat Transfer Analysis	3
1.2.1	The Thermal Stress Analysis	4
1.2.3	The Optimal Studies of the Heating Processes	6
1.3	The Objectives of the Present Investigation	10

## CHAPTER 2

## THE TRANSIENT HEAT TRANSFER ANALYSIS OF THE INGOT

2.1	Introduction	14
2.2	The Mathematical Formulation	15
2.3	The Formulation of Elemental Matrices	24
2.3.1	The Capacitance Matrix $[C_1^e]$	24
2.3.2	The Conduction Matrix $[K_1^e]$	25
2.4	The Formulation of Elemental Force Vectors	27
2.4.1	The Force Vector, $\{F_Q^e\}$ Due to the Heat Generation	27
2.4.2	The Force Vector, $\{F_q^e\}$ Due to the Heat Flux	28
2.4.3	The Force Vector, $\{F_C^e\}$ Due to the Convection	29
2.4.4	The Force Vector, $\{F_r^e\}$ due to the Radiation	29

	<u>Page</u>
2.5 The Solution of the Nonlinear Transient Heat Transfer Problems	32
2.5.1 The Transformation of the Simultaneous Differential Equations	32
2.5.2 The Iteration Method	35
2.5.3 The Newton-Raphson Method	36
2.5.4 The Nonlinear Optimization Method	38
2.6 Numerical Example	40
2.7 The Computer Simulation of the Heat Transfer Process Within the Ingot	49
2.7.1 The System of Equations for the Heat Transfer Within the Ingot	49
2.7.2 The Temperature Distribution Within the Ingot	51
2.7.3 The Temperature Gradient Distribution Within the Ingot	61
2.8 Conclusions	70

## CHAPTER 3

## THE THERMOELASTIC STRESS ANALYSIS OF THE INGOT

3.1 Introduction	72
3.2 The Mathematical Formulation	73
3.3 The Failure Theories	79
3.4 The Three-Dimensional Finite Element Analysis	81
3.5 The Verification of the Axisymmetric Finite Element Model	82
3.6 The Comparison of the Axisymmetric Finite Element Analysis With the Finite Difference Analysis	83
3.7 The Linearization of Heat Transfer Equations	96
3.8 The Effect of the Slenderness Ratio	98
3.9 Conclusions	102

## CHAPTER 4

## THE OPTIMAL HEATING SCHEDULE OF THE INGOT

4.1 Introduction	105
4.2 The Furnace Temperature Paths and the Thermal Stresses	107
4.2.1 Discussion on the Various Furnace Temperature Paths	107
4.2.2 The Constant Furnace Temperature Heating	107

	<u>Page</u>
4.2.3 The Variable Furnace Temperature Heating	112
4.3 The Optimal Heating Schedule	119
4.3.1 The Description of the Heating Cycle of the Ingot	119
4.3.2 The Analysis of the Various Methods of Obtaining the Optimal Furnace Temperature Path	125
4.3.3 The Single Variable Optimization Method	131
4.4 Conclusions	136
CHAPTER 5	
CONCLUSIONS AND RECOMMENDATIONS	
5.1 A Brief Discussion	141
5.2 Conclusions	142
5.3 Limitations of the Present Investigation and Recommendations for Future Work	145
REFERENCES	146
APPENDIX A	
DIFFERENTIATION OF MATRICES AND VECTORS WITH RESPECT TO $\{T\}^e$	150
APPENDIX B	
THE EXPRESSIONS FOR THE ELEMENTAL MATRICES AND VECTORS OF THE SOLID	152
APPENDIX C	
THE REPRESENTATION OF $T^e$ IN THE MATRIX FORM	156
APPENDIX D	
DESCRIPTION AND LISTING OF THE COMPUTER PROGRAMS	158

LIST OF FIGURES

NO:	DESCRIPTION	
1.1	Schematic Arrangement of the Vacuum-Casting Installation, Employing the Stream Degassing Technique (after McGannon [1]).	2
1.2	The Diametral Cross-section of the Cylindrical Ingot.	7
1.3	The Rate of Heating of the 1.016 m Dia. Ingot under the Programmed Heating Practice (after Sun [8]).	11
2.1	The Details of the Axisymmetric Triangular Element.	20
2.2	The System Configuration with Various Boundary Conditions.	41
2.3	The Discretization of the System into Finite Elements.	43
2.4	The Time-Temperature Plot of the Ceramic Body.	44
2.5	The Time-Temperature Plot at the Node 1.	46
2.6	The Time-Temperature Plot at the Node 13.	47
2.7	The Time-Temperature Plot at the Node 23.	48
2.8	The Discretization of the Ingot into Finite Elements.	52
2.9	The Time-Temperature Plot of the Ingot Corresponding to the Furnace Heating Rate of $0.014^{\circ}\text{K}/\text{sec}$ ( $51.5^{\circ}\text{K}/\text{hour}$ ).	54
2.10	The Time-Temperature Plot of the Ingot Corresponding to the Furnace Heating Rate of $0.017^{\circ}\text{K}/\text{sec}$ ( $64.375^{\circ}\text{K}/\text{hour}$ ).	55
2.11	The Time-Temperature Plot of the Ingot Corresponding to the Furnace Heating Rate of $0.024^{\circ}\text{K}/\text{sec}$ ( $85.833^{\circ}\text{K}/\text{hour}$ ).	56

No.	DESCRIPTION	PAGE
2.12	The Time-Temperature Plot of the Ingot Corresponding to the Furnace Heating Rate of 0.0355°K/sec (128.76°K/hour).	57
2.13	The Time-Temperature Plot of the Ingot Corresponding to the Furnace Heating Rate of 0.071°K/sec (257.5°K/hour).	58
2.14	The Time-Temperature Plot of the Ingot Corresponding to a Constant Furnace Temperature of 810°K.	60
2.15	The Variation of the Radial Temperature Gradient Along the Section AB ( $T_F = 810^\circ\text{K}$ ).	63
2.16	The Variation of the Radial Temperature Gradient Along the Section CD ( $T_F = 810^\circ\text{K}$ ).	64
2.17	The Variation of the Radial Temperature Gradient Along the Section EF ( $T_F = 810^\circ\text{K}$ ).	65
2.18	The Variation of the Axial Temperature Gradient Along the Section AB ( $T_F = 810^\circ\text{K}$ ).	67
2.19	The Variation of the Axial Temperature Gradient Along the Section CD ( $T_F = 810^\circ\text{K}$ ).	68
2.20	The Variation of the Axial Temperature Gradient Along the section EF ( $T_F = 810^\circ\text{K}$ ).	69
3.1	The Elemental Stresses in the Cylindrical Coordinate System.	75
3.2	Finite Difference Subdivision of the Cylinder.	84
3.3	The Comparison of the 2-D Finite Difference and 3-D Finite Element $\sigma_d$ Results of $T_F = 1000^\circ\text{K}$ .	87
3.4	The Comparison of the 2-D Finite Difference and 3-D Finite Element $\sigma_s$ Results at $T_F = 1000^\circ\text{K}$ .	88

NO.	DESCRIPTION	PAGE
3.5	The Comparison of the 2-D Finite Difference and 3-D Finite Element $\sigma_n$ Results at $T_F=1000^{\circ}K$ .	89
3.6	The Comparison of the Two and Three Dimensional Finite Element $\sigma_d$ Results at $T_F=1000^{\circ}K$ .	92
3.7	The Comparison of the Two and Three Dimensional Finite Element $\sigma_s$ Results at $T_F=1000^{\circ}K$ .	93
3.8	The Comparison of the Two and Three Dimensional Finite Element $\sigma_n$ Results at $T_F=1000^{\circ}K$ .	94
3.9	The Distribution of $\sigma_r$ , $\sigma_{\theta}$ and $\sigma_z$ Along the Radius of the Ingot, AB, at $T_F = 1000^{\circ}K$ and $t = 2$ hours.	97
3.10	The Comparison of the Linearized and Nonlinearized $\sigma_d$ Results at $T_F=1000^{\circ}K$ .	99
3.11	The Comparison of the Linearized and Nonlinearized $\sigma_s$ Results at $T_F=1000^{\circ}K$ .	100
3.12	The Comparison of the Linearized and Nonlinearized $\sigma_n$ Results at $T_F=1000^{\circ}K$ .	101
3.13	The Effect of the Slenderness Ratio on $\sigma_d$ values.	103
4.1	The Variation of the Normalized Stresses and Temp. as a Function of Time Corresponding to $T_F = 500^{\circ}K$ .	109
4.2	The Variation of the Normalized Stresses and Temp. as a Function of Time Corresponding to $T_F = 800^{\circ}K$ .	110
4.3	The Variation of the Normalized Stresses and Temp. as a Function of Time Corresponding to $T_F = 1100^{\circ}K$ .	111



No.	DESCRIPTION	PAGE
4.4	The Variation of the Normalized Stresses and $\Delta T$ as a Function of Time Corresponding to the Furnace Heating Rate of $0.023^{\circ}\text{K}/\text{sec}$ , and Final $T = 800^{\circ}\text{K}$ . F	113
4.5	The Variation of the Normalized Stresses and $\Delta T$ as a Function of Time Corresponding to the Furnace Heating Rate of $0.035^{\circ}\text{K}/\text{sec}$ and Final $T = 800^{\circ}\text{K}$ . F	114
4.6	The Variation of the Normalized Stresses and $\Delta T$ as a Function of Time Corresponding to the Furnace Heating Rate of $0.070^{\circ}\text{K}/\text{sec}$ and Final $T = 800^{\circ}\text{K}$ . F	115
4.7	The Variation of the Normalized Stresses and $\Delta T$ as a Function of Time Corresponding to the Furnace Heating Rate of $0.037^{\circ}\text{K}/\text{sec}$ and Final $T = 1100^{\circ}\text{K}$ . F	116
4.8	The Variation of the Normalized Stresses and $\Delta T$ as a Function of Time Corresponding to the Furnace Heating Rate of $0.056^{\circ}\text{K}/\text{sec}$ and Final $T = 1100^{\circ}\text{K}$ . F	117
4.9	The Variation of the Normalized Stresses and $\Delta T$ as a Function of Time Corresponding to the Furnace Heating Rate of $0.112^{\circ}\text{K}/\text{sec}$ and Final $T = 1100^{\circ}\text{K}$ . F	118
4.10	The Stress and Temperature Variations in the Ingot.	121
4.11	The Minimum Heating Time of the Ingot.	122

No.	DESCRIPTION	PAGE
4.12	The Constrained Minimum Heating Time of the Ingot.	124
4.13	The Initial Value Multistage Decision Problem.	126
4.14	One of the Feasible Paths in the Multivariable Optimization.	130
4.15	The Optimal Furnace Heating Path Considering $\sigma$ as the Failure Criteria. d	133
4.16	The Optimal Furnace Heating Path Considering $\sigma$ as the Failure Criteria. s	134
4.17	The Optimal Furnace Heating Path Considering $\sigma$ as the Failure Criteria. n	135
4.18	The Optimal Positive Slope Furnace Heating Path Considering $\sigma$ as the Failure Criteria. d	137
4.19	The Optimal Positive Slope Furnace Heating Path Considering $\sigma$ as the Failure Criteria. s	138
4.20	The Optimal Positive Slope Furnace Heating Path Considering $\sigma$ as the Failure Criteria. n	139

LIST OF TABLES

No.	DESCRIPTION	PAGE
2.1	The Variations of $\Delta T_{\max}$ , $t^*$ and $t_s$ for Different Rates of Furnace Heating.	62
3.1	The Absolute Normalized Stresses and Their Locations at Different Instants of the Heating Time ( $T_F=1000^\circ\text{K}$ ).	95

NOMENCLATURE

{ }	vector
[ ]	matrix
$A^e$	area of the triangular element
[A]	Jacobian matrix
$[B_1]$	thermal gradient matrix
$[B_2]$	elastic gradient matrix
c	specific heat
$[C_1]$	capacitance matrix
d	diameter of the ingot
$[D_1]$	thermal material property matrix
$[D_2]$	elastic material property matrix
E	modulus of elasticity
$\{f^i\}$	residual vector
$\{F\}$	elastic force vector
$\{F_c\}$	force vector due to convection
$\{F_q\}$	force vector due to the heat flux
$\{F_Q\}$	force vector due to heat generation within the body
$\{F_r\}$	force vector due to radiation
h	convection heat transfer coefficient
i, j, k	nodes of the triangular element
$k_r, k_z$	thermal conductivities in the r and z directions respectively.
[K]	elastic stiffness matrix
$[K_1]$	thermal conduction matrix

$i_r, i_z$	direction cosines normal to the surface
$L_{ij}, L_{jk}, L_{ki}$	length of sides i-j, j-k, k-i of the triangular element
$n_1$	total number of elements
$n_2$	total number of nodes
$[N_1]$	shape function matrix
$q$	heat flux
$Q$	heat generated within the body
$\bar{r}$	coordinate of the centroid of the triangular element in the r-direction
$r_i, r_j, r_k$	coordinates of the nodes i, j, k of the element in the r-direction
$\Delta r$	distance between two nodes
$S_1$	surface experiencing heat flux
$S_2$	surface experiencing convection and radiation heat transfer
$t$	time
$\Delta t$	time increment
$t_s$	time required to reach steady state temperature
$t^*$	time where $\Delta T_{\max}$ occurs
$t^+$	time required for $T_s$ to reach the finishing temperature
$T$	temperature
$\{T\}$	nodal temperature vector
$T_f$	furnace temperature
$T_i, T_j, T_k$	temperature of nodes i, j, k of the element
$T_B$	maximum ingot temperature

$T_S$	surface nodal temperatures
$\Delta T$	temperature difference between nodes A and B
$\Delta T_{max}$	maximum temperature difference of nodes A and B
$\Delta T_1$	difference between the temperature of an element and the initial temperature
$\{T_o\}$	optimization temperature vector
$\{T_c\}$	calculated temperature vector
$u, v$	displacements of the element in r and z directions respectively
$\{U\}$	displacement vector
$U$	objective function for the optimum furnace temperature path to be minimized
$w$	work done
$\alpha$	coefficient of thermal expansion
$\epsilon$	emissivity of the body
$\epsilon_r, \epsilon_z, \epsilon_\theta, \gamma_{rz}$	radial, axial, circumferential and shear strains respectively
$\{\epsilon\}$	strain vector
$\{\epsilon_0\}$	initial strain vector
$\theta$	objective function to be minimized for the solution of nonlinear heat transfer equations
$A$	strain energy
$\gamma$	Poisson's ratio
$\pi$	Potential energy
$\rho$	density of the material
$\sigma$	Stefan-Boltzmann Constant
$\sigma_1, \sigma_2, \sigma_3$	principal stresses

$\sigma_r, \sigma_z, \sigma_\theta, \tau_{rz}$	radial, axial, circumferential and shear stresses respectively
$\sigma_d, \sigma_d'$	distortion energy stress and normalized distortion energy stress respectively
$\sigma_n, \sigma_n'$	maximum normal stress and normalized maximum normal stress respectively
$\sigma_s, \sigma_s'$	maximum shear stress and normalized maximum shear stress respectively
$\sigma_y$	yield stress of the material
$\chi$	variational functional to be minimized

---

The superscript e refers to the element and G, the global matrices and vectors.

CHAPTER 1

INTRODUCTION AND LITERATURE SURVEY

1.1 The Forging of an Ingot,

A large number of primary or secondary metal forming processes involve complex heat transfer and stress analysis calculations. The solutions of such problems require enormous computations which are possible now with the advent of the fast digital computers. The benefits of these computations are that these processes can be done safely and within much shorter time thus saving a large sum of capital. One of these processes is the heating of ingots in a soaking pit.

In conventional steel mill practice, the molten steel is first poured into a preheated ingot molds which can be vacuum degassed as shown in Fig. 1.1 and left to solidify for several days before the ingot is stripped away from the mold [1,2]. Then the ingot is sent to a soaking furnace for heating to a convenient temperature for hot working. A large number of steels are heated to a temperature around 1225°C for forging. After initial forging, the ingot is reheated in preparation for further work such as forming, rolling, annealing, drawing, etc. During the heating of the ingot in a furnace the surface gets heated fairly rapidly whereas the



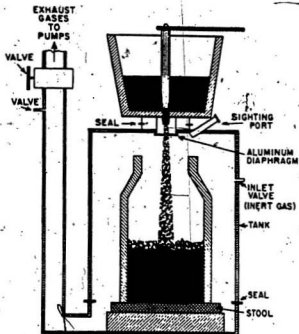


Fig. 1.1: Schematic Arrangement of the Vacuum-Casting Installation, Employing the Stream Degassing Technique (after McGannon [1]).

core remains at a comparatively lower temperature. Thus, the thermal stresses are developed in the ingot due to the temperature variation within the ingot. —

In practice, these ingots are charged into a furnace maintained at a lower temperature in the first stage, and then the furnace temperature is raised to 1498°K(1225°C) along a certain path such that the thermal stresses do not cause cracking failure of the material. One can heat the ingots to a higher temperature range without causing thermal cracking by choosing different furnace temperature paths. But, this heating process has to be carried out in an optimum time in order to minimize the production time as well as production cost. This problem involves the calculation of the transient temperatures and the corresponding thermal stress distributions within the ingot and then the optimal furnace temperature path is obtained.

## 1.2 The Literature Survey

### 1.2.1 The Heat Transfer Analysis

The numerical studies of the heat transfer process of a solid exchanging heat with the surroundings have been carried out [3,4]. In [3], the heat balance of the system was formulated using the finite difference method. The temperature decay rate in the gases in an annealing furnace was studied. The numerical results were obtained by using an

implicit method. In the investigation carried out in [4], the transient temperature distribution within an I-beam was analyzed using the finite element method. The radiative as well as convective heat transfer from the surrounding fluid medium was represented by an equivalent convective heat transfer coefficient, which if multiplied by the temperature difference between the boundary node and the ambient temperature equalled the total amount of heat transfer. This amounted to linearizing the boundary condition.

The calculation of the internal temperature distribution within the cylindrical ingot during heating is a problem in unsteady-state heat conduction and the equations governing this heat transfer process are given in [5,6]. Hunt [7] outlined a numerical method for the solution of the internal temperature distribution in a heated ingot which involved the knowledge of the initial temperature distribution in the ingot, the variation of the ingot skin temperature with time, etc. The heat transfer process within the cylindrical ingot has been studied by several other researchers also [8,9]. In these studies, the temperature distributions within the ingot were obtained using the finite difference method. A number of assumptions were made in these investigations which can be written as

- (a) The whole of the ingot surface was at the same temperature and the absorption of the heat was symmetrical.
- (b) The ingot was assumed to be infinite in length so that the heat flow was radial, i.e. there was no heat input to the flat surfaces which are the top and bottom surfaces of the ingot.
- (c) Each temperature zone was sufficiently small so that a single temperature could be assigned to it and over a small time  $\Delta t$ , the difference of temperature between the adjacent zones was regarded as constant.

### 1.2.2 The Thermal Stress Analysis

In recent years considerable amount of effort has been devoted towards calculation of the thermal stresses in infinite and semi-infinite solids, thick plates and infinitely long cylinders. Adequate references on these types of work can be found in [10]. There are numerous processes in the ceramic as well as in metallurgical engineering fields where one has to have a very good idea about the thermal stresses. These stresses are usually generated by the creation of temperature variation within the body due to the imposed surface conditions; these stresses can also occur if there is a heat source within the body. The solution of such problems involves simultaneous solution

of the elasticity and thermal problems. The thermal stresses generated by nonuniform temperature distribution during the heating of large-diameter Hastelloy X ingots were studied in [8]. In this study, the temperature distribution and the corresponding thermal stresses along the horizontal section AB (refer to Fig. 1.2) were calculated. In the temperature distribution calculations, the heat flux in the axial direction was neglected. The equations for the thermal stress calculations given in [11] were used. The thermal stresses along the vertical axis at the centre of the ingot (in tension) was selected as the critical parameter, and a maximum allowable stress of 90 per cent of 0.2 per cent yield strength was considered as the fracture criteria. The effect of the variation of material properties, which change with temperature, on the thermal stresses in the cylinder was studied in [12]. In [13], the uncoupled thermoelastic brittle fracture problem has been discussed in terms of the types of stress fields produced by surface heating or cooling.

### 1.2.3 The Optimization Studies of the Heating Processes

Any industrial operation should be carried out in an optimal manner. For example, in the case of heating of alloys, ceramics, etc., the process should be done in the minimum time and in doing so, all the constraints must be

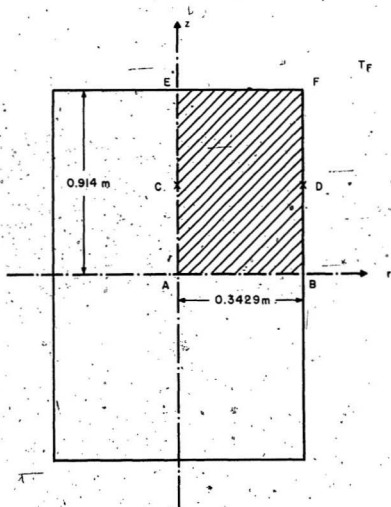


Fig. 1.2: The Diametral Cross-section of the Cylindrical Ingot

satisfied. In a heating process care should be taken that the material temperatures at various points in the solid do not exceed a certain specified value, and the thermal stresses during the heating should not cause failure of the material. In the forging operation of steels, the hot working is carried out in the higher austenitic range. If a close control on the finishing temperatures are not maintained then the solid temperatures can rise into the two-phase region where one of the phases is liquid or, even within the solid-phase temperature range, the problem of burning or oxidation can occur if the finishing temperature is exceeded. Thus, this operation requires a very close control on the solid temperatures.

Meric [14-19] has done quite a considerable amount of work in optimizing the heating time of solids. In [14], an infinitely long solid slab having temperature dependent thermal conductivity was heated optimally under certain ambient conditions. The objective in this work was to heat the slab to a higher temperature level at the end of a fixed time period, while keeping the ambient temperature as low as possible. The boundary control problem of optimal heating of an infinitely long slab with temperature-dependent thermal conductivity, subjected to a convection and radiation boundary condition, was analyzed using the finite element method in [15]. In [16], a stationary variational

formulation of the necessary conditions for optimality was derived for an optimal control problem governed by a parabolic equation and mixed boundary conditions. A simple model problem in optimal boundary heating of solids was analyzed in [17]. The objective of this study was to achieve a desired temperature profile along a segment of solid boundary with a minimum amount of a boundary heat flux which acts as the controlling function. The conjugate gradient method of optimization was used in the minimization process. In [18], the unsteady optimal heating of solids by a boundary heat flux was formulated for a solid of arbitrary geometry. Through the use of the Lagrange multiplier, the problem was reduced to an unconstrained optimization problem. An optimal steady-state control problem governed by an elliptic state equation was solved by several finite element methods in [19]. A nonlinearly constrained problem which involved minimization of the energy consumption of an industrial furnace was formulated in [20]. The variables of the optimization method represented the profile of fuel consumptions along the furnace. The sum of these variables was minimized. The constraints were formulated to satisfy the functioning limits of the furnace and the desired characteristics of the product. In all these analyses, constraints such as the thermal stresses were not considered. In [8], the thermal stresses were included in the



optimization of the furnace heating schedule but the optimum furnace path was approximated by a series of finite-length constant-slope paths which is shown in Fig. 1.3. In this study, the temperature and thermal stress distributions were calculated using two-dimensional finite-difference analysis. This analysis has two drawbacks: The first one is that the optimum path should be a continuous smooth curve rather than a series of straight lines and the second one is that axial heat flux should also be considered. This is because in actual practice, the heat flows from both the radial as well as the axial directions.

Based on a review of the available literature, it can be inferred that the nonlinear three-dimensional transient thermal and stress analyses of the cylindrical ingot during heating in the furnace, and the optimum (minimum) time heating cycle of the ingot considering the thermal cracking of the material have not been done so far. These are the objectives of the present investigation. A brief description of the objectives is presented in the next section.

### 1.3 The Objectives of the Present Investigation

In this thesis, the equations for the transient temperature distribution within the cylindrical ingot due to

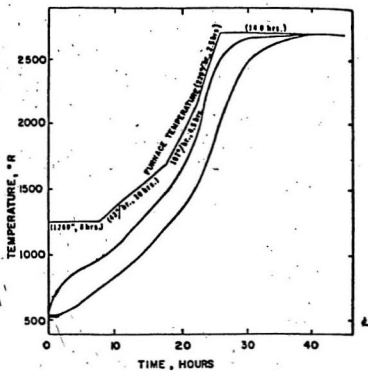


Fig. 1.3. The Rate of Heating of the 1.016 m Dia. Ingot under the Programmed Heating Practice (after Sun [8]).

the radiative and convective heat flux from the furnace have been obtained using the finite element method. This problem has been formulated as an axisymmetric field problem. The thermal stresses due to nonuniform temperature distribution of the ingot are calculated using the linear elasticity theory. The heating rate of the ingot has been varied with a view to optimize the heating schedule of the ingot. Therefore, the following are the objectives of the present investigation:

1. The derivation of the temperature distribution equations in an ingot using the nonlinear finite element analysis.
2. The study of the temperature distributions within the ingot due to various furnace heating paths.
3. The study of the thermal stresses due to the various furnace heating paths.
4. The optimal heating schedule of the heating process.

In Chapter 2, using the finite element method, the equations for the nonlinear thermal analysis of the ingot during heating in the furnace are derived. The Crank-Nicholson finite difference method has been used to express the system of differential equations as a system of nonlinear algebraic equations. Several numerical methods are discussed for solving these nonlinear equations. The effect of the heating rate of the furnace on the ingot temperatures has also been studied.

In Chapter 3, a mathematical model for the axisymmetric thermal stress distribution within the ingot due to nonuniform temperature distribution has been established using the finite element method. The thermal stresses are calculated using the linear-elasticity theory. To demonstrate the importance of the three-dimensional model, the thermal stresses of this analysis are compared with those of the two-dimensional model. The effect of linearizing the heat transfer equations and slenderness ratio of the ingot on the thermal stresses are also studied.

In Chapter 4, the temperature and thermal stress distributions are analyzed for various feasible constants as well as linear slope furnace temperature paths. The different optimization methods applicable for the study of minimum heating time are discussed. The optimum heating furnace temperature path is obtained by maintaining the thermal stress energies at 90% of the 0.2 per cent yield stress of the material throughout the heating period. This optimum path is achieved by carrying out the single variable optimization at each stage during the heating of the ingot.

The conclusions and recommendations for future work are presented in Chapter 5.

## CHAPTER 2

THE TRANSIENT HEAT TRANSFER ANALYSIS OF THE INGOT2.1 Introduction

The cylindrical ingots are heated in a furnace to higher temperature range for hot working. The heat flux enters into the ingot through the top and bottom flat surfaces as well as the cylindrical surface during heating. In the ingot, the thermal stresses while heating are developed due to the nonuniform temperature distribution. In the study of optimal heating of the ingot without the thermal cracking of the material, one always has to consider the magnitudes of maximum thermal stresses within the ingot. The calculation of the thermal stresses involves, at first, the determination of the transient temperature distribution at certain instant of time, and then these are used for the corresponding stress calculations. Therefore, in this chapter as the first step, the transient temperature distributions are calculated. A mathematical model for the nonlinear transient heat transfer analysis within the ingot has been formulated using the three dimensional finite element method, where the boundary elements exchange heat with the surrounding furnace by the convection and radiation mechanisms. The resulting first-order matrix differential

equation is expressed as the system of nonlinear algebraic equations by using the Crank-Nicholson finite difference method. This system of equations are solved for nodal temperatures of ingot by using an iteration method. Finally, the effect of rate of heating on the ingot temperature is studied. The mathematical formulation of the finite element heat transfer analysis is presented in the next section.

## 2.2 The Mathematical Formulation

The diametral cross-section of an ingot is shown in Fig. 1.2. When this ingot is charged into the hot furnace the heat flows both radially and axially. The governing heat transfer equation for the heat flow can be written as [21,22].

$$k_r \frac{\partial^2 T}{\partial r^2} + \frac{k_r}{r} \frac{\partial T}{\partial r} + k_z \frac{\partial^2 T}{\partial z^2} + Q = \rho c \frac{\partial T}{\partial t} \quad (2.1)$$

with the boundary condition

$$k_r \frac{\partial T}{\partial r} \Big|_r + k_z \frac{\partial T}{\partial z} \Big|_z + q + h(T - T_F) + \sigma \epsilon (T^4 - T_F^4) = 0 \quad (2.2)$$

where

$k_r, k_z$  = thermal conductivities in  $r$  and  $z$  directions respectively

$T$  = temperature

$Q$  = heat generated within the body per unit volume

$\rho$  = density of the material

$c$  = specific heat

$t$  = time

$i_r, i_z$  = direction cosines normal to the surface

$q$  = heat flux per unit area

$h$  = convection heat transfer coefficient

$T_F$  = furnace temperature

$\sigma$  = Stefan-Boltzmann Constant

$\epsilon$  = emissivity of the surface

It can be shown by calculus of variations [21] that the solution to the above differential equation, Eqn. (2.1) and boundary condition, Eqn. (2.2), can alternately be obtained by minimizing the corresponding variational functional and solving the resulting set of algebraic equations. Therefore, we seek a functional such that its first variation with respect to temperature,  $T$ , is zero. Eqn. (2.1) can be rewritten as

$$-k_r r \frac{\partial^2 T}{\partial r^2} - k_r \frac{\partial T}{\partial r} - k_z r \frac{\partial^2 T}{\partial z^2} - r(Q - \rho c \frac{\partial T}{\partial t}) = 0 \quad (2.3)$$

Similarly, one can rewrite Eqn. (2.2) as

$$\begin{aligned}
 & k_r \tau \frac{\partial T}{\partial r} i_r + k_z \tau \frac{\partial T}{\partial z} i_z + \tau q + \tau h (T - T_P) \\
 & + \tau \sigma \epsilon (T^4 - T_P^4) = 0 \quad (2.4)
 \end{aligned}$$

Multiplying Eqn. (2.3) and Eqn. (2.4) by the first variation of  $T$  which is  $\delta T$ , and integrating over the domain, we get

$$\begin{aligned}
 \delta \chi = & \int_V [-k_r \tau \frac{\partial^2 T}{\partial r^2} - k_r \tau \frac{\partial T}{\partial r} - k_z \tau \frac{\partial^2 T}{\partial z^2} - \tau(Q - \rho c \frac{\partial T}{\partial t})] \delta T \, dV \\
 & + \int_S [k_r \tau \frac{\partial T}{\partial r} i_r + k_z \tau \frac{\partial T}{\partial z} i_z + \tau q + \tau h (T - T_P) \\
 & + \tau \sigma \epsilon (T^4 - T_P^4)] \delta T \, dS \quad (2.5)
 \end{aligned}$$

Eqn. (2.5) can be rearranged as

$$\begin{aligned}
 \delta \chi = & \int_S k_r \tau \frac{\partial T}{\partial r} i_r \delta T \, dS - \int_V k_r \tau \frac{\partial^2 T}{\partial r^2} \delta T \, dV - \int_V k_r \tau \frac{\partial T}{\partial r} \delta T \, dV \\
 & + \int_S k_z \tau \frac{\partial T}{\partial z} i_z \delta T \, dS - \int_V k_z \tau \frac{\partial^2 T}{\partial z^2} \delta T \, dV \\
 & - \int_V \tau(Q - \rho c \frac{\partial T}{\partial t}) \delta T \, dV + \int_S \tau q \delta T \, dS + \int_S \tau h (T - T_P) \delta T \, dS \\
 & + \int_S \tau \sigma \epsilon (T^4 - T_P^4) \delta T \, dS \quad (2.6)
 \end{aligned}$$

Using Green's divergence theorem, the following integrals can be expressed as



$$\int_S k_r r \frac{\partial T}{\partial r} \delta T \, dS = \int_V k_r r \frac{\partial^2 T}{\partial r^2} \delta T \, dV + \int_V k_r r \frac{\partial T}{\partial r} \delta T \, dV$$

$$+ \int_V \frac{k_r}{2} r \delta \left( \frac{\partial T}{\partial r} \right)^2 \, dV \quad (2.7)$$

$$\int_S k_z r \frac{\partial T}{\partial z} \delta T \, dS = \int_V k_z r \frac{\partial^2 T}{\partial z^2} \delta T \, dV + \int_V \frac{k_z}{2} r \delta \left( \frac{\partial T}{\partial z} \right)^2 \, dV$$

$$(2.8)$$

By substituting Eqns. (2.7) and (2.8) in Eqn. (2.6), we obtain

$$\delta \chi = \int_V \frac{k_r}{2} r \delta \left( \frac{\partial T}{\partial r} \right)^2 \, dV + \int_V \frac{k_z}{2} r \delta \left( \frac{\partial T}{\partial z} \right)^2 \, dV - \int_V r \delta T (Q - \rho c \frac{\partial T}{\partial t}) \, dV$$

$$+ \int_S r q \delta T \, dS + \int_S \frac{rh}{2} \delta (T - T_F)^2 \, dS + \int_S r \sigma \epsilon \delta \left( \frac{T^5}{5} - T_F^4 T \right) \, dS$$

$$(2.9)$$

The above equation can be rearranged as

$$\delta \chi = \int_V \delta \left[ \frac{k_r}{2} r \left( \frac{\partial T}{\partial r} \right)^2 + \frac{k_z}{2} r \left( \frac{\partial T}{\partial z} \right)^2 - r T (Q - \rho c \frac{\partial T}{\partial t}) \right] \, dV$$

$$+ \int_S \delta \left[ r q T + \frac{rh}{2} (T - T_F)^2 + r \sigma \epsilon \left( \frac{T^5}{5} - T_F^4 T \right) \right] \, dS \quad (2.10)$$

The variational operator  $\delta$  can be removed from both sides of Eqn. (2.10) and then it becomes

$$\begin{aligned}
 \chi = & \int_V \left[ \frac{k_r}{2} r \left( \frac{\partial T}{\partial r} \right)^2 + \frac{k_z}{2} r \left( \frac{\partial T}{\partial z} \right)^2 - r T (Q - \rho c \frac{\partial T}{\partial t}) \right] dV + \int_{S_1} r q T ds \\
 & + \int_{S_2} \left[ \frac{rh}{2} (T - T_P)^2 + r \sigma \epsilon \left( \frac{T^5}{5} - T_P^4 T \right) \right] ds \quad (2.11)
 \end{aligned}$$

where

$S_1$  is the surface experiencing heat flux

$S_2$  is the surface experiencing convection and radiation heat exchange

Let  $T^e$  represent the temperature of an axisymmetric triangular element shown in Fig. 2.1. Defining the following elemental matrices

$$T^e = [N_1^e] \{T^e\} \quad (2.12a)$$

$$[D_1^e] = \begin{bmatrix} r k_r^e & 0 \\ 0 & r k_z^e \end{bmatrix} \quad (2.12b)$$

$$[B_1^e] = \begin{bmatrix} \frac{\partial N_1^e}{\partial r} & \frac{\partial N_1^e}{\partial r} & \frac{\partial N_k^e}{\partial r} \\ \frac{\partial N_1^e}{\partial z} & \frac{\partial N_1^e}{\partial z} & \frac{\partial N_k^e}{\partial z} \end{bmatrix} \quad (2.12c)$$

$$\begin{aligned}
 \{g_1^e\} &= \left[ \frac{\partial T^e}{\partial r} \quad \frac{\partial T^e}{\partial z} \right]^T \\
 &= [B_1^e] \{T^e\} \quad (2.12d)
 \end{aligned}$$

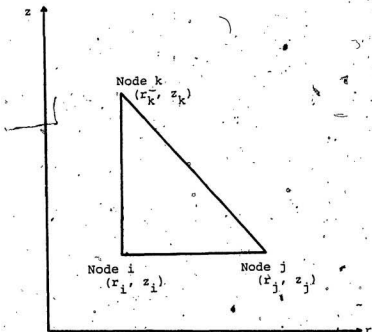


Fig. 2.1: The Details of the Axisymmetric Triangular Element.

and

$$\frac{\partial T^e}{\partial t} = [N_1^e] \frac{\partial \{T^e\}}{\partial t} \quad (2.12e)$$

One can express Eqn. (2.11) for an element as

$$\begin{aligned} \chi^e = & \int_{V^e} \frac{1}{2} \{T^e\}^T [B_1^e]^T [D_1^e] [B_1^e] \{T^e\} dV - \int_{V^e} r Q^e [N_1^e] \{T^e\} dV \\ & + \int_{V_1^e} r \rho c^e [N_1^e] \frac{\partial \{T^e\}}{\partial t} [N_1^e] \{T^e\} dV + \int_{S_1^e} r q^e [N_1^e] \{T^e\} dS \\ & + \int_{S_2^e} \frac{r h^e}{2} ([N_1^e] \{T^e\})^2 dS - \int_{S_2^e} r h^e T_F [N_1^e] \{T^e\} dS \\ & + \int_{S_2^e} \frac{r h^e}{2} T_F^2 dS + \int_{S_2^e} \frac{r c c^e}{5} ([N_1^e] \{T^e\})^5 dS \\ & \int_{S_2^e} r c c^e T_F^4 [N_1^e] \{T^e\} dS \end{aligned} \quad (2.13)$$

The functions for temperature  $T$  are not continuous over the region but, are defined over the individual triangular elements.

Minimizing the variational functional  $\chi$  with respect to  $\{T^e\}$  will yield a stationary value of  $\chi$  that will satisfy the differential equation, Eqn. (2.1), and the boundary condition, Eqn. (2.2). This can be mathematically written as

$$\frac{\partial \chi}{\partial \{T^e\}} = \frac{\partial \chi^1}{\partial \{T^e\}} + \frac{\partial \chi^2}{\partial \{T^e\}} + \dots + \frac{\partial \chi^{n_1}}{\partial \{T^e\}} = 0 \quad (2.14)$$

where  $n_1$  denotes the total number of elements.

Differentiating Eqn. (2.13) with respect to  $\{T^e\}$ , using the relationships given in the Appendix A, and adding the contribution of each of the elements as shown in Eqn. (2.14) we obtain

$$\begin{aligned} \frac{\partial \chi}{\partial \{T^e\}} = & \sum_{e=1}^{n_1} \left[ \int_{V^e} [B_1^e]^T [D_1^e] [B_1^e] \{T^e\} dv - \int_{V^e} r \rho^e [N_1^e]^T dv \right. \\ & + \int_{V^e} r \rho c^e [N_1^e]^T [N_1^e] \frac{\partial \{T^e\}}{\partial t} dv + \int_{S_1^e} r q^e [N_1^e]^T ds \\ & + \int_{S_2^e} r h^e [N_1^e]^T [N_1^e] \{T^e\} ds - \int_{S_2^e} r h^e T_F [N_1^e]^T ds \\ & \left. + \int_{S_2^e} r \alpha c^e [N_1^e]^T ([N_1^e] \{T^e\})^4 ds - \int_{S_2^e} r \alpha c^e T_F^4 [N_1^e]^T ds \right] = 0 \end{aligned} \quad (2.15)$$

The above equation can be expressed as

$$\begin{aligned} [C_1^G] \frac{\partial \{T^G\}}{\partial t} + [K_1^G] \{T^G\} \\ = \{F_Q^G\} - \{F_q^G\} + \{F_c^G\} + \{F_r^G\} \end{aligned} \quad (2.16)$$

where  $[C_1^G]$  and  $[K_1^G]$  refer to the global capacitance and conduction matrices respectively;  $\{F_Q^G\}$ ,  $\{F_q^G\}$ ,  $\{F_c^G\}$  and  $\{F_r^G\}$  are the global force vectors due to the heat generation, heat flux, convection and radiation respectively.

The expressions for the elemental  $[C_1^e]$ ,  $[K_1^e]$ ,  $\{F_c^e\}$  and  $\{F_r^e\}$  are

$$[C_1^e] = \int_{V^e} \rho c^e r [N_1^e]^T [N_1^e] dV \quad (2.17a)$$

$$[K_1^e] = \int_{V^e} [B_1^e]^T [D_1^e] [B_1^e] dV + \int_{S_2^e} r h^e [N_1^e]^T [N_1^e] ds \quad (2.17b)$$

$$\{F_Q^e\} = \int_{V^e} r Q^e [N_1^e]^T dV \quad (2.17c)$$

$$\{F_q^e\} = \int_{S_1^e} r q^e [N_1^e]^T ds \quad (2.17d)$$

$$\{F_c^e\} = \int_{S_2^e} r h^e T_F [N_1^e]^T ds \quad (2.17e)$$

$$\begin{aligned}
 \{F_r^e\} &= \int_{S_2^e} r \sigma \epsilon T_F^4 [N_1^e]^T dS \\
 &= \int_{S_2^e} r \sigma \epsilon [N_1^e]^T ([N_1^e] \{T^e\})^4 dS \quad (2.17f)
 \end{aligned}$$

### 2.3 The Formulation of Elemental Matrices

#### 2.3.1 The Capacitance Matrix $[C_1^e]$

Fig. 2.1 shows the location of various nodes of the axisymmetric triangular element. Using the volume coordinate system to integrate over the volume, the Eqn. (2.17a) can be written as

$$[C_{11}^e] = \frac{\pi \Lambda^e \rho c^e}{90} \begin{bmatrix} C_{11} & C_{12} & C_{13} \\ & C_{22} & C_{23} \\ \text{Symmetric} & & C_{33} \end{bmatrix} \quad (2.18)$$

where

$$C_{11} = 12 r_i^2 + 2 r_j^2 + 2 r_k^2 + 6 r_i r_j + 6 r_i r_k + 2 r_j r_k$$

$$C_{12} = 3 r_i^2 + 3 r_j^2 + r_k^2 + 4 r_i r_j + 2 r_i r_k + 2 r_j r_k$$

$$C_{13} = 3 r_i^2 + r_j^2 + 3 r_k^2 + 2 r_i r_j + 4 r_i r_k + 2 r_j r_k$$

$$C_{22} = 2r_i^2 + 12r_j^2 + 2r_k^2 + 6r_i r_j + 2r_i r_k + 6r_j r_k$$

$$C_{23} = r_i^2 + 3r_j^2 + 3r_k^2 + 2r_i r_j + 2r_i r_k + 4r_j r_k$$

$$C_{33} = 2r_i^2 + 2r_j^2 + 12r_k^2 + 2r_i r_j + 6r_i r_k + 6r_j r_k$$

### 2.3.2 The Conduction Matrix $[K_1^e]$

The expression for the conduction matrix  $[K_1^e]$ , can be written as

$$[K_1^e] = [K_k^e] + [K_h^e] \quad (2.19)$$

where

$$[K_k^e] = \int_{V^e} [B_1^e]^T [D_1^e] [B_1^e] dV = [B_1^e]^T [D_1^e] [B_1^e] \int_{V^e} dV \quad (2.20)$$

The volume integral  $\int_{V^e} dV$  can be evaluated as

$$\int_{V^e} dV = \int_{A^e} 2\pi r dA = 2\pi \bar{r} A^e \quad (2.21)$$

where

$$\bar{r} = \frac{r_i + r_j + r_k}{3}$$

$A^e$  = area of the triangular element.

Now the Eqn. (2.20) can be written as



$$\begin{aligned}
 [K_k^e] &= \frac{2\pi r^2 k_r e}{4A^e} \begin{bmatrix} b_i b_i & b_i b_j & b_i b_k \\ b_j b_i & b_j b_j & b_j b_k \\ b_k b_i & b_k b_j & b_k b_k \end{bmatrix} \\
 &+ \frac{2\pi r^2 k_z e}{4A^e} \begin{bmatrix} c_i c_i & c_i c_j & c_i c_k \\ c_j c_i & c_j c_j & c_j c_k \\ c_k c_i & c_k c_j & c_k c_k \end{bmatrix} \quad (2.22)
 \end{aligned}$$

The expressions for  $b_i$ ,  $b_j$ ,  $b_k$ ,  $c_i$ ,  $c_j$  and  $c_k$  are given in the Appendix C.

The  $[K_h^e]$  matrix is due to the convective heat transfer. This matrix is zero if none of the triangular element sides exchange heat by convection mechanism. For elements having convection boundary condition, this matrix is dependent on the side of the element experiencing convective heat transfer. In this case

$$[K_h^e] = \int_{S_2^e} r h^e [N_1^e]^T [N_1^e] ds \quad (2.23)$$

Using area coordinates, the above integral for the side  $i$ - $j$  of the element can be evaluated as

$$[k_h^e]_{ij} = \frac{2\pi \bar{r} h^e L_{ij}}{12} \begin{bmatrix} 3r_i + r_j & r_i + r_j & 0 \\ r_i + r_j & 3r_j + r_i & 0 \\ 0 & 0 & 0 \end{bmatrix} \quad (2.24)$$

Similarly, for the convection on side j-k of the element one can write

$$[k_h^e]_{jk} = \frac{2\pi \bar{r} h^e L_{jk}}{12} \begin{bmatrix} 0 & 0 & 0 \\ 0 & 3r_j + r_k & r_j + r_k \\ 0 & r_j + r_k & 3r_k + r_j \end{bmatrix} \quad (2.25)$$

and for the side k-i, it will be

$$[k_h^e]_{ki} = \frac{2\pi \bar{r} h^e L_{ki}}{12} \begin{bmatrix} 3r_i + r_k & 0 & r_i + r_k \\ 0 & 0 & 0 \\ r_i + r_k & 0 & 3r_k + r_i \end{bmatrix} \quad (2.26)$$

where

$L_{ij}$ ,  $L_{jk}$ ,  $L_{ki}$  = length of sides i-j, j-k, k-i of the element respectively.

$h^e$  = convection heat transfer coefficient of the element

## 2.4 Formulation of Elemental Force Vectors

### 2.4.1 The Force Vector $\{F_Q^e\}$ Due to the Heat Generation

Using the volume coordinate system to integrate over the volume, the Eqn. (2.17c) can be written as

$$\{F_Q^e\} = \frac{2\pi\bar{r} Q^e \Lambda^e}{12} \begin{Bmatrix} 2r_i + r_j + r_k \\ r_i + 2r_j + r_k \\ r_i + r_j + 2r_k \end{Bmatrix} \quad (2.27)$$

#### 2.4.2 The Force Vector, $\{F_Q^e\}$ Due to the Heat Flux

The vector,  $\{F_Q^e\}$  is dependent on the side of the element experiencing the heat flux. Using area coordinates to integrate over the surface, the Eqn. (2.17d), for the side i-j of the element can be written as

$$\{F_Q^e\}_{ij} = \frac{2\pi\bar{r} q^e L_{ij}}{6} \begin{Bmatrix} 2r_i + r_j \\ r_i + 2r_j \\ 0 \end{Bmatrix} \quad (2.28)$$

Similarly, for the side j-k of the element one obtains

$$\{F_Q^e\}_{jk} = \frac{2\pi\bar{r} q^e L_{jk}}{6} \begin{Bmatrix} 0 \\ 2r_j + r_k \\ r_j + 2r_k \end{Bmatrix} \quad (2.29)$$

and for the side k-i, it will be

$$\{F_Q^e\}_{ki} = \frac{2\pi\bar{r} q^e L_{ki}}{6} \begin{Bmatrix} 2r_i + r_k \\ 0 \\ r_i + 2r_k \end{Bmatrix} \quad (2.30)$$

### 2.4.3 The Force Vector $\{F_c^e\}$ Due to the Convection

This vector is also dependent on the side exchanging heat by convection. Using area coordinates the surface integral, Eqn. (2.17e) for the side  $i-j$  of the element can be written as

$$\{F_c^e\}_{ij} = \frac{2\pi \bar{r} h^e T_F L_{ij}}{6} \begin{Bmatrix} 2r_i + r_j \\ r_i + 2r_j \\ 0 \end{Bmatrix} \quad (2.31)$$

Similarly, for the side  $j-k$ , it will be

$$\{F_c^e\}_{jk} = \frac{2\pi \bar{r} h^e T_F L_{jk}}{6} \begin{Bmatrix} 0 \\ 2r_j + r_k \\ r_j + 2r_k \end{Bmatrix} \quad (2.32)$$

and for the side  $k-i$ , it can be written as

$$\{F_c^e\}_{ki} = \frac{2\pi \bar{r} h^e T_F L_{ki}}{6} \begin{Bmatrix} 2r_i + r_k \\ 0 \\ r_i + 2r_k \end{Bmatrix} \quad (2.33)$$

### 2.4.4 The Force Vector, $\{F_r^e\}$ Due to the Radiation

The expression for the vector  $\{F_r^e\}$  can be written as

$$\{F_r^e\} = \{F_1^e\} - \{F_2^e\} \quad (2.34)$$

where

$$\{F_1^e\} = \int_{S_2^e} r \sigma \epsilon T_F^4 [N_1^e]^T ds. \quad (2.35)$$

$$\{F_2^e\} = \int_{S_2^e} r \sigma \epsilon [N_1^e]^T ([N_1^e] \{T^e\})^4 ds \quad (2.36)$$

Both the vectors,  $\{F_1^e\}$  and  $\{F_2^e\}$ , are dependent on the side of the element experiencing radiation heat transfer. The surface integrals in Eqn. (2.34) are evaluated using the area coordinates. The vector  $\{F_1^e\}$ , Eqn. (2.35), for the side i-j of the element will be

$$\{F_1^e\}_{ij} = \frac{2\pi \bar{r} \sigma \epsilon T_F^4 L_{ij}}{6} \begin{Bmatrix} 2r_i + r_j \\ r_i + 2r_j \\ 0 \end{Bmatrix}; \quad (2.37)$$

Similarly, for the side j-k, it can be written as

$$\{F_1^e\}_{jk} = \frac{2\pi \bar{r} \sigma \epsilon T_F^4 L_{jk}}{6} \begin{Bmatrix} 0 \\ 2r_j + r_k \\ r_j + 2r_k \end{Bmatrix}, \quad (2.38)$$

and for the side k-i, it will be

$$\{F_1^e\}_{ki} = \frac{2\pi \bar{r} \sigma \epsilon T_F^4 L_{ki}}{6} \begin{Bmatrix} 2r_i + r_k \\ 0 \\ r_i + 2r_k \end{Bmatrix} \quad (2.39)$$

Similarly, the vector  $\{F_2^e\}$ , Eqn. (2.36) for the side i-j of

the element is

$$\{F_2^e\}_{ij} = \frac{2\pi \bar{r} \sigma \epsilon L_{ij}}{420} \begin{Bmatrix} c_1 \\ c_2 \\ 0 \end{Bmatrix} \quad (2.40)$$

where

$$C_1 = (60T_i^4 + 40T_i^3 T_j + 24T_i^2 T_j^2 + 12T_i T_j^3 + 4T_j^4) r_i \\ + (10T_i^4 + 16T_i^3 T_j + 18T_i^2 T_j^2 + 16T_i T_j^3 + 10T_j^4) r_j$$

$$C_2 = (10T_j^4 + 16T_j^3 T_i + 18T_j^2 T_i^2 + 16T_j T_i^3 + 10T_i^4) r_i \\ + (60T_j^4 + 40T_j^3 T_i + 24T_j^2 T_i^2 + 12T_j T_i^3 + 4T_i^4) r_j$$

and for the side j-k it will be

$$\{F_2^e\}_{jk} = \frac{2\pi \bar{r} \sigma \epsilon L_{jk}}{420} \begin{Bmatrix} 0 \\ C_2 \\ C_3 \end{Bmatrix} \quad (2.41)$$

where

$$C_2 = (60T_j^4 + 40T_j^3 T_k + 24T_j^2 T_k^2 + 12T_j T_k^3 + 4T_k^4) r_j \\ + (10T_j^4 + 16T_j^3 T_k + 18T_j^2 T_k^2 + 16T_j T_k^3 + 10T_k^4) r_k$$

$$C_3 = (10T_k^4 + 16T_k^3 T_j + 18T_k^2 T_j^2 + 16T_k T_j^3 + 10T_j^4) r_j \\ + (60T_k^4 + 40T_k^3 T_j + 24T_k^2 T_j^2 + 12T_k T_j^3 + 4T_j^4) r_k$$

Similarly, for the side k-i, it can be written as

$$\{F_2^e\}_{ki} = \frac{2\pi \bar{r} \sigma \epsilon L_{ki}}{420} \begin{Bmatrix} C_1 \\ 0 \\ C_3 \end{Bmatrix} \quad (2.42)$$

where

$$C_1 = (60T_i^4 + 40T_i^3 T_k + 24T_i^2 T_k^2 + 12T_i T_k^3 + 4T_k^4) r_i \\ + (10T_i^4 + 16T_i^3 T_k + 18T_i^2 T_k^2 + 16T_i T_k^3 + 10T_k^4) r_k$$

$$C_3 = (10T_k^4 + 16T_k^3 T_i + 18T_k^2 T_i^2 + 16T_k T_i^3 + 10T_i^4) r_i \\ + (60T_k^4 + 40T_k^3 T_i + 24T_k^2 T_i^2 + 12T_k T_i^3 + 4T_i^4) r_k$$

## 2.5 The Solution of the Nonlinear Transient Heat Transfer Problems

### 2.5.1 The Transformation of the Simultaneous Differential Equations

There are two commonly known methods for solving the nonlinear set of transient temperature equations Eqn. (2.16). It is a system of first order nonlinear differential equation. The first method of solving these equations is by using the finite element method defined in the time domain [21]. The second method [23] for solving these equations is by approximating the time derivative using a finite difference scheme. However, the number of computations involved in the first method are very large. On the other hand, the Crank-Nicholson central finite difference

method [22,23] is unconditionally stable and can be easily used in the present investigation for obtaining the temperature distribution. Using this method, the first derivative of the nodal temperatures between two points in the time domain can be approximated as

$$\frac{d\{T^G\}_t}{dt} = \frac{\{T^G\}_{t+\frac{\Delta t}{2}} - \{T^G\}_{t-\frac{\Delta t}{2}}}{\Delta t} \quad (2.43)$$

where  $\Delta t$  is the time step.

Similarly, we can also express  $\{T^G\}_t$  and  $\{F^G\}_t$  as

$$\{T^G\}_t = \frac{\{T^G\}_{t+\frac{\Delta t}{2}} + \{T^G\}_{t-\frac{\Delta t}{2}}}{2} \quad (2.44)$$

and

$$\{F^G\}_t = \frac{\{F^G\}_{t+\frac{\Delta t}{2}} + \{F^G\}_{t-\frac{\Delta t}{2}}}{2} \quad (2.45)$$

Substitution of Eqns. (2.43), (2.44), (2.45) into Eqn. (2.16) gives

$$\begin{aligned} \frac{1}{\Delta t} [C_1^G] \{T^G\}_{t+\frac{\Delta t}{2}} - \frac{1}{\Delta t} [C_1^G] \{T^G\}_{t-\frac{\Delta t}{2}} + \frac{1}{2} [K_1^G] \{T^G\}_{t+\frac{\Delta t}{2}} \\ + \frac{1}{2} [K_1^G] \{T^G\}_{t-\frac{\Delta t}{2}} = \frac{1}{2} \{F_Q^G\}_{t+\frac{\Delta t}{2}} + \frac{1}{2} \{F_Q^G\}_{t-\frac{\Delta t}{2}} \end{aligned}$$



$$\begin{aligned}
& -\frac{1}{2} [F_q^G]_{t+\frac{\Delta t}{2}} - \frac{1}{2} [F_q^G]_{t-\frac{\Delta t}{2}} + \frac{1}{2} [F_c^G]_{t+\frac{\Delta t}{2}} \\
& + \frac{1}{2} [F_c^G]_{t-\frac{\Delta t}{2}} + \frac{1}{2} [F_r^G]_{t+\frac{\Delta t}{2}} + \frac{1}{2} [F_r^G]_{t-\frac{\Delta t}{2}}
\end{aligned} \quad (2.46)$$

The above equation can be rearranged as

$$\begin{aligned}
& ([K_1^G] + \frac{2}{\Delta t} [C_1^G]) \{T^G\}_{t+\frac{\Delta t}{2}} = (\frac{2}{\Delta t} [C_1^G] - [K_1^G]) \{T^G\}_{t-\frac{\Delta t}{2}} \\
& + [F_Q^G]_{t+\frac{\Delta t}{2}} + [F_Q^G]_{t-\frac{\Delta t}{2}} - [F_q^G]_{t+\frac{\Delta t}{2}} - [F_q^G]_{t-\frac{\Delta t}{2}} \\
& + [F_c^G]_{t+\frac{\Delta t}{2}} + [F_c^G]_{t-\frac{\Delta t}{2}} + [F_r^G]_{t+\frac{\Delta t}{2}} + [F_r^G]_{t-\frac{\Delta t}{2}}
\end{aligned} \quad (2.47)$$

In the above equation, the force vectors due to radiative heat transfer,  $[F_r^G]_{t-\frac{\Delta t}{2}}$  and  $[F_r^G]_{t+\frac{\Delta t}{2}}$  are nonlinear. They contain the high powers of some of the nodal temperatures of the elements along the surface of the ingot. Here nodal temperature vector  $\{T^G\}$  at time  $t+\frac{\Delta t}{2}$  is unknown whereas the other quantities (vectors and matrices) are known. The substitution of  $\{T^G\}_{t-\frac{\Delta t}{2}}$  on the right side

of Eqn. (2.47) reduces to

$$\begin{aligned}
 ([K_1^G] + \frac{2}{\Delta t} [C_1^G]) \{T^G\}_{t+\frac{\Delta t}{2}} = [A_1] + \{F_O^G\}_{t+\frac{\Delta t}{2}} - \{F_Q^G\}_{t+\frac{\Delta t}{2}} \\
 + \{F_C^G\}_{t+\frac{\Delta t}{2}} + \{F_R^G\}_{t+\frac{\Delta t}{2}}
 \end{aligned} \quad (2.48)$$

where  $[A_1]$  is known.

The Eqn. (2.48) has vectors  $\{F_R^G\}_{t+\frac{\Delta t}{2}}$  and  $\{F_C^G\}_{t+\frac{\Delta t}{2}}$  on the right hand side and these vectors contain the unknown nodal temperatures at the time  $t+\frac{\Delta t}{2}$ . Therefore, this equation can only be solved by iteration techniques. Some of these techniques are

- 1) The Iteration Method
- 2) The Newton-Raphson Method
- 3) The Nonlinear Optimization Method

Some discussion on these methods are mentioned in the following sections.

### 2.5.2 The Iteration Method

In this method, [24] the nodal temperatures at time  $t+\frac{\Delta t}{2}$  are initially assumed to be the same as the temperatures at time  $t-\frac{\Delta t}{2}$ , and used on the right hand side

of Eqn. (2.48). Then the force vectors,  $\{F_Q^G\}$ ,  $\{F_C^G\}$ ,  $\{F_R^G\}$  and  $\{F_T^G\}$  in Eqn. (2.48) are evaluated with the assumed nodal temperatures. At this stage Eqn. (2.48) reduces to

$$([K_1^G] + \frac{2}{\Delta t} [C_1^G]) \{T^G\}_{t + \frac{\Delta t}{2}} = \{A_2\} \quad (2.49)$$

where  $\{A_2\}$  is known.

The linear equation, Eqn. (2.49) can be easily solved for  $\{T^G\}_{t + \frac{\Delta t}{2}}$ . The calculated nodal temperatures are then compared with those assumed ones. If they do not meet the convergence criteria then, the average of the assumed and calculated temperatures are used in the next iteration.

### 2.5.3 The Newton-Raphson Method

It is a commonly known method for solving the nonlinear equations [23,25]. In this method the unknown temperature vector  $\{T^G\}$  at the  $i$ th stage of iteration is substituted in Eqn. (2.48) and rearranging this equation one can write

$$\begin{aligned} \{f\}^i = & ([K_1^G] + \frac{2}{\Delta t} [C_1^G]) \{T^G\}_{t + \frac{\Delta t}{2}}^i - \{A_1\} - \{F_Q^G\}_{t + \frac{\Delta t}{2}}^i \\ & + \{F_C^G\}_{t + \frac{\Delta t}{2}}^i - \{F_C^G\}_{t + \frac{\Delta t}{2}}^i - \{F_R^G\}_{t + \frac{\Delta t}{2}}^i \quad (2.50a) \end{aligned}$$

In this equation  $\{f\}^i$  is the residual vector whose all the elements are zero only when the assumed vector  $\{T^G\}^i$  converges. Clearly,  $\{f\}^i$  is a function of all the nodal temperatures, therefore, one can evaluate the matrix  $[A]^i$ , the Jacobian matrix whose general term  $A_{jk}^i$  can be defined as

$$A_{jk}^i = \frac{\partial f_j}{\partial T_k} \Big|_i \quad (2.50b)$$

The correction vector  $\{\Delta T^G\}^i$  can be obtained using

$$[A]^i \{\Delta T^G\}^i = -\{f\}^i \quad (2.50c)$$

Then, the improved temperature vector can be known using the relation

$$\{T^G\}_{t+\frac{\Delta t}{2}}^{i+1} = \{T^G\}_{t+\frac{\Delta t}{2}}^i + \{\Delta T^G\}_{t+\frac{\Delta t}{2}}^i \quad (2.50d)$$

The iteration can be terminated if

$$|f_j| < f_{tol} \quad (j = 1, 2, \dots, n)$$

Alternately, the iteration can also be terminated if

$$|\Delta T_j^G| < \Delta T_{tol}^G \quad (j=1, 2, \dots, n)$$

#### 2.5.4 The Nonlinear Optimization Method

The nonlinear optimization methods can also be used [26] for solving Eqn. (2.48) for the unknown nodal temperature vector  $\{T^G\}_{t+\frac{\Delta t}{2}}$ . As an example, the solution of Eqn. (2.48) can be obtained by the Davidon-Fletcher-Powell method [27,28] which is a very stable method and converges quadratically.

If we denote the global temperature vector at the  $i$ th iteration stage of the optimization as  $\{T_o^i\}_{t+\frac{\Delta t}{2}}$  and substitute on the right hand side of Eqn. (2.48) then we can compute the force vectors  $\{F_c^G\}_{t+\frac{\Delta t}{2}}$  and  $\{F_r^G\}_{t+\frac{\Delta t}{2}}$ . Then, this equation reduces to system of linear equations which can be solved for the unknown temperature vector at time  $t+\frac{\Delta t}{2}$ . This calculated vector can be denoted as  $\{T_c^i\}_{t+\frac{\Delta t}{2}}$ . So we can define the objective function,  $\theta$  for the minimization as

$$\theta = \sum_{i=1}^{n_2} (T_c^i - T_o^i)^2_{t+\frac{\Delta t}{2}} \quad (2.51)$$

where  $n_2$  denotes the total number of nodes.

Therefore, the global temperature vector  $\{T^G\}_{t+\frac{\Delta t}{2}}$

is obtained by minimizing the objective function  $\theta$ . The iterative procedure of this method can be stated as follows [27]:

(1) Start with an initial assumed vector  $\{T_o^i\}$  and a positive definite symmetric matrix  $[H^i]$ . Usually we consider  $[H^i]$  as the identity matrix. Set iteration number  $i$  to 1.

(2) Compute the gradient of the objective function  $\nabla \theta^i$ , at  $\{T_o^i\}$ , and evaluate  $\{G^i\}$  such that

$$\{G^i\} = -[H^i] \{\nabla \theta^i\} \quad (2.52.1)$$

(3) Obtain the optimal step length  $\lambda_i^*$  in the direction  $\{G^i\}$  and set

$$\{T_o^{i+1}\}_{t + \frac{\Delta t}{2}} = \{T_o^i\}_{t + \frac{\Delta t}{2}} + \lambda_i^* \{G^i\} \quad (2.52.2)$$

Substitute  $\{T_o^{i+1}\}_{t + \frac{\Delta t}{2}}$  in  $[F_c^G]_{t + \frac{\Delta t}{2}}$  and  $[F_r^G]_{t + \frac{\Delta t}{2}}$ . Solve for  $\{T_c^{i+1}\}_{t + \frac{\Delta t}{2}}$ . Compute the value of objective function

$\theta_{t + \frac{\Delta t}{2}}^{i+1}$  and test for optimality. If the objective function

attains an optimum value, then terminate the iterative procedure. The temperature vector corresponding to optimum objective function represents the global temperature vector at time  $t + \frac{\Delta t}{2}$ . Otherwise go to the next step.

(5) Update the matrix [H] using the relation

$$[H^{i+1}] = [H^i] + [M^i] + [N^i] \quad (2.52.3)$$

where

$$[M^i] = \frac{\lambda_i^* [G^i] \{G^i\}^T}{\{G^i\}^T \{P^i\}} \quad (2.52.4)$$

$$[N^i] = \frac{-[[H^i] \{P^i\}] [\{H^i\} \{P^i\}]^T}{\{P^i\}^T [H^i] \{P^i\}} \quad (2.52.5)$$

and

$$\{P^i\} = v\theta(\{T_o^{i+1}\}) - v\theta(\{T_o^i\}) = v\theta^{i+1} - v\theta^i \quad (2.52.6)$$

6) Set the new iteration number  $i=i+1$  and go to Step 2.

## 2.6 Numerical Example

The transient heat transfer process of the body shown in Fig. 2.2 was studied using the finite element method, [24]. It is a ceramic body whose sides were maintained at 300°C, the bottom surface was insulated. The top surface exchanged heat with the surrounding fluid which was at 50°C. This heat transfer process was by convection and radiation mechanisms. Initially the whole body was at 300°C. This problem was analyzed as a two-dimensional problem. Because of the symmetry about the vertical axis, the heat transfer analysis was carried out for the right half

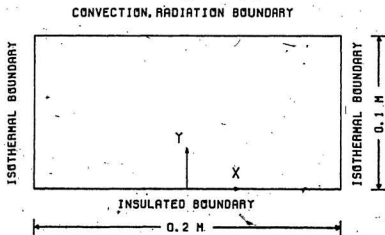


Fig. 2.2: The System Configuration with Various Boundary Conditions.



of the body only. The linear finite triangular elements were used in this study. The finite element discretization of the system is shown in Fig. 2.3. The unsteady heat transfer process of this body was represented by Eqn. (2.48). The expressions for the elemental matrices  $[K_1^e]$ ,  $[C_1^e]$  and elemental force vectors  $\{F_Q^e\}$ ,  $\{F_q^e\}$ ,  $\{F_C^e\}$ ,  $\{F_r^e\}$  are given in the Appendix B. The Eqn. (2.48) was solved for  $\{T^G\}_{t+\frac{\Delta t}{2}}$  by the three methods mentioned earlier i.e. the iteration method, the Newton-Raphson method and the optimization method.

Fig. 2.4 shows the temperature distribution of the solid using the iteration technique. This figure shows the continuous decline of temperature for all the salient nodes with time. The temperatures of various nodes oscillate in the beginning, and then die out after some time. At a given time, the oscillation amplitudes are higher at the top surface nodes compared to the nodes at the insulated boundary. The rate of decrease of the temperature at the top surface is very high, whereas the temperatures at the nodes which are on insulated boundary decrease very slowly. At any given time, node 21 is at the lowest temperature. This is because it lies on the symmetrical axis loosing heat to the surrounding fluid by convection as well as radiation.

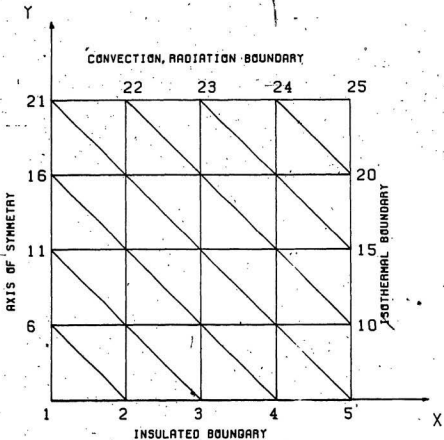


Fig. 2.3: The Discretization of the System into Finite Elements.

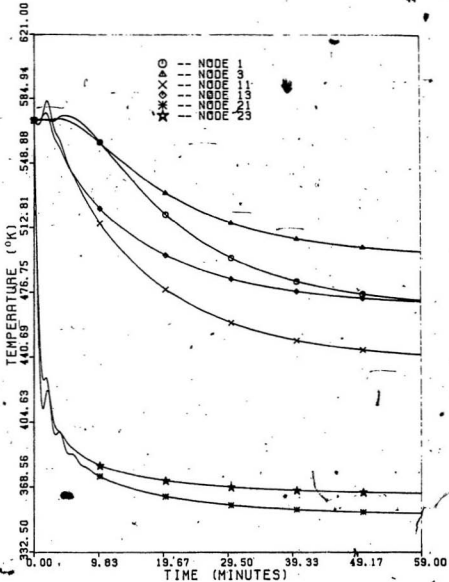


Fig. 2.4: The Time-Temperature Plot of the Ceramic Body.

Moreover, it is the farthest point from insulated and isothermal surfaces. Figs. 2.5 - 2.7 show the time-temperature plot of the nodes 1, 13, 23 respectively. It is clear from these figures that the temperature distributions obtained by different numerical methods are quite close. As expected, the finite element results show oscillations in the initial time period, whereas finite difference results do not exhibit such a behaviour. However, one has to take care of the stability criteria in the finite difference method. The finite element equation Eqn. (2.48) is unconditionally stable.

In order to solve the heat transfer equation Eqn. (2.48) by Newton-Raphson method, one has to compute the Jacobian matrix,  $[A]$ . The computation of Jacobian matrix requires more computer memory storage and involves more number of computations as compared to the iteration method. Similarly, the solution of Eqn. (2.48) by the nonlinear optimization method required more computation time [26]. The iteration method was found to be the most efficient among the three methods for solving nonlinear heat transfer equations. Using this method the solution was obtained using the least amount of CPU time compared to the Newton-Raphson method or the nonlinear optimization method.

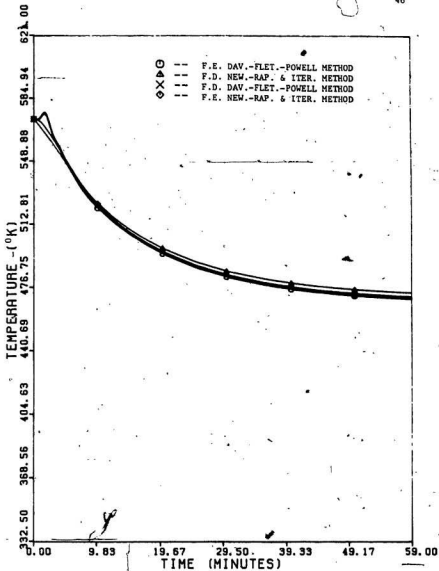


Fig. 2.5: The Time-Temperature Plot at the Node 1.

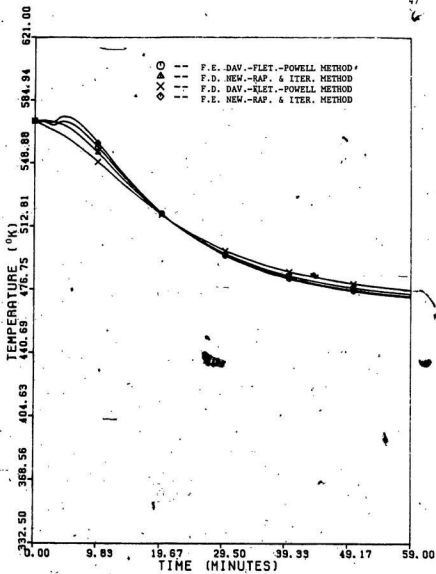


Fig. 2.6: The Time-Temperature Plot at the Node 13.

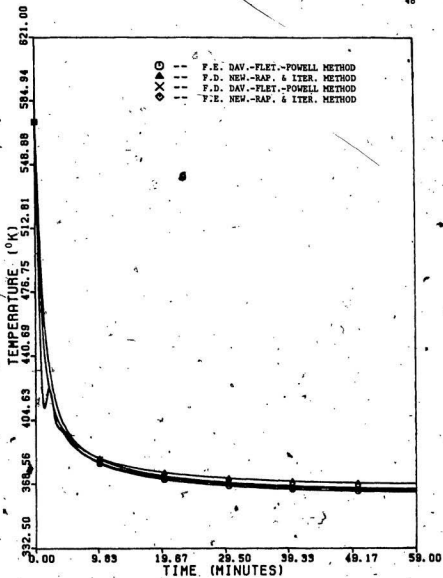


Fig. 2.7: The Time-Temperature Plot at the Node 23.

Therefore, this iterative method was used for solving heat transfer equation of the ingot which is carried out in the next section.

## 2.7 Computer Simulation of the Heat Transfer Process Within the Ingot

### 2.7.1 The System of Equations for the Heat Transfer Within the Ingot

There are a lot of industrial processes which can be modelled on a digital computer. These simulated models can be used very economically to study the effects of the variation of some of the control variables on the state variables and thus the feasibility of any modification of the process can be easily implemented. As an example, in a heat treatment process, the furnace temperature can be considered as a control variable and the resulting temperatures at various points of the solid as the state variables. By varying the furnace temperature one can obtain the desirable distribution of the temperature within the solid. A computer model of such a process can be very easily established.

There are several types of metallurgical processes where a material is required to be heated to a very high temperature before processing. Some of these processes are annealing, forging, rolling, etc. During the heating process the surface gets heated fairly rapidly whereas the core remains at a comparative lower temperature. The thermal



stresses are developed due to this temperature difference. If this temperature difference is large then it can lead to the thermal cracking of the material. Therefore, the material should be heated in such a way that this maximum difference in the temperature at any instant should be less than certain amount so that the cracking does not take place. This necessitates a thorough analysis of the heat transfer process within such materials [29].

In the forge-shop, steel ingots are heated to the higher austenitic temperature range which is close to 1225°C. In practice, these ingots are charged into a furnace maintained at a lower temperature in the first stage, and then the furnace temperature is raised in the successive stages [1].

The heat transfer analysis was studied using finite element method. The boundary elements of ingot exchanged heat with the surrounding furnace by means of convection and radiation mechanisms while being heated. The ingot gains heat from the furnace through the top and bottom flat surfaces as well as the cylindrical surface. In this heat transfer process both the heat flux,  $q$ , and heat generation term within the ingot,  $Q$ , are zero. Therefore, the Eqn. (2.47) for this problem reduces to

$$\begin{aligned}
 & \left( [K_1^G] + \frac{2}{\Delta t} [C_1^G] \right) \{T^G\}_{t+\frac{\Delta t}{2}} = \left( \frac{2}{\Delta t} [C_1^G] - [K_1^G] \right) \{T^G\}_{t-\frac{\Delta t}{2}} \\
 & + \{F_c^G\}_{t+\frac{\Delta t}{2}} + \{F_c^G\}_{t-\frac{\Delta t}{2}} + \{F_r^G\}_{t+\frac{\Delta t}{2}} + \{F_r^G\}_{t-\frac{\Delta t}{2}}
 \end{aligned}
 \tag{2.53}$$

The iteration method was used for solving  $\{T^G\}_{t+\frac{\Delta t}{2}}$  in the above equation. The results of the solution are discussed in the next subsection.

#### 2.7.2 The Temperature Distribution Within the Ingot

The temperature distribution within the ingot was obtained [29] using Eqn. (2.53). Fig. 1.2 shows the diametral cross-section of the ingot where AB represents the radius and AE half the height of the ingot. Due to the symmetry about the horizontal and vertical axis, the finite element analysis was carried out for the shaded region only. In this figure,  $T_F$  represents the furnace temperature. The zone of interest was divided into several linear axisymmetric triangular elements (the details are given in the Appendix C). The finite element discretization of the system is shown in Fig. 2.8. In the heating process, the temperature gradients at the surface were quite high therefore, the size of the elements near the surface were smaller. It was assumed that the ingot was made of 1% Cr steel, and the

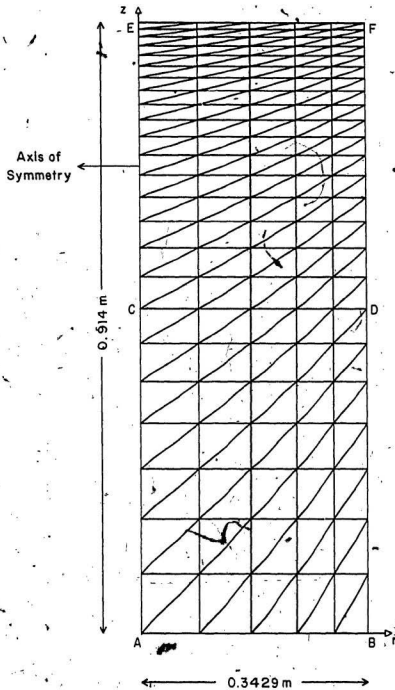


Fig. 2.8: The Discretization of the Ingot into Finite Elements.

material properties were obtained from [30]. The thermal conductivity, ( $k_r$ ,  $k_z$ ) specific heat, ( $c$ ) and convection heat transfer coefficient, ( $h$ ) had nonlinear variations with the temperature of the ingot.

The assumed variation of heat transfer coefficient,  $h$ , with ingot temperature can be written as [31]

$$h = \frac{0.5413(T_F - T_S)^{0.25}}{d} \quad \text{W/m}^2 \cdot \text{K} \quad (2.54)$$

where

$T_F$  is the furnace temperature

$T_S$  is the surface nodal temperature

$d$  is the diameter of the ingot

In order to study the heat transfer process within the ingot the furnace temperature was raised from the room temperature, 295°K, to final temperature, 810°K, along a linear path but with various heating rates, which are shown in Figs. 2.9-2.13. Fig. 2.9 shows the temperature variation of some of the typically selected points such as A, B, C and F. In these figures the fastest temperature rise takes place at the corner point F. The point A shows the slowest response. This is, because at the point F, the heat from both the top as well as the cylindrical surfaces is being received. The point A is slowest to respond because it is the interior-most point. The rate of increase of the

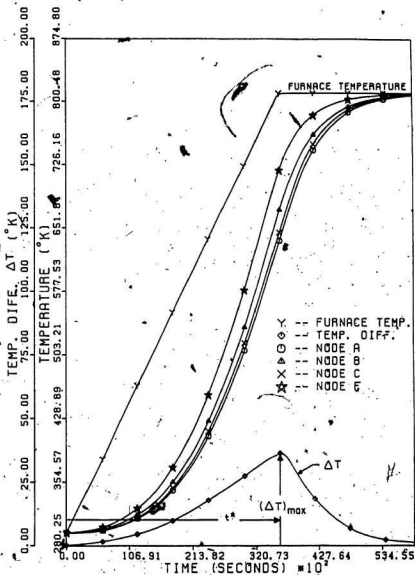


Fig. 2.9: The Time-Temperature Plot of the Ingot Corresponding to the Furnace Heating Rate of  $0.014^{\circ}\text{K}/\text{sec}$  ( $51.5^{\circ}\text{K}/\text{hour}$ ).

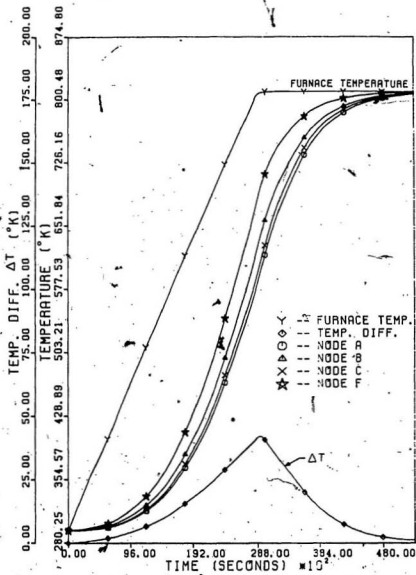


Fig. 2.10: The Time-Temperature Plot of the Ingot Corresponding to the Furnace Heating Rate of  $0.017^{\circ}\text{K}/\text{sec}$  ( $64.375^{\circ}\text{K}/\text{hour}$ ).

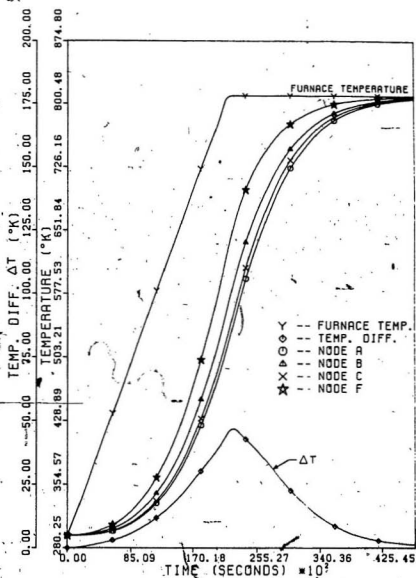


Fig. 2.11: The Time-Temperature Plot of the Ingot Corresponding to the Furnace Heating Rate of  $0.024^{\circ}\text{K}/\text{sec}$  ( $85.833^{\circ}\text{K}/\text{hour}$ ).

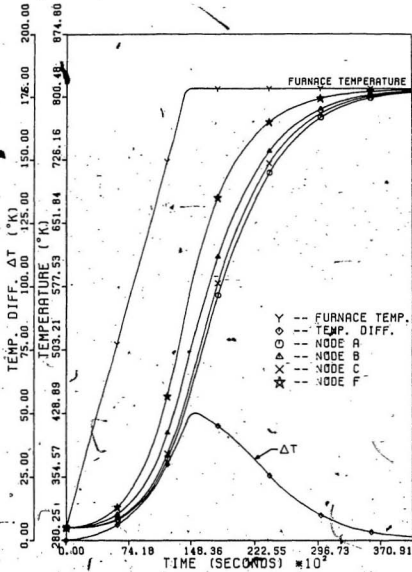


Fig. 2.12: The Time-Temperature Plot of the Ingot Corresponding to the Furnace Heating Rate of  $0.0355^{\circ}\text{K}/\text{sec}$  ( $128.76^{\circ}\text{K}/\text{hour}$ ).



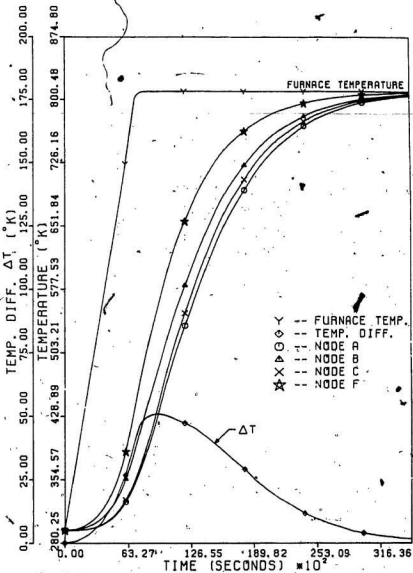


Fig.2.13: The Time-Temperature Plot of the Ingot Corresponding to the Furnace Heating Rate of  $0.071^{\circ}\text{K}/\text{sec}$  ( $257.5^{\circ}\text{K}/\text{hour}$ ).

temperature at the point B is greater than C because it happens to be at the cylindrical surface. In these figures, there is also a plot of  $\Delta T$  versus time.  $\Delta T$  represents the temperature difference between the nodes B and A. These two points were selected because the temperature difference per unit length was greater than between points A and E or A and F. In other words, the average gradient along AB was greater than AE or AF. The parameter  $\Delta T_{\max}$  is the maximum temperature difference between these points and it causes maximum thermal stresses. While heating the ingot care is taken so that this quantity does not exceed a certain value which would cause thermal cracking. An interesting fact to be observed is that  $\Delta T_{\max}$  takes place 36000 seconds (10 hours) after the furnace temperature starts rising (refer to Fig. 2.9). At this instant, the point B is already close to the final temperature.

The effect of the variation of the furnace heating rate on  $\Delta T_{\max}$  is shown in Figs. 2.9 to 2.13. In Fig. 2.14, the furnace is already at the finishing temperature i.e. the ingot is charged into the hot furnace maintained at the finishing temperature. In these figures the heating characteristics of the various points shown in Fig. 2.9, do not change but the occurrence of  $\Delta T_{\max}$  shifts to the left i.e., the maximum temperature difference between the points B and A takes place sooner as the heating rate of the furnace

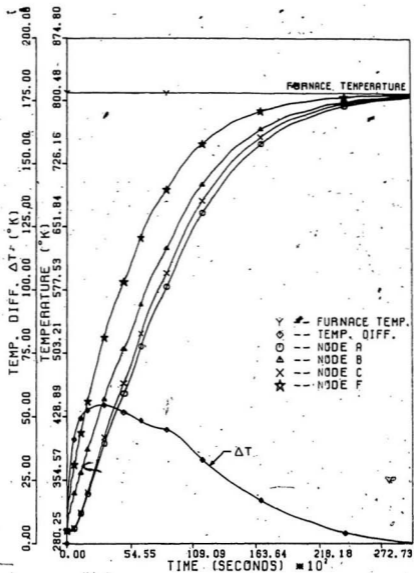


Fig.2.14: The Time-Temperature Plot of the Ingot Corresponding to a Constant Furnace Temperature of 810 $^{\circ}\text{K}$ .

is increased. This fact is shown in the Table 2.1. As can be seen in this table the time  $t^*$ , the time at which  $\Delta T_{\max}$  takes place, decreases as the heating rate increases, but the magnitude of  $\Delta T_{\max}$  increases with the increase in the heating rate.

In this table it is quite clear that as the heating rate increases then  $t_s$ , the time required for the ingot to reach the steady state temperature, decreases. One is always interested in minimizing  $t_s$ , which would amount to decreasing the production time of heating the ingots but one has to keep in mind the quantity  $\Delta T_{\max}$ , a very high value of which can lead to thermal cracking.

### 2.7.3 The Temperature Gradient Distribution

#### Within The Ingot

The temperature gradients were calculated using Eqn. (2.12d) for a constant furnace temperature of 810°K. In Figs. 2.15 - 2.17, the radial temperature gradients along the sections AB, CD and EF respectively are shown. In all of these figures the gradient characteristics are similar. After 120 seconds (2 minutes) of heating, the gradients are very high near the cylindrical surface; the core is unaffected by the heating process. As the heating time increases these gradients increase, and then as the surface and the core temperatures come close to each other, these

Table 2.1 The Variations of  $\Delta T_{\max}$ ,  $t^*$  and  $t_s$  for  
Different Rates of Furnace Heating

Furnace Heating Rate $\times 10^2$ ( $^{\circ}\text{K}/\text{sec}$ )	$\Delta T_{\max}$ ( $^{\circ}\text{K}$ )	$t^* \times 10^{-3}$ (seconds)	$t_s \times 10^{-3}$ (seconds)
1.43	36.26	36.0	66.0
1.78	41.50	28.8	61.2
2.38	46.28	22.8	55.2
3.57	50.14	15.6	50.4
7.15	53.08	8.4	45.6
"	55.47	3.0	43.2

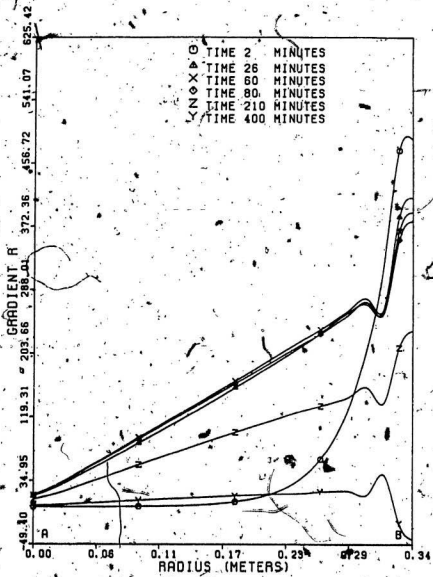


Fig.2.15: The Variation of the Radial Temperature Gradient Along the Section AB ( $T_s = 910^{\circ}\text{K}$ ).

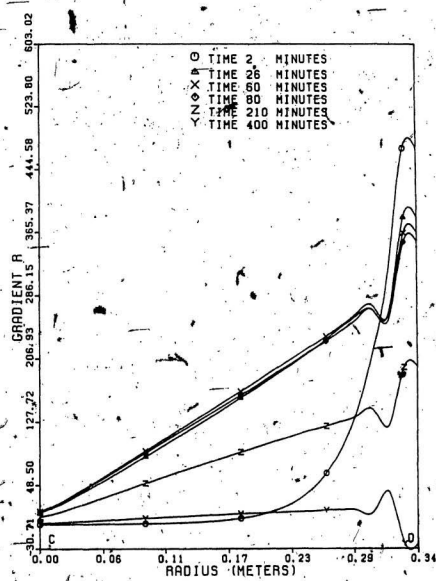


Fig. 2.16: The Variation of the Radial Temperature-Gradient Along the Section CD. ( $T_F = 810^\circ K$ ).

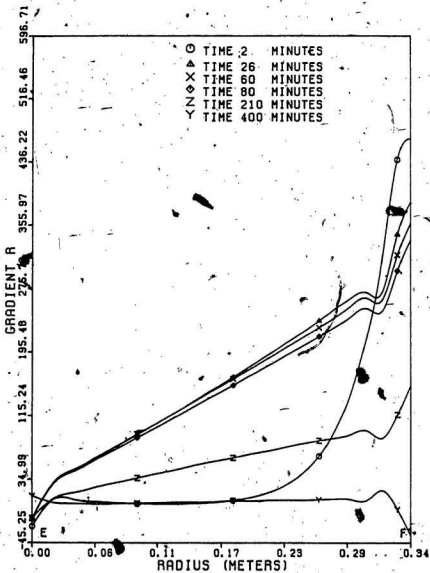


Fig. 2.17: The Variation of the Radial Temperature Gradient Along the Section EF ( $T_p = 810^\circ\text{K}$ ).



gradients decrease. These curves go through a maxima and a minima near the cylindrical surface due to the bi-directional heat-flux. These figures clearly show that one-dimensional heat flow study in ingots would not lead to reliable values of the temperature gradients.

The gradients in the vertical or z direction, along the same sections i.e. AB, CD, EF as discussed earlier, are shown in Figs. 2.18 - 2.20. These gradients have positive values due to the heat flux entering from the top surface. Referring to these figures the temperature gradients are maximum at the time equal to 120 seconds (2 minutes) at the top surface (refer to Fig. 2.20) whereas, at this instant, the points along the line AB are too far away for the heat flux from the top to diffuse through the body. In other words, the fastest response due to the heat flux from the z direction is felt by the top surface. The maximum value of the gradient along the line CD is felt after 4800 seconds (80 minutes); the same effect is experienced along the line AB after 12,600 seconds (210 minutes). These gradient curves show very important aspects of the dynamics of the heat transfer process. In addition, the variations of the gradients along the radial as well as the vertical directions clearly show that one has to use polynomials of higher powers of T to indicate the distribution of the temperature field in the ingot.

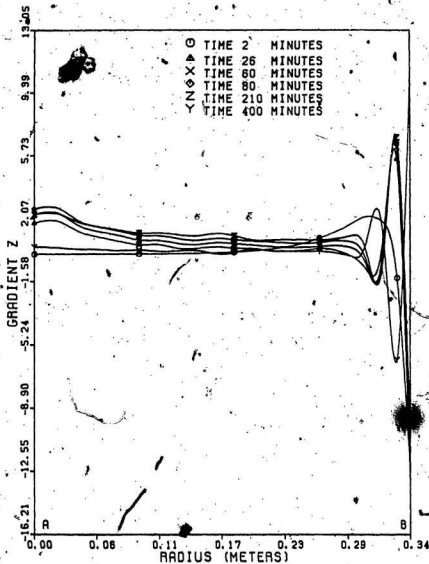


Fig. 2.18: The Variation of the Axial Temperature Gradient Along the Section AB ( $T_p = 810^\circ\text{K}$ ).

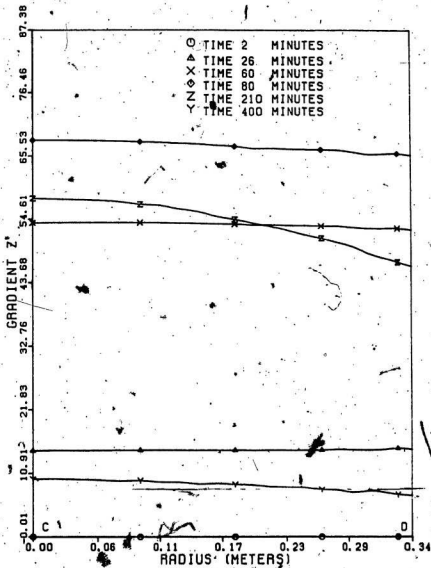


Fig. 2.19: The Variation of the Axial Temperature Gradient Along the Section CD ( $T_0 = 810^\circ\text{K}$ ).

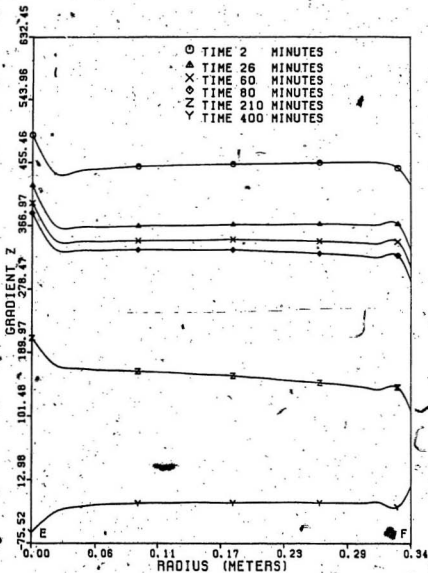


Fig. 2.20: The Variation of the Axial Temperature Gradient Along the section EP ( $T_p=810^\circ\text{K}$ ).

As a point of clarification it should be mentioned here that the temperatures reported were obtained by varying the mesh size until there was no significant change in their values.

## 2.8 CONCLUSIONS

In this chapter, the equations for the transient nonlinear temperature distribution within the ingot due to convective and radiative heat flux from the furnace was obtained using a combination of finite element and finite difference methods. The nonlinearities of this analysis were due to two reasons: the first reason was due to the variation of material properties of the ingot with its temperature and the second reason was the nonlinear boundary conditions due to radiative heat transfer at the surface of the ingot. The resulting nonlinear heat transfer equations of the solid were solved by the iteration, the Newton-Raphson and the nonlinear optimization methods. Based on these studies the following conclusions can be drawn:

1. The optimization methods can be used for solving nonlinear heat transfer problems.
2. The iteration method is very efficient and requires less CPU time for solving nonlinear heat transfer equations compared to the other methods.

3. The axisymmetric analysis of the heat transfer process yields better insight into the temperature distribution within the ingot as compared to the analysis where the heat flux from the axial direction is not considered.
4. The temperature distribution of the ingot along either the radial or the vertical direction is nonlinear.
5. The time  $t^*$  decreases as the heating rate increases.
6. The quantity  $\Delta T_{\max}$  increases as the heating rate increases.
7. The temperature gradients provide very useful information regarding the heat flux from the radial and vertical directions:

## CHAPTER 3

THE THERMOELASTIC STRESS ANALYSIS OF THE INGOT3.1 Introduction

In the previous chapter, the transient temperature distribution within the ingot during heating in a furnace was formulated using the finite element method. The nonlinear transient temperatures at various nodes of the ingot were calculated for different furnace heating rates using the linear finite triangular elements. In this chapter, the axisymmetric thermal stress analysis equations have been obtained using the finite element method. These thermal stresses are due to the nonuniform temperature distribution within the ingot and are dependent upon nodal temperatures. The same axisymmetric triangular finite elements are used in both the thermal and stress analysis since the latter analysis is based on the former one. The mechanical as well as thermal properties have been assumed to vary nonlinearly with the temperature. The thermal and stress distributions of the nodes along the horizontal section AB (refer to Fig. 1.2) are also compared using the two-dimensional finite difference method and the results are then compared. The influence of the linearization and slenderness ratio on the maximum normalized thermal stress energies are also analyzed.

The axisymmetric finite element formulation of the thermal stress analysis is presented in the next section.

### 3.2 The Mathematical Formulation

Principle of virtual displacement can be used in the finite element formulation of the axisymmetric thermal stress analysis [21]. According to this principle, the thermal stress equations of the ingot are obtained by minimization of the potential energy. The potential energy,  $\pi_1$  of the ingot can be expressed as,

$$\pi_1 = \text{strain energy, } (\Lambda) - \text{work done } (W) \quad (3.1)$$

Since, the region of interest is subdivided into a number of linear triangular elements, the above equation can be written as

$$\pi_1 = \sum_{e=1}^{n_1} \pi_1^e \quad (3.2)$$

where

$n_1$  denotes the total number of elements

$\pi_1^e$  denotes the potential energy contribution of the element  $e$

The strain energy,  $\Lambda^e$ , of the element can be written as

$$\Lambda^e = \int_{V^e} \frac{1}{2} (\{\epsilon^e\}^T \{\sigma^e\} - \{\epsilon_0^e\}^T \{\sigma^e\}) dV \quad (3.3)$$



where

$\{\epsilon^e\}$  is the elemental strain vector

$\{\epsilon_0^e\}$  is the elemental initial strain vector

$\{\sigma^e\}$  is the elemental stress vector

Using Hooke's law, the elemental stress and strain vectors are related as

$$\{\sigma^e\} = [D_2^e]\{\epsilon^e\} - [D_2^e]\{\epsilon_0^e\} \quad (3.4)$$

where  $[D_2^e]$  is the material property matrix. It can be expressed as

$$[D_2^e] = \frac{E}{(1+\nu)(1-2\nu)} \begin{bmatrix} 1-\nu & \nu & \nu & 0 \\ \nu & 1-\nu & \nu & 0 \\ \nu & \nu & 1-\nu & 0 \\ 0 & 0 & 0 & \frac{1-2\nu}{2} \end{bmatrix} \quad (3.5)$$

The stress components for the thermal stress analysis are shown in Fig. 3.1. The stress vector for the ingot can be represented as

$$\{\sigma^e\}^T = [\sigma_r^e, \sigma_\theta^e, \sigma_z^e, \tau_{rz}^e] \quad (3.6)$$

Similarly the strain vector, for this case, can be written as

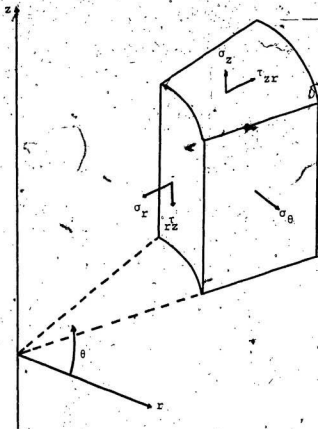


Fig. 3.1: The Elemental Stresses in the Cylindrical Coordinate System.

$$\{\epsilon^e\} = \begin{Bmatrix} \epsilon_r^e \\ \epsilon_\theta^e \\ \epsilon_z^e \\ \gamma_{rz}^e \end{Bmatrix} = \begin{Bmatrix} \frac{\partial u^e}{\partial r} \\ \frac{u^e}{r} \\ \frac{\partial v^e}{\partial z} \\ \frac{\partial u^e}{\partial z} + \frac{\partial v^e}{\partial r} \end{Bmatrix} \quad (3.7)$$

where  $u^e, v^e$  are the displacement components in the  $r, z$  directions respectively.

Using interpolation functions for both  $u^e$  and  $v^e$  as

$$u^e = [N_1^e] \{u^e\} \quad (3.8a)$$

$$v^e = [N_1^e] \{v^e\} \quad (3.8b)$$

Eqn. (3.7) can be rewritten as

$$\{\epsilon^e\} = [B_2^e] \{U^e\} \quad (3.9)$$

where

$$[B_2^e] = \frac{r}{2A^e} \begin{bmatrix} b_1 & 0 & b_j & 0 & b_k & 0 \\ \frac{2A^e N_1^e}{r} & 0 & \frac{2A^e N_j^e}{r} & 0 & \frac{2A^e N_k^e}{r} & 0 \\ 0 & c_r & 0 & c_j & 0 & c_k \\ p_1 & b_1 & c_j & b_j & c_k & b_k \end{bmatrix} \quad (3.10)$$

The expressions of various terms such as  $b_i$ ,  $c_i$ , etc., are given in the Appendix C, and

$$\{U^e\} = \begin{Bmatrix} u_i^e \\ v_i^e \\ u_j^e \\ v_j^e \\ u_k^e \\ v_k^e \end{Bmatrix} \quad (3.11)$$

Similarly, the initial strain vector  $\{\epsilon_0^e\}$  for the element can be written as

$$\{\epsilon_0^e\} = \begin{Bmatrix} \alpha \Delta T_1^e \\ \alpha \Delta T_1^e \\ \alpha \Delta T_1^e \\ 0 \end{Bmatrix} \quad (3.12)$$

where

$\alpha$  denotes the coefficient of thermal expansion

$\Delta T_1^e$  denotes the difference between the initial and the temperature at time  $t$

The work done (W) in this problem is zero. By substituting Eqns. (3.3), (3.4) and (3.9) in Eqn. (3.2), it can be rewritten as

$$\begin{aligned} \pi = \sum_{e=1}^{n_1} \int_{V^e} & \left[ \frac{1}{2} \{U^e\}^T [B_2^e]^T [D_2^e] [B_2^e] \{U^e\} dv \right. \\ & \left. - \{U^e\}^T [B_2^e]^T [D_2^e] \{\epsilon_0^e\} dv + \frac{1}{2} \{\epsilon_0^e\}^T [D_2^e] \{\epsilon_0^e\} \right] dv \end{aligned} \quad (3.13)$$

where  $n_1$  denotes the total number of elements.

To minimize potential energy,  $\pi$ , we differentiate Eqn. (3.13) with respect to the elemental displacement vector  $\{U^e\}$  and set it equal to zero. This can be written as

$$\begin{aligned} \frac{\partial \pi}{\partial \{U^e\}} = \sum_{e=1}^{n_1} & \left[ \int_{V^e} [B_2^e]^T [D_2^e] [B_2^e] dv \{U^e\} \right. \\ & \left. - \int_{V^e} [B_2^e]^T [D_2^e] \{\epsilon_0^e\} dv \right] = 0 \end{aligned} \quad (3.14)$$

The above equation can be expressed as

$$[K^G] \{U^G\} = \{F^G\} \quad (3.15)$$

where

$[K^G]$  refers to the global stiffness matrix

$\{F^G\}$  refers to the global force vector due to thermal loading

The expressions for the elemental stiffness matrix,  $[K^e]$  and the corresponding force vector,  $\{F^e\}$  are written as [21]

$$[K^e] = [B_2^e]^T [D_2^e] [B_2^e] 2\pi \bar{r} A^e \quad (3.16)$$

and

$$\{F^e\} = \frac{\alpha E \Delta T_1^e}{(1-2\nu)} [B_2^e]^T \begin{Bmatrix} 1 \\ 1 \\ 1 \\ 0 \end{Bmatrix} 2\pi \bar{r} A^e \quad (3.17)$$

where  $\bar{r}$  denotes the coordinate in the  $r$  direction of the centroid of the triangular element under consideration. These elemental matrices and vectors,  $[K^e]$  and  $\{F^e\}$ , are assembled to obtain the corresponding global  $[K^G]$  and  $\{F^G\}$  as shown in Eqn. (3.15). Once the global displacement vector is obtained using Eqn. (3.15) then the elemental stress vectors are calculated using the relation [21]

$$\{\sigma^e\} = [D_2^e] [B_2^e] \{u^e\} - [D_2^e] \{\epsilon_0^e\} \quad (3.18)$$

### 3.3 The Failure Theories

The properties of the alloys which can be forged vary very widely. Therefore, an engineer who is planning the heating schedule must consider all the failure theories and then choose the one which applies very closely to the alloy being forged. In [8] it was assumed that failure occurred when the stress exceeded 90 percent of the 0.2 percent yield

stress. As far as the failure analysis is concerned one can use some of the important theories which are [32]: (a) the distortion-energy theory, (b) the maximum normal-stress theory, and (c) the maximum shear-stress theory.

According to the distortion energy theory [33], the failure occurs if

$$\sigma_d = \left[ \frac{1}{2} (\sigma_z - \sigma_r)^2 + \frac{1}{2} (\sigma_r - \sigma_\theta)^2 + \frac{1}{2} (\sigma_\theta - \sigma_z)^2 + 3\tau_{rz}^2 \right]^{1/2} > \sigma_y \quad (3.19)$$

In terms of the principal stresses, Eqn. (3.19) can be rewritten as

$$\sigma_d = \frac{1}{\sqrt{2}} [(\sigma_1 - \sigma_2)^2 + (\sigma_2 - \sigma_3)^2 + (\sigma_3 - \sigma_1)^2]^{1/2} > \sigma_y \quad (3.20)$$

where the principal stresses  $\sigma_1, \sigma_2, \sigma_3$  are obtained as the roots of the cubic equation [11]

$$\sigma^3 - (\sigma_r + \sigma_z + \sigma_\theta) \sigma^2 + (\sigma_r \sigma_z + \sigma_z \sigma_\theta + \sigma_r \sigma_\theta - \tau_{rz}^2) \sigma - (\sigma_r \sigma_\theta \sigma_z - \sigma_\theta \tau_{rz}^2) = 0 \quad (3.2.1)$$

where  $|\sigma_1| > |\sigma_2| > |\sigma_3|$ .

If one uses the normal-stress theory then a material fails when

$$\sigma_n = |\sigma_1| > \sigma_y \quad (3.2.2)$$

Similarly, for the material to fail in accordance with the maximum shear-stress theory, the condition

$$\sigma_s = |\sigma_1 - \sigma_3| > \sigma_y \quad (3.2.3)$$

must be satisfied.

### 3.4 The Three-Dimensional Finite Element Analysis

The diametral cross section of a cylindrical steel ingot, used in this analysis, is shown in Fig. 1.2. This ingot was made of AISI 4140 steel whose thermal and mechanical properties were obtained from [34]. All the properties varied nonlinearly with change in the ingot temperature. The assumed variation of 0.2% yield stress ( $\sigma_y$ ) and Young's modulus (E) of this material are

$$\sigma_y(T) = 4.484144 \times 10^8 (1 - 4.1667 \times 10^{-4}(T-298)) \quad (3.24)$$

$$E(T) = 206482 \times 10^6 (1 - 4.1667 \times 10^{-4}(T-298)) \quad (3.25)$$

where T denotes the average temperature of the element under consideration.

The procedure for calculation of the thermal stresses in the ingot can be outlined as follows:

- (a) First, compute the global temperature vector  $\{T^G\}_t + \frac{\Delta t}{2}$  at time  $t + \frac{\Delta t}{2}$  by solving the nonlinear transient heat transfer equation, Eqn. (2.53).



- (b) Calculate the global force vector  $\{F^G\}$  in Eqn. (3.15) using the temperature vector  $\{T^G\}$  at  $t + \frac{\Delta t}{2}$ .
- (c) Solve Eqn. (3.15) for the unknown displacement vector  $\{U^G\}$ .
- (d) Calculate the elemental stress vector,  $\{\sigma^e\}$  by using the elemental displacement vector  $\{U^e\}$  given in the Eqn. (3.18).

### 3.5 The Verification of the Axisymmetric

#### Finite Element Model

This verification was carried out by assuming a linear temperature profile between the centre and the surface along the section AB. Then, the thermal stresses corresponding to this profile were calculated using the following relations [11]:

$$\sigma_r = \frac{\alpha}{1-\nu} \left( \frac{4}{d^2} \int_0^{d/2} E T r \, dr - \frac{1}{r^2} \int_0^r E T r^2 \, dr \right) \quad (3.26)$$

$$\sigma_\theta = \frac{\alpha}{1-\nu} \left( \frac{4}{d^2} \int_0^{d/2} E T r \, dr + \frac{1}{r^2} \int_0^r E T r \, dr - E T \right) \quad (3.27)$$

$$\sigma_z = \frac{\alpha}{1-\nu} \left( \frac{8}{d^2} \int_0^{d/2} E T r \, dr - E T \right) \quad (3.28)$$

where  $d$  denotes the diameter of the ingot.

Here, the stresses  $\sigma_r$ ,  $\sigma_\theta$  and  $\sigma_z$  calculated using the above relations were the principal stresses in the  $r$ ,  $\theta$  and  $z$  directions respectively. The stresses,  $\sigma_d$ ,  $\sigma_s$  and  $\sigma_n$  were then obtained using the Eqns. 3.19 to 3.23.

The thermal stresses using the finite element model developed in this work, were also calculated corresponding to the same temperature profile. These stress values were found to be the same. In this way, the model developed in this work was verified.

### 3.6 The Comparison of the Axisymmetric

#### Finite Element Analysis With the Finite Difference Analysis

In the studies carried out in [8], the heat flux from the axial direction was neglected. The temperatures and stresses at various nodes along the section AB of the ingot were obtained by using the finite-difference method. In the real practice, when the ingot is heated in the furnace, the heat enters into the ingot from the radial and axial directions. If the heat flux in the axial direction is neglected then all the horizontal sections of the ingot will have essentially the same temperature profile. Therefore, the temperature distribution along the horizontal section AB was calculated using the finite difference equations [6]. For the intermediate nodes (refer to Fig. 3.2) it is

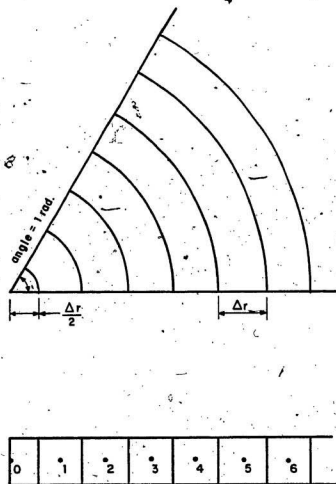


Fig. 3.2: Finite Difference Subdivision of the Cylinder.

$$T_{n,t+\frac{\Delta t}{2}} = T_{n,t-\frac{\Delta t}{2}} + \frac{1}{M} \left[ \frac{2 + \frac{\Delta r}{r}}{2} (T_{n+1,t-\frac{\Delta t}{2}} - T_{n,t-\frac{\Delta t}{2}}) + \frac{2 - \frac{\Delta r}{r}}{2} (T_{n-1,t-\frac{\Delta t}{2}} - T_{n,t-\frac{\Delta t}{2}}) \right] \quad (3.29)$$

For the center node it can be written as

$$T_{0,t+\frac{\Delta t}{2}} = \frac{4}{M} T_{1,t-\frac{\Delta t}{2}} + (1 - \frac{4}{M}) T_{0,t-\frac{\Delta t}{2}} \quad (3.30)$$

For the surface node it is

$$T_{n,t+\frac{\Delta t}{2}} = \frac{8r-4\Delta r}{M(4r-\Delta r)} T_{n-1,t-\frac{\Delta t}{2}} + \frac{8rN}{M(4r-\Delta r)} T_F + (1 - \frac{8rN+8r-4}{M(4r-\Delta r)}) T_{n,t-\frac{\Delta t}{2}} \quad (3.31)$$

where

$n$  denotes the node number

$\Delta r$  denotes the distance between two nodes

$r$  denotes the distance of the node from centre

$M$  denotes the Fourier Modulus ( $\frac{\Delta r^2 \rho c}{K \Delta t}$ )

$N$  denotes the Biot Modulus ( $\frac{h \Delta r}{K}$ )

The heat transfer coefficient,  $h$  was calculated using the relation [13]

$$h = \sigma \varepsilon A_1 \left( \frac{T_F^4 - T_S^4}{T_F - T_S} \right) + 0.5413 \left( \frac{T_F - T_S}{d} \right)^{0.25} \quad (3.32)$$

where

$T_S$  denotes the surface nodal temperature

$d$  is the diameter of the ingot

$A_1$  is the area of the flame surface.

After obtaining the temperatures at various nodes the stress values at each of these nodes were calculated using Eqns. 3.26 to 3.28. Here  $\sigma_x$ ,  $\sigma_\theta$  and  $\sigma_z$  were the three principal stresses because the temperature variations along the vertical axis of the cylinder was neglected.

In the finite element model developed in this work, the temperatures were obtained using Eqn. (2.53), and the stresses were obtained using Eqns. (3.15) and (3.18).

Figs. 3.3 - 3.5 show the temperature as well as the normalized stress ( $\sigma_d$ ,  $\sigma_s$ ,  $\sigma_n$  normalized with respect to  $\sigma_y$ , the yield stress and was denoted as  $\sigma_d$ ,  $\sigma_s$ ,  $\sigma_n$  respectively) variations of the three dimensional finite element and two dimensional finite difference analyses results with time corresponding to the constant furnace temperature at 1000°K. Here, the ingot which was initially at room temperature was charged into the hot furnace. These figures are divided into two sections; the top section shows the normalized stresses whereas the bottom one shows the temperature variations at

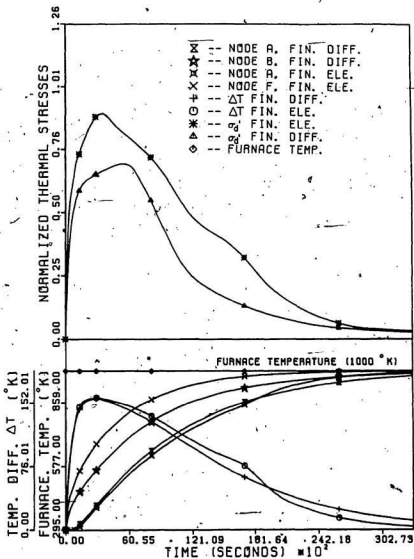


Fig. 3.3: The Comparison of the 2-D Finite Difference and 3-D Finite Element  $\sigma_d$  Results of  $T_p = 1000^{\circ}$ K.

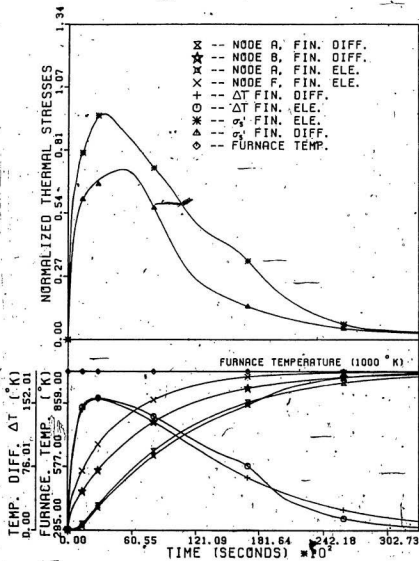


Fig. 3.4: The Comparison of the 2-D Finite Difference and 3-D Finite Element  $\sigma_x$  Results at  $T_F=1000$  K.

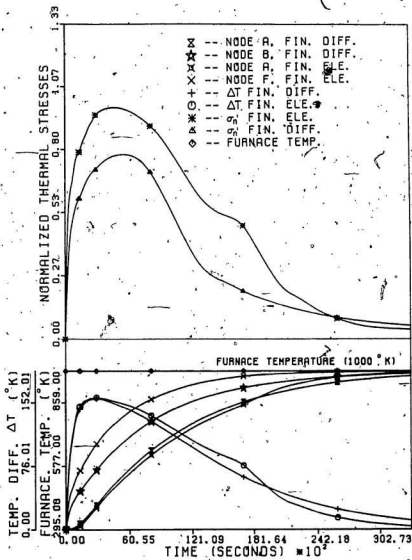



Fig. 3.5: The Comparison of the 2-D Finite Difference and 3-D Finite Element  $\sigma_n$  Results at  $T_F = 1000^\circ\text{K}$ .





various points in the ingot. The corner point F (refer to Fig. 1.2) has the highest temperature within the ingot due to the heat flux both from the axial as well as the radial directions. The temperatures of the nodes A, B and F rise quite rapidly in the beginning but as these temperatures approach the furnace temperature, the slope of each of these curves diminishes. The difference of temperatures between nodes A and B is shown in the lower half of the plots. In these plots  $\Delta T$ , which represents the average temperature gradient along AB, is also shown (the average gradient =  $2\Delta T/d$ ).

It can be clearly seen in these three figures that the normalized stresses based on the two-dimensional finite difference analysis are less than those obtained by the three-dimensional finite element analysis. Thus, the furnace scheduling based on the two-dimensional finite difference analysis would not be safe. In other words, these results show that one has to consider the heat flow from the axial direction also. Another fact which can be observed in these figures is that the peak values of  $\Delta T$  and the normalized stresses occur almost at the same instant of time.

To analyze further the importance of the axial heat flow, the top and bottom flat surfaces were insulated and the temperatures and stresses corresponding to the furnace temperature,  $T_F$  equal to  $1000^\circ\text{K}$  were calculated using the

finite element analysis. The results obtained are shown in Figs. 3.6 - 3.8. It was found that all the horizontal sections such as AB, CB, EF, etc. (refer to Fig. 1.2) had identical temperature profiles. The temperatures and stresses obtained by the three-dimensional finite element analysis are also shown in these figures for the comparison purpose. The three-dimensional stresses are again higher than the two-dimensional stresses in all these figures. However, temperatures of the nodes A and B in both the analyses are the same. This is due to the fact that the points along the section AB are too far away for the heat flux from the top to diffuse through the body.

It is worth mentioning here that the maximum value of the normalized stresses  $\sigma_d'$ ,  $\sigma_s'$  and  $\sigma_n'$  occurred at different nodes during the course of the heating. This is shown in the Table 3.1. It can be seen in this table that in the beginning the maximum stresses  $\sigma_d'$ ,  $\sigma_s'$  and  $\sigma_n'$  occur at the node F which is the right top corner point in the Fig. 1.2. This fact can be observed only in the three-dimensional model because the two-dimensional results are based on zero axial heat flux conditions which correspond to the temperature and stress variations along the section AB which is too far away from the top and bottom faces of the ingot. This section AB is a symmetrical section and there is no axial heat flow on this section.

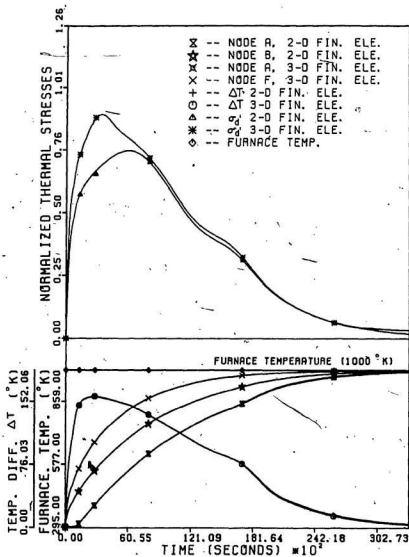


Fig. 3.6: The Comparison of the Two and Three Dimensional Finite Element  $\sigma_z$  Results at  $T_p=1000^\circ\text{K}$ .



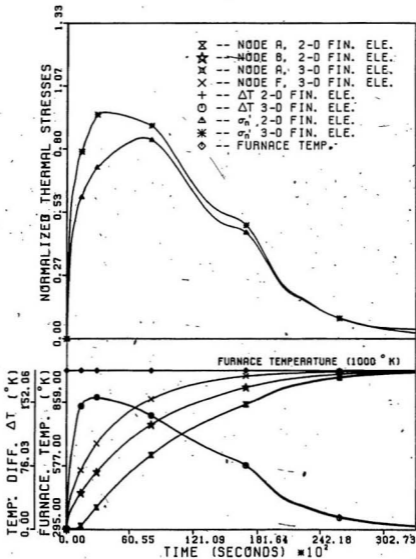


Fig. 3.8: The Comparison of the Two and Three Dimensional Finite Element  $\sigma_n$  Results at  $T_p=1000^\circ\text{K}$ .

Table 3.1 The Absolute Normalized Stresses and Their Locations at Different Instants of the Heating Time ( $T_p = 1000^\circ\text{K}$ )

Time (seconds) $\times 0,0166$	$(\sigma_d')_{\max}$	Node	$(\sigma_n')_{\max}$	Node	$(\sigma_s')_{\max}$	Node
5	0.555	F	0.636	F	0.637	F
30	0.769	F	0.811	F	0.816	F
60	0.889	F	0.933	F	0.939	F
150	0.698	B	0.858	A	0.702	B
270	0.374	B	0.506	A	0.382	B
390	0.104	B	0.142	A	0.107	B
600	0.0313	E	0.0373	Near E	0.0313	E

In Fig. 3.9, the finite element results of  $\sigma_r$ ,  $\sigma_\theta$ ,  $\sigma_z$  along the section AB, at the heating time equal to 7,200 seconds (2 hours) corresponding to the constant furnace temperature at 1000°K, are shown. The radial stress is maximum at the core and very close to zero at the centroid of the surface element. This is because the surface element is free to expand thus no radial stresses are developed at the free surface. On the other hand, the displacement of the points along the axis is zero therefore the stresses are maximum at the axis. The stress components  $\sigma_z$  and  $\sigma_\theta$  are tensile at the core but compressive near the surface. During the heating, the surface region tends to expand in the  $\theta$  and  $z$  directions also. However, the ingot cannot expand freely along these directions, thus the compressive stresses are developed in this region and the corresponding tensile stresses are developed towards the core region. Similar nature of the curves were reported in [8] where the calculations were done using the finite-difference method.

### 3.7 The Linearization of Heat Transfer Equations

In the present investigation, the nonlinearity due to the radiative boundary condition requires an iterative solution of the heat transfer equation, Eqn. (2.53). However, the computations can be significantly reduced if one can use a linearization scheme. One of such schemes [35] can

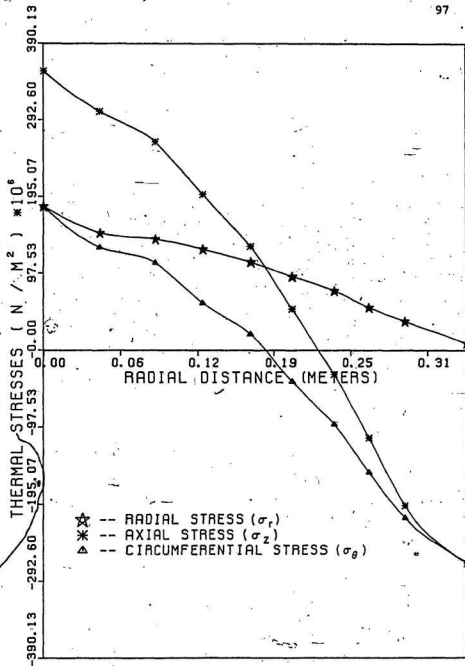


Fig. 3.9: The Distribution of  $\sigma_r$ ,  $\sigma_\theta$  and  $\sigma_z$  Along the Radius of the Ingot, AB, at  $T_p = 1000^\circ\text{K}$  and  $t = 2$  hours.



be used in Eqn. (2.2) where one can expand the term,  $\sigma\epsilon(T^4 - T_F^4)$  as  $\sigma\epsilon(T^2 + T_F^2)(T - T_F)(T + T_F)$ . Then approximating  $T = T_F$ , this term can be written as  $4\sigma\epsilon T_F^3(T - T_F)$ . This is the linearized form because one can replace  $4\sigma\epsilon T_F^3$  by  $h_r$  where  $h_r$  is the equivalent radiative heat transfer coefficient. If such a scheme is used then Eqn. (2.53) can be expressed as a system of linear equations with  $\{F_R^G\} = 0$ .

The stresses and temperatures corresponding to the constant furnace temperature  $T_F$  at 1000°K using this linearization scheme are shown in Figs. 3.10-3.12. In all these figures the linearized temperatures are much higher than the corresponding nonlinearized ones. This is because in the linearization process, the surface temperatures have been replaced by the furnace temperature which is initially much higher, therefore, the corresponding peak normalized stress values are also much higher. Thus, one can see that the linearized model results deviate quite significantly from the actual nonlinearized three-dimensional model results.

### 3.8 The Effect of the Slenderness Ratio

The effect of the slenderness of the ingot on the normalized  $\sigma_d'$  corresponding to the constant furnace temperature at 1000°K is shown in Fig. 3.13. Here, the diameter was kept constant (same value as before) but the height of the ingot was varied. This figure shows that the

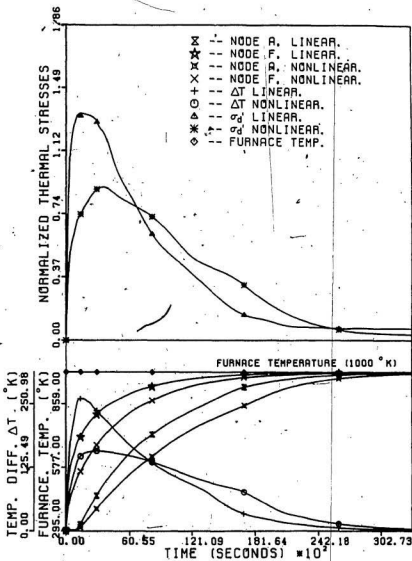


Fig. 3.10: The Comparison of the Linearized and Nonlinearized  $\sigma_d$  Results at  $T_F=1000^{\circ}$ K.

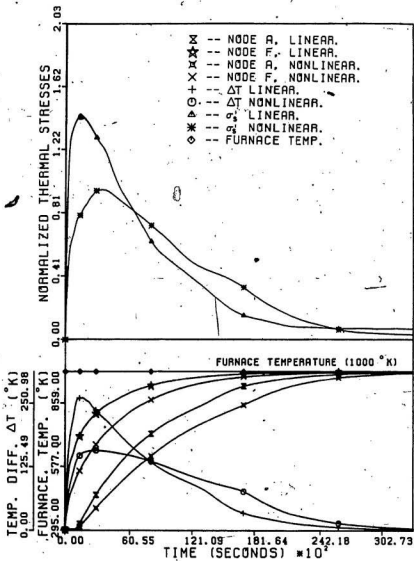


Fig. 3.11: The Comparison of the Linearized and Nonlinearized  $\sigma_x$  Results at  $T_F=1000^\circ\text{K}$ .

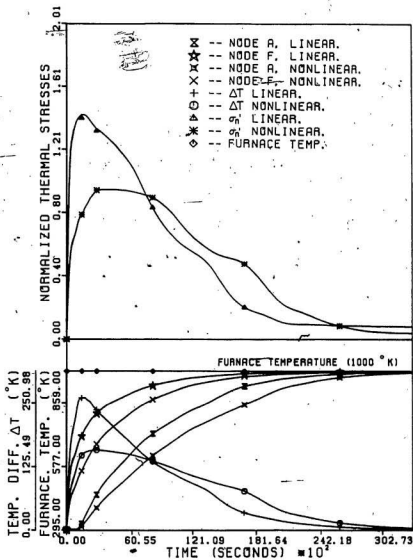


Fig. 3.12: The Comparison of the Linearized and Nonlinearized  $\sigma_n$  Results at  $T_p=1000^\circ\text{K}$ .

peak normalized stress increases as the height of the ingot is increased. Thus, a very slender ingot would not be very desirable because this would lead to higher value of the peak normalized stress for given furnace conditions. Similar results were observed when  $\sigma_n'$  or  $\sigma_s'$  were used in place of  $\sigma_d'$ .

### 3.9. Conclusions

In this chapter, a mathematical model using the finite element analysis for the axisymmetric stress distribution within the ingot has been established. The variable material properties and the radiative boundary conditions required a nonlinear thermal analysis of this problem. After obtaining the temperature distribution of the ingot, the corresponding thermally induced stresses were calculated using the linear-elasticity theory. The stress and temperature distributions for the comparison purpose were also obtained using the two-dimensional finite difference as well as finite element models. The effect of linearization of the nonlinear heat transfer equation and slenderness ratio of the ingot on the normalized thermal stresses  $\sigma_d'$ ,  $\sigma_s'$ ,  $\sigma_n'$  were also studied. Based on this investigation the following conclusions can be drawn:

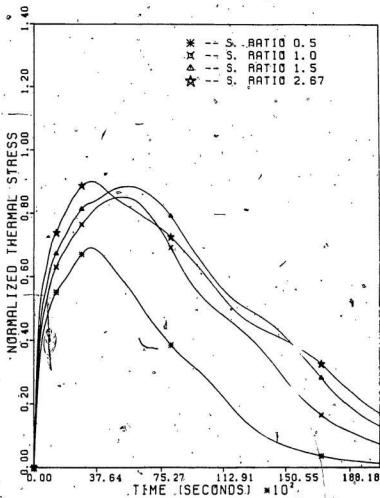


Fig. 3.13: The Effect of the Slenderness Ratio on  $\sigma_d$  values.

1. The three-dimensional finite element analysis yields higher values of the normalized stresses as compared to the two-dimensional finite difference and finite element analyses. The three-dimensional analysis results are safer to use.
2. The two-dimensional model cannot always predict the exact location of the maximum stresses in the ingot..
3. The maximum normalized thermal stresses,  $\sigma_d'$ ,  $\sigma_b'$ ,  $\sigma_n'$  occur at the top corner node F in the beginning.
4. The linearization of the radiative boundary conditions yield unreliable results because the peak normalized stresses are much higher than the nonlinearized results.
5. The peak normalized stresses increase as the slenderness ratio of the ingot is increased.

## CHAPTER 4

THE OPTIMAL HEATING SCHEDULE OF THE INGOTS4.1 Introduction

The thermal stress distribution of the ingot using axisymmetric finite element analysis was presented in the previous chapter. There are many industrial processes in which a close control on the temperature of the material during the heating is required. Such a situation arises in the glass industry, for example, where in the final processing stage the entire solid body must be brought to a uniform temperature to prevent unwanted inhomogeneities in the final product [14]. In iron and steel industry also, during heating of ingots before rolling, it is important to heat the metal rapidly with sufficient uniformity. The productive capacity of the furnace is increased by the rapid heating of the metal, at the same time uniformly heated ingots ensure less residual stresses. While heating the ingots, care should be taken so that the maximum solid temperature does not exceed the finishing temperature and the thermal stresses developed in the ingot should not cause failure of the material. If the temperature at any point in the ingot exceeds the maximum value, the problem of burning or oxidation can occur. Thus, this operation requires a very



close control on the solid temperatures. In this chapter, the thermal and stress distributions are calculated for various feasible furnace temperature paths. The objective of the problem is to obtain the furnace heating path so that one can heat the ingot to the finishing temperature in the minimum time considering thermal failure of the material. The optimization methods such as dynamic programming, multi-variable optimization, etc. are discussed. After considering various alternatives the single parameter nonlinear optimization method is chosen as the optimization method and the optimum furnace paths are obtained for different stress energy criteria. All the material properties, both mechanical and thermal are varied with the ingot temperature. Two types of constraints are used in this analysis: the first one is that the maximum allowed stresses should not exceed 90% of the yield stress (a safety factor of 10%) and the second one is that the temperatures of any of the points within the ingot should not exceed the finishing temperature (1225°C). The first constraint is due to the failure theory of the material and the second one is to avoid oxidation or burning of the alloy.

The temperature and thermal stress calculations for various feasible constant and linear slope furnace paths are presented in the next section.

## 4.2 The Furnace Temperature Paths and the Thermal Stresses

### 4.2.1 Discussion on the Various Furnace Temperature Paths

Before attempting to obtain the optimal furnace path one has to have a very clear idea of the influence of the heating cycle on the the maximum thermal stresses developed within ingot. With this in mind, several constant furnace temperature paths and constant slope paths should be chosen and the corresponding thermal stresses calculated. For obtaining the optimal furnace path, the furnace temperature at the time,  $t=0$ , should be as high as possible, at the same time the maximum thermal stresses developed in the ingot corresponding to the high initial furnace temperature should be less than yield stress of the material. The different furnace paths should give fairly good idea about the optimum furnace path. In order to apply the various failure theories, the absolute maximum values of the stresses,  $\sigma_d$ ,  $\sigma_s$  and  $\sigma_n$ , can be normalized with respect to the yield stress,  $\sigma_y$  and denoted as  $\sigma_d'$ ,  $\sigma_s'$  and  $\sigma_n'$  respectively. The stress calculations involve obtaining the vectors  $\{U^G\}$  and  $\{\sigma^e\}$  using Eqns. (3.15) and (3.18) respectively and then  $\sigma_d'$ ,  $\sigma_n'$ ,  $\sigma_s'$  are calculated from  $\{\sigma^e\}$ .

### 4.2.2 The Constant Furnace Temperature Heating

Fig. 4.1 shows the variation of the normalized stresses and nodal temperatures as a function of the heating

time corresponding to the constant furnace temperature  $T_F$  at  $500^\circ\text{K}$ . These figures are divided into two parts. In the lower half of this figure, the variation of the furnace temperature, the difference of the surface (node A) and core temperatures (node B),  $\Delta T$ , and the temperature of some of the nodes A, B and F (refer to Fig. 1.2) are shown. The upper half of this figure shows the variation of the normalized stresses,  $\sigma_d'$ ,  $\sigma_s'$  and  $\sigma_n'$  with time. The magnitude of these normalized stresses are very small. It is evident from this figure that the maximum of the normalized stresses occurs at a time close to the maximum of the temperature difference  $\Delta T$ . This figure also shows that the maximum of  $\sigma_d'$  is always less than maximum of  $\sigma_s'$  and  $\sigma_n'$ .

The variations of the normalized stresses,  $\sigma_d'$ ,  $\sigma_s'$  and  $\sigma_n'$  and the nodal temperatures corresponding to the constant furnace temperatures of  $800^\circ\text{K}$  and  $1100^\circ\text{K}$  are shown in Figs. 4.2 and 4.3 respectively. The nature of these curves resembles the previous figure, i.e., Fig. 4.1. The magnitude of all the normalized stresses in Fig. 4.2 are higher as compared to the stresses in Fig. 4.1. In Fig. 4.3 all the peak normalized stresses exceeded one. From this, one can infer that the ingot cannot be heated at a constant furnace temperature,  $1100^\circ\text{K}$  without causing thermal cracking of the material.

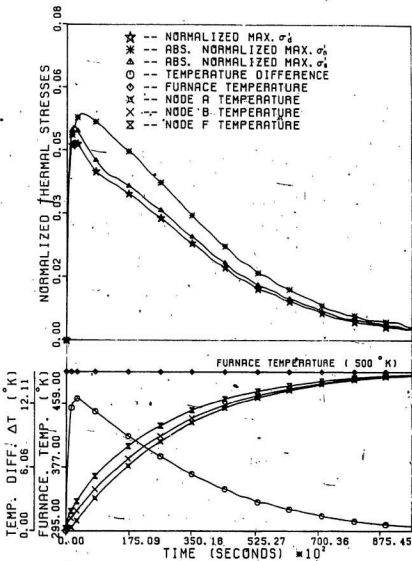


Fig. 4.1: The Variation of the Normalized Stresses and Temp. as a Function of Time Corresponding to  $T_p = 500^\circ\text{K}$ .

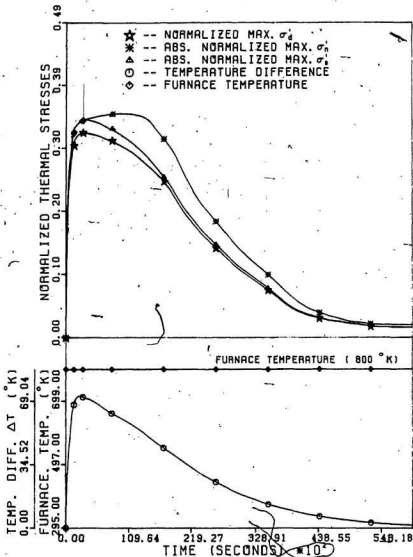


Fig. 4.2: The Variation of the Normalized Stresses and Temp. as a Function of Time Corresponding to  $T_p = 800^{\circ}$ K.

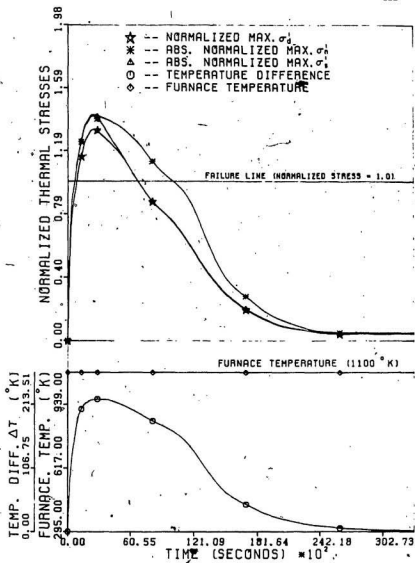


Fig. 4.3: The Variation of the Normalized Stresses and Temp. as a Function of Time Corresponding to  $T_p = 1100^{\circ}$ K.

In Figs. 4.1 - 4.3, the temperature difference  $\Delta T$ , is zero when the ingot is at room temperature and it approaches zero when the ingot reaches steady state temperature. The peak normalized stresses occur when  $\Delta T$  is close to the maximum, which indicates that the maximum stresses are directly related to the average gradient along the line AB (refer to Fig. 1.2) and not to the local values of the gradients along  $r$  or  $z$  directions. For example, when the ingot is charged into the furnace the local values of the gradients near the point B are quite high but the stresses do not reach the peak value at that instant of time.

#### 4.2.3 The Variable Furnace Temperature Heating

To control the peak normalized stresses,  $\sigma_d'$ ,  $\sigma_s'$  and  $\sigma_n'$  the furnace temperature paths were varied with different slopes. Figs. 4.4 to 4.6 show the final furnace temperature equal to 800°K, whereas in the Figs. 4.7 to 4.9 the final furnace temperature is 1100°K. The time required to reach the final constant temperature in Figs. 4.4 and 4.7 is 21,600 seconds (6 hours); it is 14,400 seconds (4 hours) in Figs. 4.5 and 4.8, and 7,200 seconds (2 hours) in Figs. 4.6 and 4.9. In all these figures, the peak values of the normalized stresses as well as the temperature difference  $\Delta T$ , occur at the same instant of time. In Figs. 4.4 to 4.9, the higher is

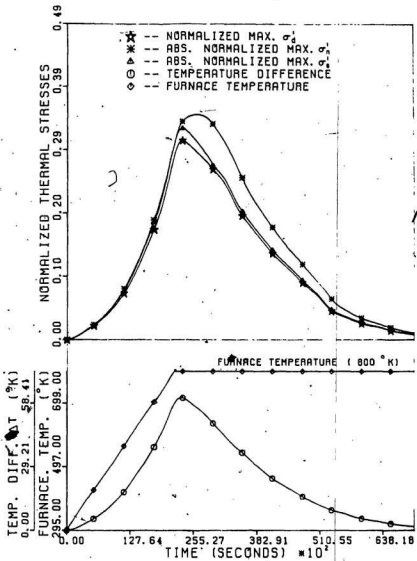


Fig. 4.4: The Variation of the Normalized Stresses and  $\Delta T$  as a Function of Time Corresponding to the Furnace Heating Rate of  $0.023^\circ\text{K}/\text{sec}$ , and Final  $T_F=800^\circ\text{K}$ .



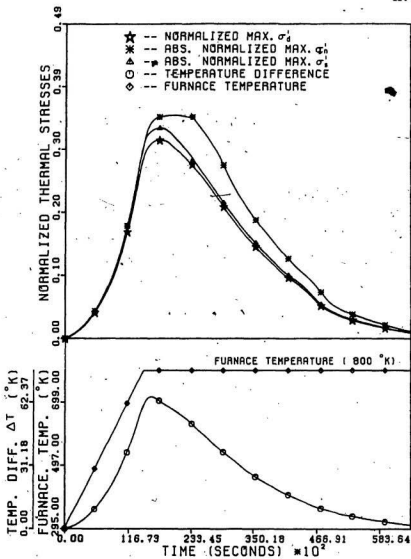


Fig. 4.5: The Variation of the Normalized Stresses and  $\Delta T$  as a Function of Time Corresponding to the Furnace Heating Rate of  $0.035^{\circ}\text{K}/\text{sec}$  and Final  $T_p=800^{\circ}\text{K}$

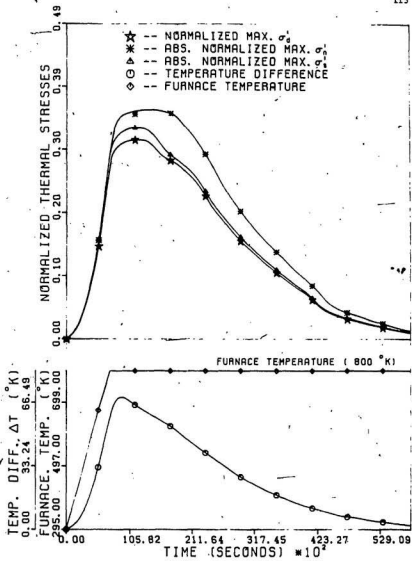


Fig. 4.6: The Variation of the Normalized Stresses and  $\Delta T$  as a Function of Time Corresponding to the Furnace Heating Rate of  $0.070^{\circ}$ K/sec and Final  $T=800^{\circ}$ K.

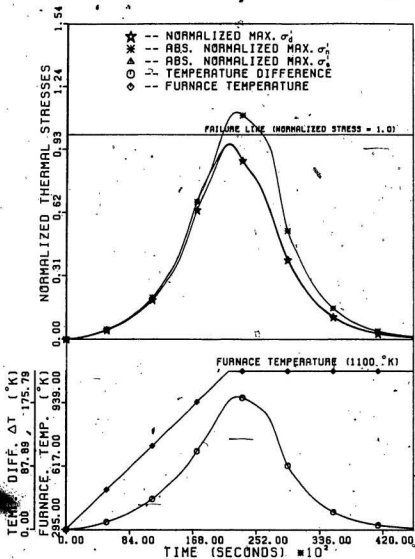


Fig. 4.7: The Variation of the Normalized Stresses and  $\Delta T$  as a Function of Time Corresponding to the Furnace Heating Rate of  $0.037^{\circ}\text{K}/\text{sec}$  and Final  $T_p = 1100^{\circ}\text{K}$ .

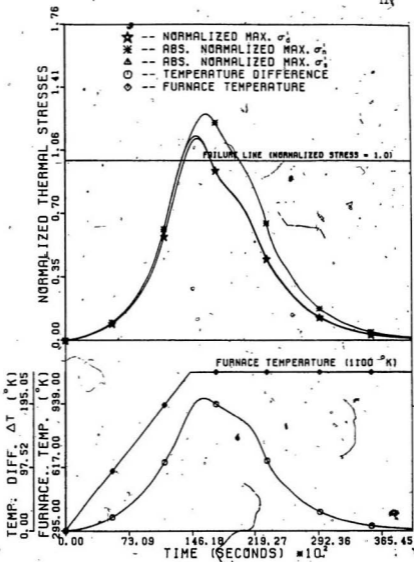


Fig. 4.8: The Variation of the Normalized Stresses and  $\Delta T$  as a Function of Time Corresponding to the Furnace Heating Rate of 0.056°K/sec and Final  $T_p = 1100^\circ K$ .

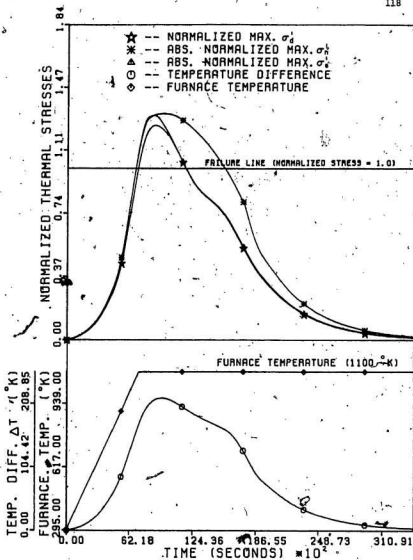


Fig. 4.9: The variation of the Normalized Stresses and  $\Delta T$  as a Function of Time Corresponding to the Furnace Heating Rate of 0.112 $^{\circ}$ K/sec and Final  $T_F=1100^{\circ}$ K.

the slope of the furnace temperature path, the higher are the peak normalized stresses. However, these stresses do not exceed one in Figs. 4.4 to 4.6 where the final temperature is 800°K; they exceed one in the Figs. 4.7 to 4.9 where the final furnace temperature is 1100°K. The maximum of  $\sigma_n$  is always greater than the maximum of  $\sigma_d$  and  $\sigma_s$  respectively.

Thus, it is clear that to heat the ingot to 1498°K one can start at the furnace temperature above 800°K but below 1100°K so that normalized stresses,  $\sigma_d$ ,  $\sigma_s$  and  $\sigma_n$  do not exceed one. Secondly, as the slope of the straight line furnace paths is increased the occurrence of the peak stress is shifted towards the left i.e. it occurs sooner. For example, for the final furnace temperature of 800°K, there are four plots which are Figs. 4.2, 4.4, 4.5 and 4.6. Fig. 4.2 can be considered as having slope equal to infinity (the furnace temperature  $T_f$  jumps from the room temperature to 800°K instantly). The shift of the maxima to the left can be seen by comparing the slopes of these figures. The starting temperature of the optimal furnace path was guessed with these facts in mind.

### 4.3 The Optimal Heating Schedule

#### 4.3.1 The Description of the Heating Cycle of the Ingot

In the previous section, the stress as well as the temperature distributions within the ingot were obtained for

constant and linear slope furnace temperature paths. The essential features of all these studies is shown in Fig. 4.10. In this figure, the stresses build up to a peak value in the beginning and then decrease. The furnace temperature  $T_F$  is always higher than the maximum ingot temperature,  $T_S$ , until  $T_S$  reaches the finishing temperature. After that the  $T_F$  is maintained at the finishing temperature so that the core temperature also reaches finishing temperature later on. Here, the total processing time has been divided into two periods. The first period is called the heating period [1] and the second one is called the soaking period. Fig. 4.11 shows the variation of the ingot temperature where  $T_F$  is equal to infinity between  $t = 0$ , and  $t = t^+$ , and at the time  $t^+$ ,  $T_S$  reaches the finishing temperature. At this instant,  $T_F$  is lowered down from infinity to the finishing temperature, and then the soaking period starts. According to the bang-bang control theory [36],  $t^+$  would be the minimum processing time because the control variable  $T_F$  has been raised to infinity at  $t = 0$  and maintained at infinity until the state variable, the maximum solid temperature  $T_S$ , reaches the finishing temperature; and at this instant of time  $T_F$  is brought down to the finishing temperature. But, we cannot process the material in this time  $t^+$  because of two reasons: the first reason is that the

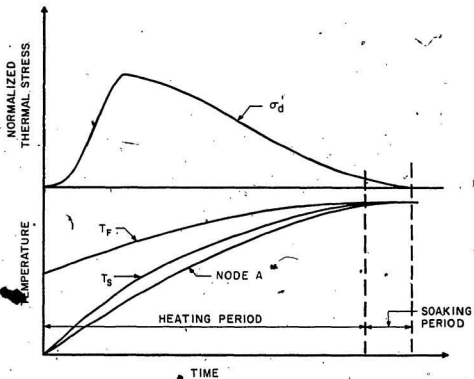


Fig. 4.10: The Stress and Temperature Variations in the Ingot.



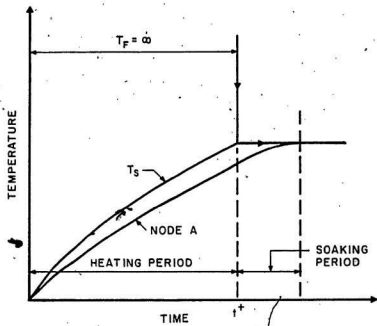


Fig. 4.11: The Minimum Heating Time of the Ingot.

furnace cannot be maintained at infinity and secondly, the thermal stresses would exceed the allowable limit. Therefore, the minimum processing time would be obtained if we follow a path for  $T_p$  such that the normalized stress is equal to one throughout the heating period. The soaking period depends upon the material properties. The variation of the normalized stress, the ingot temperatures, and the optimal  $T_p$  path are shown in Fig. 4.12. In this figure, the normalized stress is equal to one although the heating period and then it decreases in the soaking period when the maximum difference in the temperature within the solid decreases. However, one should always use a safety factor, say 10% of  $\sigma_y$ , while computing the normalized stresses as constraints. In other words, one should not let these stresses exceed  $0.9 \sigma_y$  at any time during the heating cycle.

This factor can vary depending upon the control of the furnace temperature. If the furnace temperature cannot be very closely controlled then higher safety factors should be used. It should be borne in mind that the lower the safety factor, the higher is the utilization of the elastic range of the material and therefore shorter will be the optimal heating time.

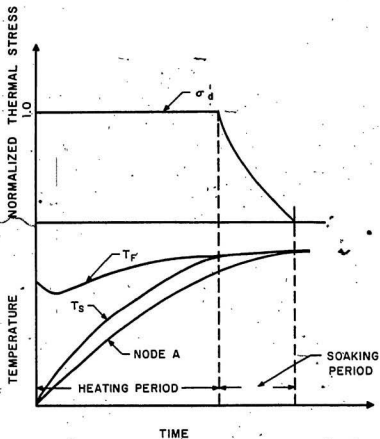


Fig. 4.12: The Constrained Minimum Heating Time of the Ingot.

#### 4.3.2 The Analysis of the Various Methods of Obtaining the Optimal Furnace Temperature Path

The optimum furnace temperature path of the ingot can be obtained in different ways. One of the methods of solving this problem is by using the dynamic programming [27]. This method can be used for obtaining the optimum furnace path by defining the entire path as an initial value multistage problem which is shown in Fig. 4.13. Here,  $\{X_n\}$ ,  $\{X_{n-1}\}$ , ...,  $\{X_i\}$ , ...,  $\{X_1\}$  denote the control variables at stages  $n$ ,  $n-1$ , ...,  $i$ , ..., 1 respectively;  $\{S\}$  denotes the state variables (global nodal temperature vector of the ingot). Here the furnace temperature  $T_p$  is the single design or control variable and is denoted as  $X$ . The vector  $\{S_{n+1}\}$  denotes the global nodal temperatures at  $t=0$ , which are known.  $R_n$ ,  $R_{n-1}$ , ...,  $R_i$ , ...,  $R_1$  denote the return functions at stages  $n$ ,  $n-1$ , ...,  $i$ , ..., 1 respectively. They represent the objective function to be minimized in each stage and can be denoted for the stage  $i$  for the present problem as

$$R_i(X_i, \{S_{i+1}\}) = 0.9 - (\sigma_d')_{\max} \quad (4.1)$$

Therefore, our objective is to minimize the objective function  $f$ , which is the sum of all individual stage returns. Thus one can write

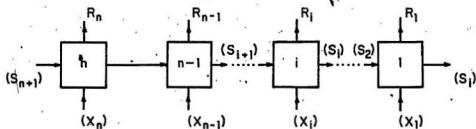


Fig. 4.13: The Initial Value Multistage Decision Problem.

$$\begin{aligned} \text{minimize } f = & R_n(X_n, \{S_{n+1}\}) + R_{n-1}(X_{n-1}, \{S_n\}) \\ & + \dots + R_1(X_1, \{S_2\}) \end{aligned} \quad (4.2)$$

This multistage optimization can be used for finding the optimum furnace path during the heating period only (there is no minimization in the soaking period). The number of stages,  $n$ , in this problem is also variable. The final stage of this problem is the one in which at least one of the output state variables reaches the finishing temperature of the ingot.

The minimization of the objective function,  $f$ , can be done as follows:

First, consider the first subproblem by starting at the final stage,  $i=1$ . The design variable  $X_1$  must be selected such that  $R_1(X_1, \{S_2\})$  is an optimum for the input vector  $\{S_2\}$ . The optimum of the objective function at the stage  $i=1$  can be denoted as

$$f_1^*(\{S_2\}) = \text{opt}_{X_1} [R_1(X_1, \{S_2\})] \quad (4.3)$$

Once the input state vector  $\{S_2\}$  is known, the optimal values of  $R_1$ ,  $X_1$ , and  $\{S_1\}$  can be calculated by performing single parameter optimization at that stage. But, the vector  $\{S_2\}$  is not known at this time. In general, optimization can be carried out for possible values of  $\{S_2\}$

and the corresponding optimal  $\{S_1\}$ ,  $X_1$  and  $R_1$  values are stored.

Next, consider the second subproblem by grouping the last two stages. Then the objective function to be minimized in this case can be written as

$$f_2(\{S_3\}) = R_2(X_2, \{S_3\}) + R_1(X_1, \{S_2\}) \quad (4.4)$$

The objective function is dependent upon the design variables  $X_2$  as well as  $X_1$ . Again, the input state vector  $\{S_3\}$  is not known. For various possible values of  $\{S_3\}$ , the above function can be minimized. In this minimization procedure, if any of the calculated  $\{S_2\}$  vectors matches with the previous assumed  $\{S_2\}$  vector, then the optimal values of  $X_1$ ,  $R_1$  and  $\{S_1\}$  corresponding to that vector are used in these calculations thereby avoiding repetitive computations. If  $f_2^*$  denotes the optimum objective value then it can be written as:

$$f_2^* \{S_3\} = \text{opt}_{X_1, X_2} [R_2(X_2, \{S_3\}) + R_1(X_1, \{S_2\})] \quad (4.5)$$

Extending the same logic, the optimum objective function at the stage  $n$  can be written as

$$f_n^* (\{S_{n+1}\}) = \text{opt}_{X_1, X_2, \dots, X_n} [R_n(X_n, \{S_{n+1}\}) + \dots + R_1(X_1, \{S_2\})] \quad (4.6)$$

The number of computations involved for minimizing the above objective function are quite large. These computations increase drastically with the increase in the number of stages and the number of elements in the state vector. In the present problem, the vector  $[S]$  contains 150 elements. Therefore, using the dynamic programming would be quite impractical in the present investigation.

The second method can be understood from Fig. 4.14. In this figure, along path 1, the  $T_F(t)$  is represented by, selecting five temperatures which are represented by  $(T_F)_1$ ,  $(T_F)_2$ , etc. By selecting a path, the state variables (the nodal temperatures) and  $\sigma_d$  are calculated. In these computations, one would need to know the furnace temperature value between say  $(T_F)_1$  and  $(T_F)_2$ . These values can be obtained using any interpolation method such as the cubic spline interpolation. If none of the constraints is violated then the time required for the surface temperature to reach the final specified temperature is recorded and the corresponding path is considered as a feasible path. In this way, several feasible paths can be tried out and the feasible path which requires the minimum time is selected as the optimal path. As a point of clarification it should be mentioned here that the process of selection of the values of  $(T_F)_i$ ,  $i = 1, \dots, 6$ , is done by the multivariable optimization method where these are considered as design



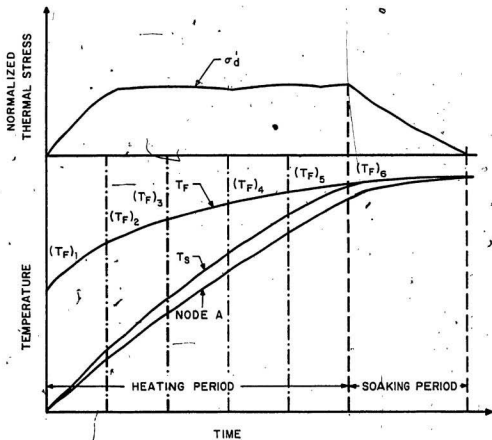


Fig. 4.14 One of the Feasible Paths in the Multivariable Optimization.

variables. These variables are allowed to vary within certain limits. Greater accuracy in the optimal path selection can be achieved if  $i$  is allowed to take a large value i.e. the design variables are selected at finer intervals of time. Even in this method, large CPU times are required due to the multivariable optimization.

The third method, which is a single variable optimization method and which requires significantly less CPU time, was briefly explained in Section 4.3.1. In this method, the furnace temperature  $T_F$  at a given time increment is allowed to vary using single variable optimization method so that the function  $U$  in Eqn. (4.1) is minimum. If one progresses this way until the final specified temperature is reached then the time taken to reach the final temperature would be the minimum time.

#### 4.3.3 The Single Variable Optimization Method

Thus, the minimization, as stated earlier, can be written as

$$\text{Minimize } U = 0.9 - (\sigma'_d)_{\max} \quad (4.1)$$

subject to the maximum temperature constraint

$$T_s < 1498^\circ\text{K} \quad (4.2)$$

In Eqn. (4.1),  $U$  is a function of  $T_F$  because  $(\sigma'_d)_{\max}$  is a function of  $T_F$ . The optimization for each time step was

carried out using the Davidon-Fletcher-Powell method [27] where  $T_F$  was the single variable. The details about this optimization technique have already been discussed in Chapter 2. The optimization was carried out until  $T_S$  attained the final hot working temperature which was 1498°K. After this, the  $T_S$  and  $T_F$  were maintained equal to 1498°K until core temperature became equal to  $T_F$  or  $T_S$ .

The results obtained for the AISI 4140 ingot are shown in Figs. 4.15-4.17 where  $\sigma_d'$ ,  $\sigma_s'$  and  $\sigma_n'$  are the failure criteria respectively. In all these figures, the  $T_F$  starts at a reasonably high value, decreases for sometime, and then increases. When the  $T_S$  reaches the finishing temperature then  $T_F$  is maintained equal to  $T_S$  because the second type of constraint becomes active i.e. the temperatures of the solid should not exceed the finishing temperature. Along this optimal furnace temperature path both types of constraints (maximum thermal stresses and maximum  $T_S$ ) have been satisfied.

If one encounters a situation where the decrease (it happens in the early part of the heating period) in the furnace temperature cannot be controlled very easily then the optimal heating schedule can be slightly modified and the results, due to the modification, are shown in Figs. 4.18 - 4.20. In this modification scheme,  $\sigma_d'$  etc. are not equal to 0.90 in the beginning; it takes a very small time for the

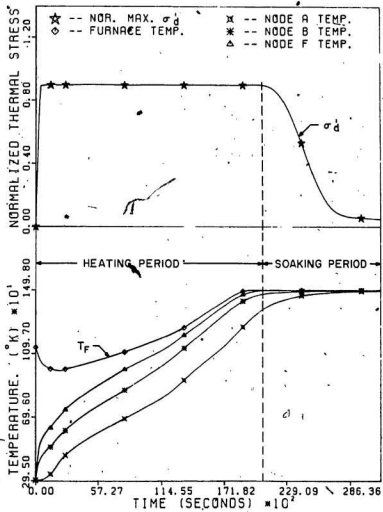


Fig. 4.15 The Optimal Furnace Heating Path Considering  $\sigma_d$  as the Failure Criteria.

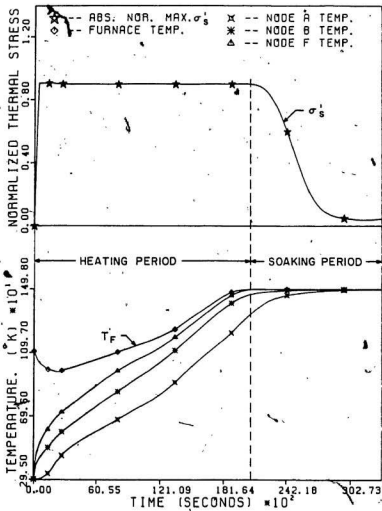


Fig. 4.16: The Optimal Furnace Heating Path Considering  $\sigma'_s$  as the Failure Criteria.

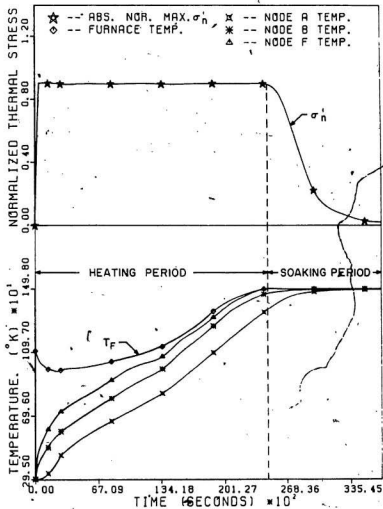


Fig. 4.17: The Optimal Furnace Heating Path Considering  $\sigma_n$  as the Failure Criteria.

stresses to build up to  $0.9 \sigma_y$  but, the furnace temperature  $T_F$  has positive slope all along. The optimal heating time in the second scheme is slightly higher than the first one in all the three cases.

#### 4.4 Conclusions

In this chapter, the solid temperature distributions as a function of furnace temperature variations were obtained and the corresponding thermal stresses were calculated. Various feasible furnace temperature paths were analyzed considering the elastic range for the thermal stresses and maximum specified temperature in the solid, as the constraints. The method for obtaining the optimal path was chosen from the three possible methods based on minimum CPU time, as the criteria. The optimal heating schedule was obtained by maximizing the utilization of the elastic range of the material. Based on this study the following conclusions can be drawn:

1. The peak normalized stresses occur close to the peak value of the temperature  $\Delta T$  when the furnace temperature is held constant.
2. The maximum stresses occur when the maximum average temperature gradients occur.

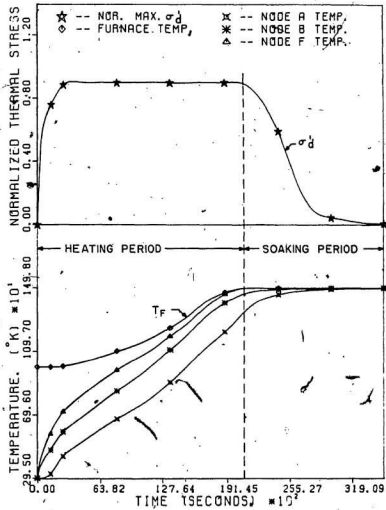


Fig. 4.18: The Optimal Positive Slope Furnace Heating Path Considering  $\sigma_d$  as the Failure Criteria.



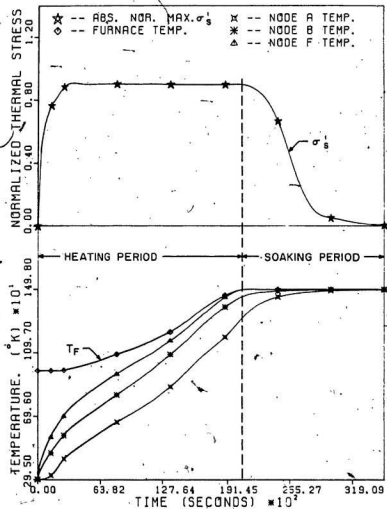


Fig. 4.19: The Optimal Positive Slope Furnace Heating Path Considering  $\sigma_s$  as the Failure Criteria.

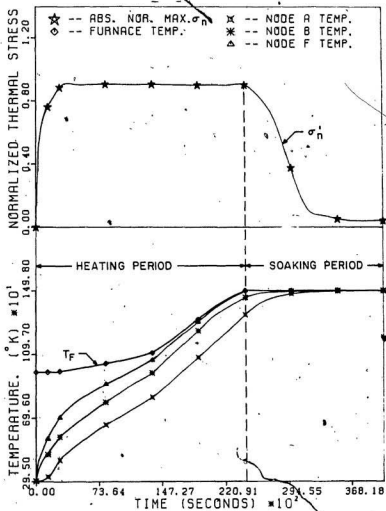


Fig. 4.20: The Optimal Positive Slope Furnace Heating Path Considering  $\sigma_n$  as the Failure Criteria.

3. The higher is the constant furnace temperature the higher are the thermally induced maximum failure theory stresses ( $\sigma_d$ ,  $\sigma_s$  and  $\sigma_n$ ).
4. The occurrence of the peak stresses ( $\sigma_d$ ,  $\sigma_s$  and  $\sigma_n$ ) can be delayed by decreasing the slope of the furnace heating paths.
5. The distortion energy stress  $\sigma_d$  is less than  $\sigma_n$  at any instant of time.
6. The optimal furnace heating path (minimum time path) can be obtained by maintaining the maximum normalized stresses equal to one throughout the heating period.
7. The single variable optimization method, which maximizes utilization of the elastic range of the material during heating is the best method for obtaining the optimal heating schedule of the ingot.

## CHAPTER 5

CONCLUSIONS AND RECOMMENDATIONS5.1 A Brief Discussion

The work presented in this thesis consisted of the mathematical formulation of the equations which describe the heat transfer process within the ingot and the corresponding thermal stresses. These temperature distributions and stresses were then used to obtain the optimal furnace temperature path. The constraints used in obtaining the optimal path were: (a) the various failure theories of the material, and (b) the maximum temperature at any point in the ingot.

The finite element technique was used to formulate the mathematical model of the unsteady nonlinear heat transfer analysis of the ingot. The thermal stresses of the ingot were calculated using the axisymmetric finite element model. Since the thermal stresses are based on the heat transfer analysis, both the analyses were carried out using the same linear finite triangular elements.

~~The temperature distributions of the ingot were~~ studied by varying various furnace heating rates. The temperatures and the stresses using the two-dimensional and three-dimensional models were obtained and it was found that

the three dimensional formulation yielded safer results. Then, the heat transfer equations were linearized and its influence on the thermal stresses were studied. The effect of height of the ingot on these distributions were also studied. Finally, the optimal furnace temperature path for heating the ingot to the finishing temperature in the minimum time without causing thermal failure was obtained by the single variable nonlinear programming technique. This method was based on the maximum utilization of the elastic range of the material during the heating period of the ingot:

## 5.2 Conclusions

Based on the present investigation the following conclusions can be drawn:

1. The heat transfer process within the ingot can be studied by deriving the equations using the nonlinear finite element analysis.
2. The optimization methods can be used for solving the nonlinear heat transfer problems.
3. The iterative method is very efficient and requires less CPU time for solving the nonlinear heat transfer equations compared to the other methods.
4. The axisymmetric analysis of the heat transfer process yields better insight into the temperature distribution

- within the ingot as compared to the analysis where the heat flux from the axial direction is not considered.
5. The temperature distribution along either the radial or the vertical direction is nonlinear.
  6. The time  $t^*$  decreases as the heating rate increases.
  7. The quantity  $\Delta T_{\max}$  increases as the heating rate increases.
  8. The temperature gradients provide very useful information regarding the heat flux from the radial and vertical directions.
  9. The three-dimensional finite-element analysis yields higher values of the normalized stresses as compared to the two-dimensional finite-difference and finite-element analyses. The three-dimensional analysis results are safer to use.
  10. The two-dimensional model cannot always predict the exact location of the maximum stresses in the ingot.
  11. The maximum normalized thermal stresses  $\sigma_d$ ,  $\sigma_s$ ,  $\sigma_n$  occur at the top corner node F in the beginning.
  12. The linearization of the radiative boundary conditions yields unreliable results because the peak stresses are much higher than the nonlinearized results.
  13. The peak normalized stresses increase as the slenderness ratio of the ingot is increased.

14. The peak normalized stresses occur close to the peak value of the temperature difference  $\Delta T$  when the furnace temperature is held constant.
15. The maximum stresses occur when the maximum average temperature gradients occur.
16. The higher is the constant furnace temperature the higher are the thermally induced maximum failure theory stresses ( $\sigma_d$ ,  $\sigma_s$  and  $\sigma_n$ ).
17. The occurrence of the peak stresses ( $\sigma_d$ ,  $\sigma_s$  and  $\sigma_n$ ) can be delayed by decreasing the slope of the furnace heating paths.
18. The distortion energy stress  $\sigma_d$  is less than  $\sigma_n$  at any instant of time.
19. The optimal furnace heating path (the minimum time path) can be obtained by maintaining the maximum normalized stresses equal to one (maximization of the elastic range of the material) throughout the heating period.
20. The single variable nonlinear optimization method, which maximizes utilization of the elastic range of the material during heating is the best method for obtaining the optimal heating schedule of the ingot.

### 5.3 Limitations of the Present Investigation and Recommendations for Future Work

1. In the nonlinear heat transfer analysis the surrounding furnace temperature was assumed to be uniform. But in the real practice this temperature is not uniform. The present finite element heat transfer model can be modified for nonuniform surrounding temperature.
2. In the finite element heat transfer model, the radiation from the furnace bricks was neglected. This can also be included in the heat transfer analysis.
3. The spectral radiation from the hot gases (participating media) was also not considered in the heat transfer model. This factor can also be accommodated in this model.
4. In the thermal stress calculations the creep phenomenon was not included. The present model can be modified to include the creep behaviour also.
5. The thermal stresses were computed only in the elastic range of the material. The elasto-plasticity of the material can also be considered and elasto-plastic analysis can be carried out.





REFERENCES

1. McGannon, H. E., "The Making, Shaping and Treating of Steel", United States Steel Corporation, Pittsburgh, 1964, pp. 546-556; 616-630.
2. Mantell, C. L., "Engineering Materials Handbook", McGraw-Hill Book Company, New York, 1958, pp. 2.21-2.39.
3. Jaluria, Y., "Numerical Study of the Thermal Processes in a Furnace", Numerical Heat Transfer, Vol. 7, 1984, pp. 211-244.
4. Beer, G. and Meek, J. L., "Transient Heat Flow in Solids", Proceedings of the International Conference on Finite Element Methods in Engineering, The University of South Wales, Australia, 1974.
5. Carslaw, H. S., and Jaeger, J. C., "Conduction of Heat in Solids", Oxford University Press, 1947.
6. Dusinberre, G. M., "Heat Transfer Calculations by Finite Differences", International Textbook Co., Scranton, 1961, pp. 8-18; 64-68.
7. Hunt, N. V., "Numerical Evaluation of Temperature Distribution in Forging Ingots", Broken Hill Proprietary Co., Australia, 1958.
8. Sun, R. C., "Determination of the Forging-Heating Schedule for a Large Hastelloy Alloy X Ingot", Metallurgical Transaction, Vol. 1, 1970, pp. 1881-1887.
9. Finlayson, P. C., and Schofield, J. S., "Heating for Forging in a Batch-type Furnace", J. Iron and Steel Institute, Vol. 193, 1959, pp. 238-252.
10. Kassir, M. K., and Sih, G. C., "Three Dimensional Crack Problems", Noordhoff International Publishing, Lyden, 1975.
11. Timoshenko, S. P., and Goodier, J. N., "Theory of Elasticity", McGraw-Hill Book Co., New York, 1970, pp. 223-226, 445.

12. Stanley, P., and Chau, F. S., "The Effects of the Temperature-Dependence of Properties on the Thermal Stresses in Cylinders", Proceedings of the International Conference on Thermal Stresses in Materials and Structures in Severe Thermal Environments, Plenum Press, New York, 1980, pp. 61-80.
13. Emery, A. F., "Thermal Stress and Fracture in Elastic-Brittle Materials", Proceedings of the International Conference on Thermal Stresses in Materials and Structures in Severe Thermal Environments, Plenum Press, New York, 1980, pp. 95-122.
14. Meric, R. A., "Finite Element Analysis of Optimal Heating of a Slab with Temperature Dependent Thermal Conductivity", International Journal of Heat and Mass Transfer, Vol. 26, 1983, pp. 1347-1353.
15. Meric, R. A., "Finite Element and Conjugate Gradient Methods for a Nonlinear Optimal Heat Transfer Control Problem", Int. J. Numer. Meth. Engr., Vol. 14, 1979, pp. 1851-1863.
16. Meric, R. A., "Finite Element for an Optimal Control Governed by a Parabolic Equation", Int. J. Numer. Meth. Engr., Vol. 14, 1979, pp. 624-628.
17. Meric, R. A., "Boundary Integral Equations and Conjugate Gradient Methods for Optimal Boundary Heating of Solids", International Journal of Heat and Mass Transfer, Vol. 26, 1983, pp. 261-267.
18. Meric, R. A., "Boundary Elements for Optimal Heating of Solids", Journal of Heat Transfer, Vol. 106, 1984, pp. 876-880.
19. Meric, R. A., "Finite Element Methods for an Optimal Steady-State Control Problem", Int. J. Numer. Meth. Engr., Vol. 12, 1978, pp. 1375-1382.
20. Bulteau, J. P. and Dupont, M., "Optimization of an Industrial Continuous Furnace", Engineering Optimization, Vol. 7, 1984, pp. 303-318.
21. Segerlind, L. J., "Applied Finite Element Analysis", John Wiley and Sons, Inc., New York, 1976, pp. 28-30; 42-46; 63-86; 199-209; 212-222; 243-249; 402-408.
22. Rao, S. S., "The Finite Element Method in Engineering", Pergamon Press, Oxford, 1982, pp. 468-474; 493-494.

23. Huebner, K., and Thronton, E. A., "The Finite Element Method for Engineers", John Wiley and Sons, Inc., New York, 1982, pp. 427-428; 431-435.
24. Reddy, B. S., and Sharan, A. M., "The Transient Heat Transfer Analysis of Solids with Radiative Boundary Condition Using Finite Element Analysis", Int. Comm. Heat Mass Transfer, Vol. 12, 1985, pp. 169-178.
25. Gerald, C. F., "Applied Numerical Analysis", Addison-Wesley Publishing Company, Inc., Reading, 1978, pp. 15-26.
26. Sharan, A. M., and Reddy, B. S., "Nonsteady Temperature Distribution in Solids Using the Optimization Principles", AIAA-85-1015, Williamsburg, Virginia.
27. Rao, S. S., "Optimization theory and applications", Wiley Eastern Limited, New Delhi, 1978, pp. 315-327; 474-501.
28. Siddall, J. N., "Optimal Engineering Design", Marcel Dekker, Inc., New York, 1982, pp. 161-167.
29. Reddy, B. S., and Sharan, A. M., "The Computer Simulation of a Heat Transfer Process within a Forging Ingot using the Finite Element Method", Proceedings of the 4th Canadian CAD/CAM and Robotics Conference, Rexdale, 1985.
30. Holman, J. P., "Heat Transfer", McGraw-Hill Book Company, New York, 1981, pp. 536-537.
31. Schuchmann, Jr., R., "Metallurgical Engineering", Addison-Wesley Publishing Co., Reading, 1952, pp. 207-234.
32. Shigley, J. E., and Mitchell, L. D., "Mechanical Engineering Design", McGraw-Hill Book Company, New York, 1983, pp. 217-237.
33. Desai, C. S. and Abel, J. F., "Introduction to the Numerical Method", Van Nostrand Reinhold Co., New York, 1972, p. 45.
34. Cubberly, W. H., "ASM Metals Reference Book, American Society for Metals", Metals Park, Ohio, 1981, pp. 164-167.

35. Myers, G. E., "Analytical Methods in Conduction Heat Transfer", McGraw-Hill Book Company, New York, 1971, p. 303.
  36. Shiners, S. M., "Modern Control System Theory and Application", Addison-Wesley Publishing Company, Inc., Reading, 1978, pp. 496-502.
- 
- 

APPENDIX ADIFFERENTIATION OF MATRICES AND VECTORS WITH RESPECT TO  $\{T^e\}$ 

Using the matrix differentiation, it can be shown that [21]

$$\begin{aligned} \frac{\partial}{\partial \{T^e\}} \int_{V^e} \frac{1}{2} \{T^e\}^T [B_1^e]^T [D_1^e] B_1^e \{T^e\} dv \\ = \int_{V^e} [B_1^e]^T [D_1^e] [B_1^e] \{T^e\} dv \end{aligned} \quad (A.1)$$

$$\frac{\partial}{\partial \{T^e\}} \int_{V^e} r Q^e [N_1^e] \{T^e\} dv = \int_{V^e} r Q^e [N_1^e]^T dv \quad (A.2)$$

$$\begin{aligned} \frac{\partial}{\partial \{T^e\}} \int_{V^e} r \rho c^e [N_1^e] \frac{\partial \{T^e\}}{\partial t} [N_1^e] \{T^e\} dv \\ = \int_{V^e} r \rho c^e [N_1^e]^T [N_1^e] \frac{\partial \{T^e\}}{\partial t} dv \end{aligned} \quad (A.3)$$

$$\frac{\partial}{\partial \{T^e\}} \int_{S_1^e} r q^e [N_1^e] \{T^e\} ds = - \int_{S_1^e} r q^e [N_1^e]^T ds \quad (A.4)$$

$$\frac{\partial}{\partial \{T^e\}} \int_{S_2^e} \frac{r h^e}{2} ([N_1^e] \{T^e\})^2 ds$$

$$= \int_{S_2^e} r h^e [N_1^e]^T [N_1^e] \{T^e\} ds \quad (A.5)$$

$$\frac{\partial}{\partial \{T^e\}} \int_{S_2^e} r h^e T_F [N_1^e] \{T^e\} ds = \int_{S_2^e} r h^e T_F [N_1^e]^T ds \quad (A.6)$$

$$\frac{\partial}{\partial \{T^e\}} \int_{S_2^e} \frac{r h^e}{2} T_F^2 ds = 0 \quad (A.7)$$

$$\frac{\partial}{\partial \{T^e\}} \int_{S_2^e} \frac{r \sigma \epsilon}{5} ([N_1^e] \{T^e\})^5 ds$$

$$= \int_{S_2^e} r \sigma \epsilon [N_1^e]^T [N_1^e] \{T^e\}^4 ds \quad (A.8)$$

$$\frac{\partial}{\partial \{T^e\}} \int_{S_2^e} r \sigma \epsilon T_F^4 [N_1^e] \{T^e\} ds = \int_{S_2^e} r \sigma \epsilon T_F^4 [N_1^e]^T ds \quad (A.9)$$

APPENDIX B

THE EXPRESSIONS FOR THE ELEMENTAL MATRICES  
AND VECTORS OF THE SOLID

The elemental capacitance matrix can be expressed as

$$[C^e] = \int_{V^e} \rho c^e [N_1^e]^T [N_1^e] dv \quad (B.1)$$

Using the volume coordinates, it can be written in the matrix form as

$$[C^e] = \frac{\rho c^e \cdot A^e}{12} \begin{bmatrix} 2 & 1 & 1 \\ 1 & 2 & 1 \\ 1 & 1 & 2 \end{bmatrix} \quad (B.2)$$

The expression for the conduction matrix  $[K_1^e]$  is

$$\begin{aligned} [K_1^e] &= \int_{V^e} [B_1^e]^T [D_1^e] [B_1^e] dv + \int_{S_2^e} h^e [N_1^e]^T [N_1^e] ds \\ &= [K_k^e] + [K_h^e] \end{aligned} \quad (B.3)$$

The  $[K_h^e]$  matrix is due to the convective heat transfer. This matrix is zero, if none of the triangular element sides exchanges heat by convection. Evaluating the integrals in the above equation using the volume and area coordinates, the matrix  $[K_1^e]$  can be written in the matrix form as

$$\begin{aligned}
 [K_1^e] = & \frac{K_x^e}{4A^e} \begin{bmatrix} b_i b_i & b_i b_j & b_i b_k \\ b_j b_i & b_j b_j & b_j b_k \\ b_k b_i & b_k b_j & b_k b_k \end{bmatrix} \\
 & + \frac{K_y^e}{4A^e} \begin{bmatrix} c_i c_i & c_i c_j & c_i c_k \\ c_j c_i & c_j c_j & c_j c_k \\ c_k c_i & c_k c_j & c_k c_k \end{bmatrix} \\
 & + \frac{h^e L_{ij}}{6} \begin{bmatrix} 2 & 1 & 0 \\ 1 & 2 & 0 \\ 0 & 0 & 0 \end{bmatrix} \quad (B.4)
 \end{aligned}$$

The matrix  $[K_h^e]$  is evaluated for the side  $i-j$  of the element, which is exchanging heat by convection.

The force vector,  $\{F_Q^e\}$  due to the heat generation can be written as

$$\{F_Q^e\} = \int_{V^e} Q [N_1^e]^T dv \quad (B.5)$$

In the vector form, it is

$$\{F_Q^e\} = \frac{Q^e V^e}{3} \begin{Bmatrix} 1 \\ 1 \\ 1 \end{Bmatrix} \quad (B.6)$$

The force vector,  $\{F_q^e\}$  due to the heat flux can be expressed as



$$\{F_q^e\} = \int_{S_1^e} q^e [N_1^e]^T ds \quad (B.7)$$

This vector is dependent on the side of the element experiencing heat flux. For the side i-j, it can be written as

$$\{F_q^e\} = \frac{q^e L_{ij}}{2} \begin{Bmatrix} 1 \\ 1 \\ 0 \end{Bmatrix} \quad (B.8)$$

The force vector,  $\{F_c^e\}$  due to the convective heat transfer can be written as

$$\{F_c^e\} = \int_{S_2^e} h^e T_F [N_1^e]^T ds \quad (B.9)$$

This vector is also dependent on the side exchanging heat by convection. For the side i-j of the element, it is

$$\{F_c^e\} = \frac{h^e T_F L_{ij}}{2} \begin{Bmatrix} 1 \\ 1 \\ 0 \end{Bmatrix} \quad (B.10)$$

The force vector,  $\{F_r^e\}$  due to the radiative heat transfer can be expressed as

$$\begin{aligned} \{F_r^e\} &= \int_{S_2^e} \sigma \epsilon T_F^4 [N_1^e]^T ds \\ &= \int_{S_2^e} \sigma \epsilon [N_1^e]^T ([N_1^e] \{T^e\})^4 ds \end{aligned} \quad (B.11)$$

This vector is also dependent on the element side exchanging heat by radiation. For the side  $i-j$  of the element the above integral can be written as

$$\{F_r^e\} = \frac{\sigma \epsilon L_{ij}}{2} \begin{Bmatrix} 1 \\ 1 \\ 0 \end{Bmatrix}$$

$$- \frac{\sigma \epsilon L_{ij}}{30} \begin{Bmatrix} 5 T_i^4 + 4 T_i^3 T_j + 3 T_i^2 T_j^2 + 2 T_i T_j^3 + T_j^4 \\ 5 T_j^4 + 4 T_j^3 T_i + 3 T_j^2 T_i^2 + 2 T_j T_i^3 + T_i^4 \\ 0 \end{Bmatrix} \quad (B.12)$$

APPENDIX C

THE REPRESENTATION OF  $T^e$  IN THE MATRIX FORM

Consider a linear axisymmetric triangular element whose details are shown in Fig. 2.1. The nodes of this element are denoted by  $i, j, k$  in the counter-clockwise direction. The shape functions for this linear triangular element are

$$N_{\beta}^e = \frac{1}{2A^e} (a_{\beta} + b_{\beta}r + c_{\beta}z), \quad \beta = i, j, k$$

where

$$a_i = r_j z_k - r_k z_j$$

$$a_j = r_k z_i - r_i z_k$$

$$a_k = r_i z_j - r_j z_i$$

$$b_i = z_j - z_k$$

$$b_j = z_k - z_i$$

$$b_k = z_i - z_j$$

$$c_i = r_k - r_j$$

$$c_j = r_i - r_k$$

$$c_k = r_j - r_i$$

The temperature of the element is given by

$$T^e = [N^e] \{T^e\} = [N_i^e \ N_j^e \ N_k^e]$$

$$\begin{Bmatrix} T_i^e \\ T_j^e \\ T_k^e \end{Bmatrix}$$

APPENDIX DDESCRIPTION AND LISTING OF THE COMPUTER PROGRAMS

The required computations were done on the VAX 11/780 digital computer, using a package of programs developed in FORTRAN language. Some of the programs make use of subroutines which are: BOUND, DECOM and SOLVE. These are provided at the end of the appendix. All these programs are self-sufficient and can be run with the corresponding input data files.

The program MESH generates the input data required for computing unsteady nonlinear temperature as well as thermal stress distribution. This program can discretize the domain into several linear right angle triangular elements of different sizes. The input data created by this program consists of the element number, node numbers of elements, coordinates of nodes of elements and boundary conditions of elements.

The program TMP SOL computes the unsteady temperature distribution of the two-dimensional body subjected to convection and radiation boundary conditions. The nodal temperatures at various time instants are solved using the iteration method. The data generated by program MESH are used as an input into TMP SOL.

The program TMPING calculates the unsteady temperatures at various nodes of the axisymmetric cylindrical ingot when it is heated in the uniform hot fluid medium. The heat flux in both radial and axial directions are considered. The axisymmetric triangular-ring elements are used. The input data for this program can also be generated using MESH.

The program TMPING1 computes the temperatures and stress distributions of the cylindrical ingot using the finite difference method. The heat flux in the axial direction is neglected. Therefore this program computes the temperatures and stress distributions at various heating time instants along a horizontal section.

The program BCOND generates the input data for the subroutine BOUND. This data corresponds to the boundary conditions in the thermal stress analysis of the ingot.

The program OPTI calculates the optimum furnace temperature at each time step. This optimization is carried out using single variable Davignon-Fletcher-Powell method. The design variable is the furnace temperature. OPTIVAR package is used in this analysis. The subroutine UREAL calculates the ingot temperatures corresponding to the optimum furnace temperature. The subroutine STRESS computes the thermal stresses within the ingot with the variations of the temperatures of the ingot.

The subroutine BOUND imposes the boundary conditions in the thermal stress calculations. The subroutine DECOMP decomposes the matrix into upper and lower triangular matrices. The subroutine SOLVE is used for solving the unknown vector using the method of backward substitution.





```
X3=X(M3-KOUNT*INCR1)
Y3=Y(KOUNT+1)
XX1=X1
YY1=Y1
XX2=X(N2-(KOUNT-1)*INCR1)
YY2=Y(KOUNT)
XX3=X2
YY3=Y2
NCOUT=NCOUT+2
NNCOUT=NCOUT+1
IF(M1.GT.(INCR1*(INCR2-2)))GO TO 40
IF(N2.EQ.(KOUNT*INCR1))GO TO 90
60 WRITE(2,101)NNCOUT,M1,M2,M3,X1,Y1,X2,Y2,X3,Y3,K1
101 WRITE(2,101)NNCOUT,N1,N2,N3,XX1,YY1,XX2,YY2,XX3,YY3,K3
   FORMAT(' ',4(I5),6F8.5,2I2)
   NSTRT=NSTRT+1
   IF((XX3.EQ.X(INCR1)).AND.(YY3.EQ.Y(INCR2)))GO TO 80
   GO TO 50
90 KOUNT=KOUNT+1
   K3=2
   NSTRT=NSTRT+1
   GO TO 60
40 K1=2
   IF((XX3.EQ.X(INCR1)).AND.(YY3.EQ.Y(INCR2)))K3=2
   GO TO 60
80 CONTINUE
STOP
END
```

```

C*****
C
C LISTING OF THE PROGRAM   +++   THPSOL   +++
C PROGRAM FOR CALCULATING THE UNSTEADY NONLINEAR TEMPERATURE
C DISTRIBUTION OF THE SOLID
C
C SUBROUTINES USED IN THIS PROGRAM ARE BOUND,DECOMP,SOLVE
C*****

```

```

REAL KT,LENG,LAMBDA
DIMENSION NS(3),ESM1(3,3),EF(3),X(3),Y(3),B(3),C(3)
DIMENSION A(20000),D(2000)
DIMENSION CAP(3,3),ESM2(3,3),PM(3),AA(3),ESM(3,3)
DATA NCL/1/

```

```

C      KT  -----  THERMAL CONDUCTIVITY OF THE MATERIAL-
C      H .  -----  CONVECTION HEAT TRANSFER COEFFICIENT
C      DELTA ---  TIME STEP IN SECONDS
C      TO   ---  FLUID TEMP. AT PREVIOUS TIME INSTANCE
C      TN   ---  FLUID TEMP. AT CURRENT TIME INSTANCE
C      SIGM ---  STEFEN - BOLTZMANN CONSTANT
C      NCL  ---  NO. OF LOADING CASES
C      ISIDE ---  SIDE WITH CONVECTION AND RADIATION BOUNDARY
C      LENG ---  LENGTH OF THE 'SIDE

```

```

TN=323.0
TO=323.0
KT=3.0
H=200.0
RHO=1600.0
SPHEAT=800.0
LAMBDA=RHO*SPHEAT
DP=LAMBDA*AR4/48.0
TOTAL=0.0
DELTA=60.0
EPSI=0.7
SIGM=5.669E-8
PRO=EPSI*SIGM

```

```

OPEN(UNIT=2,FILE='OUTPUT.DAT',TYPE='OLD')
OPEN(UNIT=3,FILE='TEMP.DAT',TYPE='NEW')

```

```

READ(2,*)NP,NE,NBW
JGF=NP
JGSM=JGF*2
JEND=JGSM+NP*NBW

```

```

DO 100 I=1,JEND
A(I)=0.0

```

```

DO 110 I=1,JGF
A(I)=573.0
CONTINUE
110
10 CONTINUE

DO 120 I=JGF+1,JEND
A(I)=0.0
CONTINUE
120

DO 130 KK=1,NE
READ(2,*) NEL,NS,X(1),Y(1),X(2),Y(2),X(3),Y(3),ISIDE
DO 140 I=1,3
AA(I)=A(NS(I))
140 CONTINUE

B(1)=Y(2)-Y(3)
B(2)=Y(3)-Y(1)
B(3)=Y(1)-Y(2)
C(1)=X(2)-X(2)
C(2)=X(1)-X(3)
C(3)=X(2)-X(1)
AR4=(X(2)*Y(3)+X(3)*Y(1)+X(1)*Y(2)-X(2)*Y(1)-X(3)*Y(2)
+ -X(1)*Y(3)) *2.0

DO 150 I=1,3
EF(I)=0.0
PM(I)=0.0
DO 150 J=1,3
ESM(I,J)=(KT*B(I)*B(J)+KT*C(I)*C(J))/AR4
150 CONTINUE

IF(ISIDE .LE. 0) GO TO 160
J=ISIDE
K=J+1
LENG=SQRT((X(K)-X(J))**2.+(Y(K)-Y(J))**2.)
HL=H*LENG
EF(J)=HL*TO/2.0
EF(K)=HL*TO/2.0
M=NS(J)
N=NS(K)
EF1=PRO*LENG*(TO**4)/2.0
EF2=PRO*LENG*(TO**4)/2.0
EF31=((5*A(M)**4)+(4*A(N)*A(M)**3)+(3*A(M)*A(M)*
+ A(N)*A(N))+(2*A(M)*A(N)**3)+(A(N)**4))
EF3=(PRO*LENG/30.0)*EF31
EF41=((5*A(N)**4)+(4*A(M)*A(N)**3)+(3*A(M)*A(M)*
+ A(N)*A(N))+(2*A(N)*A(M)**3)+(A(M)**4))
EF4=(PRO*LENG/30.0)*EF41
EF(J)=EF(J)-EF3+EF1
EF(K)=EF(K)-EF4+EF2

ESM(J,J)=ESM(J,J)+(HL*2)/6.0
ESM(J,K)=ESM(J,K)+HL/6.0
ESM(K,J)=ESM(J,K)

```

ESM(K,K)=ESM(K,K)+(HL\*2)/6.

160

CONTINUE

CAP(1,1)=DP\*2

CAP(1,2)=DP\*1

CAP(1,3)=DP\*1

CAP(2,1)=DP\*1

CAP(2,2)=DP\*2

CAP(2,3)=DP\*1

CAP(3,1)=DP\*1

CAP(3,2)=DP\*1

CAP(3,3)=DP\*2

DO 170 I=1,3

DO 170 J=1,3

ESM1(I,J)=(2.\*CAP(I,J)/DELTA)-ESM(I,J)

170

CONTINUE

DO 180 I=1,3

DO 180 J=1,3

PM(I)=PM(I)+(ESM1(I,J)\*AA(J))

180

CONTINUE

DO 210 I=1,3

EF(I)=PM(I)+EF(I)

210

CONTINUE

DO 130 I=1,3

II=NS(I)

J5=NF+II

A(J5)=A(J5)+EF(I)

130

CONTINUE

REWIND 2

DO 300 I=1,JGSM

300

D(I)=A(I)

DO 301 I=1,JGF

270

A(I)=0.5\*(A(I)+D(I))

301

D(I)=A(I)

READ(2,\*)KD,KD,KD

DO 430 KK=1,NE

READ(2,\*) NEL, NS, X(1), Y(1), X(2), Y(2), X(3), Y(3), ISIDE

B(1)=Y(2)-Y(3)

B(2)=Y(3)-Y(1)

B(3)=Y(1)-Y(2)

C(1)=X(3)-X(2)

C(2)=X(1)-X(3)

C(3)=X(2)-X(1)

AR4=(X(2)\*Y(3)+X(3)\*Y(1)+X(1)\*Y(2)-X(2)\*Y(1)-X(3)\*Y(2)

-X(1)\*Y(3)) \*2.0

```

DO 450 I=1,3
EF(I)=0:0
DO 450 J=1,3
ESH(I,J)=(KT*B(I)*B(J)+KT*C(I)*C(J))/AR4
450 CONTINUE

IF(ISIDE .LE. 0) GO TO 460
J=ISIDE
K=J+1
LENG=SQRT((X(K)-X(J))**2.+(Y(K)-Y(J))**2.)

HL=H*LENG
EF(J)=HL*TN/2.0
EF(K)=HL*TN/2.0
M=NS(J)
N=NS(K)
EF1=PRO*LENG*(TN**4)/2.0
EF2=PRO*LENG*(TN**4)/2.0
EF31=((5*A(M)**4)+(4*A(N)*A(M)**3)+(3*A(M)*A(M)*
+ A(N)*A(N))+(2*A(M)*A(N)**3)+(A(N)**4))
EF3=(PRO*LENG/30.0)*(EF31)
EF41=((5*A(N)**4)+(4*A(M)*A(N)**3)+(3*A(M)*A(M)*
+ A(N)*A(N))+(2*A(N)*A(N)**3)+(A(M)**4))
EF4=(PRO*LENG/30.0)*(EF41)

EF(J)=EF(J)-EF3+EF1
EF(K)=EF(K)-EF4+EF2

ESH(J,J)=ESH(J,J)+(HL*2.)/6.0
ESH(J,K)=ESH(J,K)+HL/6.0
ESH(K,J)=ESH(J,K)
ESH(K,K)=ESH(K,K)+(HL*2.)/6.0
460 CONTINUE

CAP(1,1)=DP*2
CAP(1,2)=DP*1
CAP(1,3)=DP*1
CAP(2,1)=DP*1
CAP(2,2)=DP*2
CAP(2,3)=DP*1
CAP(3,1)=DP*1
CAP(3,2)=DP*1
CAP(3,3)=DP*2

DO 470 I=1,3
DO 470 J=1,3
ESH2(I,J)=(2.*CAP(I,J)/DELTA)+ESH(I,J)
470 CONTINUE

DO 430 I=1,3
II=NS(I)
J5=NP+II
A(J5)=A(J5)+EF(I)
DO 190 J=1,3

```

```

JJ=NS(J)
JJ=JJ-II+1
IF(JJ)190,190,200
200 J5=JGSM*(JJ-1)*NP+II
A(J5)=A(J5)+ESM2(I,J)
190 CONTINUE
430 CONTINUE

REWIND 2

CALL BOUND(A(JGSM+1),A(JGF+1),NP,NBW,NCL)
CALL DECOMP(A(JGSM+1),NP,NBW)
CALL SOLVE(A(JGSM+1),A(JGF+1),A(1),NP,NBW,NCL)

DO 240 I=1,JGF
240 IF(ABS(D(I)-A(I)).GE.0.01)GO TO 250
CONTINUE

GO TO 290

250 CONTINUE

DO 260 I=JGF+1,JEND
260 A(I)=0.0

DO 280 I=JGF+1,JGSM
280 A(I)=0(I)
CONTINUE

GO TO 270

290 CONTINUE

TIME=TIME+DELTA/60.0
WRITE(3,*)A(1),A(3),A(11),A(13),A(21),A(23),TIME
READ(2,*)KD,KD,KD

IF(A(1).GT.323.0)GO TO 10
STOP
END

```

C\*\*\*\*\*

C

C

C

C

C

C

C

C

C

C

C

C

C

C

C

C

C

C

C

C

C

C

C

C

C

C

C

C

C

C

C

C

C

C

C

C

C

C

C

C

C

C

C

C

C

C

C

C

C

C

C

C

C

C

C

C

C

C

C

LISTING OF THE PROGRAM +++ TMPING +++  
 THIS PROGRAM COMPUTES THE UNSTEADY NONLINEAR TEMPERATURE-  
 DISTRIBUTION IN THE INGOT.  
 SUBROUTINES USED IN THIS PROGRAM ARE DECOMP,SOLVE

C\*\*\*\*\*

REAL KT, LENG, MNSE, MSSE, KTH(2000), SPHT(2000)  
 DIMENSION NS(3), ESM1(3,3), EF(3), R(3), Z(3), B(3), C(3)  
 DIMENSION A(20000), D(2000)  
 DIMENSION CAP(3,3), ESM2(3,3), PH(3), AA(3), ESM(3,3)  
 DATA NCL/1/

TOTAL=0.0  
 PHI=3.142857  
 DELTA=60.0\*5  
 dell=delta/60.0  
 EPSI=0.7  
 SIGM=5.669E-8  
 PRO=PHI\*EPSI\*SIGM  
 RHO=7840.0  
 TO=1000  
 TN=1000

OPEN(UNIT=2, FILE='OUTPUT1.DAT', TYPE='OLD')  
 OPEN(UNIT=3, FILE='CONDOC.DAT', TYPE='OLD')  
 OPEN(UNIT=6, FILE='SPHEAT.DAT', TYPE='OLD')  
 OPEN(UNIT=7, FILE='TEMP1.DAT', TYPE='NEW')

READ(2,\*)NP, NE, NBW  
 JGF=NP  
 JGSM=JGF\*2  
 JEND=JGSM+NP\*NBW

READ(3,\*)(KTH(I), I=1, 2000)  
 READ(6,\*)(SPHT(I), I=1, 2000)

100 DO 100 I=1, JEND  
 A(I)=0.0

110 DO 110 I=1, JGF  
 A(I)=29B.0  
 CONTINUE

10 continue

120 DO 120 I=JGF+1, JEND  
 A(I)=0.0  
 CONTINUE

```

DO 130 KK=1,NE
READ(2,*) NEL,NS,R(1),Z(1),R(2),Z(2),R(3),Z(3),ISIDE
RAVER=(R(1)+R(2)+R(3))/3.0
DO 140 I=1,3
AA(I)=A(NS(I))
CONTINUE

140 B(1)=Z(2)-Z(3)
B(2)=Z(3)-Z(1)
B(3)=Z(1)-Z(2)
C(1)=R(3)-R(2)
C(2)=R(1)-R(3)
C(3)=R(2)-R(1)
AR4=(R(2)*Z(3)+R(3)*Z(1)+R(1)*Z(2)-R(2)*Z(1)-R(3)*Z(2)
- R(1)*Z(3)) *2.0

ITEMP=IFIX(((A(NS(1))2+A(NS(2))2+A(NS(3))2)/3.0)-273.0)
KT=KTH(ITEMP)
SPEHT=SPHT(ITEMP)
RLAMDA=RHO*SPEHT
DP=PHI*RLAMDA*AR4/360.0
DO 150 I=1,3
EF(I)=0.0
PH(I)=0.0
DO 150 J=1,3
ESM(I,J)=((KT*B(I)*B(J)+KT*C(I)*C(J))*RAVER*RAVER*2.*PHI)/AR4
CONTINUE

150 IF(ISIDE .LE. 0) GO TO 160
J=ISIDE
K=J+1
LENG=SQRT((R(K)-R(J))2+(Z(K)-Z(J))2)
TEMP1=ITEMP+273
TEMP2=1.8*(TO-TEMP1)
H=ABS(TEMP2)/2.25
H=H**(1./4.)
H=0.27*H
H=5.6782*H

HL=H*LENG
EF(J)=EF(J)+(RAVER*HL*PHI*TO*(2.*R(J)+R(K)))/3.0
EF(K)=EF(K)+(RAVER*HL*PHI*TO*(R(J)+2.*R(K)))/3.0
M=NS(J)
N=NS(K)

EF1=(PRO*LENG*RAVER*(2*R(J)+R(K))/3.0)*(TO**4)
EF2=(PRO*LENG*RAVER*(R(J)+2*R(K))/3.0)*(TO**4)

EF31=((60*A(M)**4)+(40*A(N)*A(M)**3)+(24*A(M)*A(M)*
A(N)*A(N))+(12*A(M)*A(N)**3)+(4*A(N)**4))*R(J)
+
EF32=((10*A(M)**4)+(16*A(N)*A(M)**3)+(18*A(M)*A(M)*A(N)**2)+
(16*A(M)*A(N)**3)+(10*A(N)**4))*R(K)
+
EF3=(RAVER*PRO*LENG/210.0)*(EF31+EF32)

EF41=((60*A(N)**4)+(40*A(M)*A(N)**3)+(24*A(M)*A(M)*

```



```

+ A(N)*A(N))+(12*A(N)*A(M)**3)+(4*A(M)**4))*R(K)
EF42=((10*A(N)**4)+(16*A(M)*A(N)**3)+(18*A(M)*A(M)*A(N)**2)+
+ (16*A(N)*A(M)**3)+(10*A(M)**4))*R(J)
EF4=(RAVER*PRO*LENG/210.0)*(EF41+EF42)

EF(J)=EF(J)-EF3+EF1
EF(K)=EF(K)-EF4+EF2

ESM(J,J)=ESM(J,J)+(RAVER*HL*PHI*(3.*R(J)+R(K)))/6.0
ESM(J,K)=ESM(J,K)+(RAVER*HL*PHI*(R(J)+R(K)))/6.0
ESM(K,J)=ESM(J,K)
ESM(K,K)=ESM(K,K)+(RAVER*HL*PHI*(R(J)+3.*R(K)))/6.0

160 CONTINUE
CAP(1,1)=DP*(12.*R(1)**2.+2.*R(2)**2.+2.*R(3)**2.+6.*R(1)*R(2)
+ 6.*R(1)*R(3)+2.*R(2)*R(3))
CAP(1,2)=DP*(3.*R(1)**2.+3.*R(2)**2.+R(3)**2.+4.*R(1)*R(2)+2.*
+ R(1)*R(3)+2.*R(2)*R(3))
CAP(2,1)=CAP(1,2)
CAP(1,3)=DP*(3.*R(1)**2.+R(2)**2.+3.*R(3)**2.+2.*R(1)*R(2)+4.*
+ R(1)*R(3)+2.*R(2)*R(3))
CAP(3,1)=CAP(1,3)
CAP(2,2)=DP*(2.*R(1)**2.+12.*R(2)**2.+2.*R(3)**2.+6.*R(1)*R(2)
+ 2.*R(1)*R(3)+6.*R(2)*R(3))
CAP(2,3)=DP*(R(1)**2.+3.*R(2)**2.+3.*R(3)**2.+2.*R(1)*R(2)+2.*
+ R(1)*R(3)+4.*R(2)*R(3))
CAP(3,2)=CAP(2,3)
CAP(3,3)=DP*(2.*R(1)**2.+2.*R(2)**2.+12.*R(3)**2.+2.*R(1)*R(2)
+ 6.*R(1)*R(3)+6.*R(2)*R(3))

DO 170 I=1,3
DO 170 J=1,3
ESM1(I,J)=(2.*CAP(I,J)/DELTA)-ESM(I,J)
170 CONTINUE

DO 180 I=1,3
DO 180 J=1,3
PM(I)=PM(I)+(ESM1(I,J)*AA(J))
180 CONTINUE

DO 210 I=1,3
EF(I)=PM(I)+EF(I)
210 CONTINUE

DO 130 I=1,3
II=NS(I)
J5=NP+II
A(J5)=A(J5)+EF(I)
130 CONTINUE

REWIND 2

DO 300 I=1,JGSM
D(I)=A(I)
300

```

```

270 DO 301 I=1,JGF
    A(I)=0.5*(A(I)+D(I))
301 D(I)=A(I)

    READ(2,*)KD,KD,KD

    DO 430 KK=1,NE
    READ(2,*) NEL,NS,R(1),Z(1),R(2),Z(2),R(3),Z(3),ISIDE
    RAVER=(R(1)+R(2)+R(3))/3.0

    B(1)=Z(2)-Z(3)
    B(2)=Z(3)-Z(1)
    B(3)=Z(1)-Z(2)
    C(1)=R(3)-R(2)
    C(2)=R(1)-R(3)
    C(3)=R(2)-R(1)
    AR4=(R(2)*Z(3)+R(3)*Z(1)+R(1)*Z(2)-R(2)*Z(1)-R(3)*Z(2)
    +
    -R(1)*Z(3)) *2.0

    ITEMP=IFIX(((A(NS(1))+A(NS(2))+A(NS(3)))/3.0)-273.0)

    KT=KTH(ITEMP)
    SPEHT=SPHT(ITEMP)
    RLAMDA=RHO*SPEHT
    DP=PHI*RLAMDA*AR4/360.0
    DO 450 I=1,3
    EF(I)=0.0
    DO 450 J=1,3
    ESH(I,J)=((KT*B(I)*B(J)+KT*C(I)*C(J))*RAVER*RAVER*2.*PHI)/AR4
450 CONTINUE

    IF(ISIDE .LE. 0) GO TO 460
    J=ISIDE
    K=J+1
    LENG=SQRT((R(K)-R(J))**2.+(Z(K)-Z(J))**2.)
    TEMP1=ITEMP+273
    TEMP2=1.8*(TN-TEMP1)
    H=ABS(TEMP2)/2.25
    H=H**(1./4.)
    H=0.27*H
    H=5.6782*H
    HL=H*LENG

    EF(J)=EF(J)+(RAVER*HL*PHI*TN*(2.*R(J)+R(K)))/3.0
    EF(K)=EF(K)+(RAVER*HL*PHI*TN*(R(J)+2.*R(K)))/3.0
    M=NS(J)
    N=NS(K)

    EF1=(PRO*LENG*RAVER*(2*R(J)+R(K))/3.0)*(TN**4)
    EF2=(PRO*LENG*RAVER*(R(J)+2*R(K))/3.0)*(TN**4)

    EF31=((60*A(M)**4)+(40*A(N)*A(M)**3)+(24*A(M)*A(M)*
    +
    A(N)*A(N))+(12*A(M)*A(N)**3)+(4*A(N)**4))*R(J)
    EF32=((10*A(M)**4)+(16*A(N)*A(M)**3)+(18*A(M)*A(M)*A(N)**2)+
    +
    (16*A(M)*A(N)**3)+(10*A(N)**4))*R(K)

```

```

EF3=(RAVER*PRO*LENG/210.0)*(EF31+EF32)
EF41=((60*A(N)**4)+(40*A(M)*A(N)**3)+(24*A(M)*A(N)*
+ A(N)*A(N)*A(N))+12*A(N)*A(M)**3+(4*A(M)**4))*R(K)
EF42=((10*A(N)**4)+(16*A(M)*A(N)**3)+(18*A(M)*A(N)*A(N)**2)+
+ (16*A(N)*A(M)**3)+(10*A(M)**4))*R(J)
EF4=(RAVER*PRO*LENG/210.0)*(EF41+EF42)
EF(J)=EF(J)-EF3+EF1
EF(K)=EF(K)-EF4+EF2
ESM(J,J)=ESM(J,J)+(RAVER*HL*PHI*(3.*R(J)+R(K)))/6.0
ESM(J,K)=ESM(J,K)+(RAVER*HL*PHI*(R(J)+R(K)))/6.0
ESM(K,J)=ESM(J,K)
ESM(K,K)=ESM(K,K)+(RAVER*HL*PHI*(R(J)+3.*R(K)))/6.0
460 CONTINUE
CAP(1,1)=DP*(12.*R(1)**2.+2.*R(2)**2.+2.*R(3)**2.+6.*R(1)*R(2)
+ 6.*R(1)*R(3)+2.*R(2)*R(3))
+ CAP(1,2)=DP*(3.*R(1)**2.+3.*R(2)**2.+R(3)**2.+4.*R(1)*R(2)+2.*
+ R(1)*R(3)+2.*R(2)*R(3))
CAP(2,1)=CAP(1,2)
+ CAP(1,3)=DP*(3.*R(1)**2.+R(2)**2.+3.*R(3)**2.+2.*R(1)*R(2)+4.*
+ R(1)*R(3)+2.*R(2)*R(3))
CAP(3,1)=CAP(1,3)
+ CAP(2,2)=DP*(2.*R(1)**2.+12.*R(2)**2.+2.*R(3)**2.+6.*R(1)*R(2)
+ 2.*R(1)*R(3)+6.*R(2)*R(3))
+ CAP(2,3)=DP*(R(1)**2.+3.*R(2)**2.+3.*R(3)**2.+2.*R(1)*R(2)+2.*
+ R(1)*R(3)+4.*R(2)*R(3))
CAP(3,2)=CAP(2,3)
+ CAP(3,3)=DP*(2.*R(1)**2.+2.*R(2)**2.+12.*R(3)**2.+2.*R(1)*R(2)
+ 6.*R(1)*R(3)+6.*R(2)*R(3))
DO 470 I=1,3
DO 470 J=1,3
ESM2(I,J)=(2.*CAP(I,J)/DELTA)+ESH(I,J)
470 CONTINUE
DO 430 I=1,3
II=NS(I)
J5=NP+II
A(J5)=A(J5)+EF(I)
DO 190 J=1,3
JJ=NS(J)
JJ=JJ-II+1
IF(JJ)190,190,200
J5=JGSM+(JJ-1)*NP+II
A(J5)=A(J5)+ESM2(I,J)
200 CONTINUE
190 CONTINUE
430 CONTINUE
REWIND 2
CALL DECOMP(A(JGSM+1),NP,NBW)
CALL SOLVE(A(JGSM+1),A(JGF+1),A(1),NP,NBW,NCL)

```

DO 240 I=1,JGF  
IF(ABS(D(I)-A(I)).GE.1.0)GO TO 250  
240 CONTINUE

GO TO 290

250 CONTINUE

DO 260 I=JGF+1,JEND  
260 A(I)=0.0

DO 280 I=1,JGF  
A(JGF+I)=D(JGF+I)  
280 CONTINUE

GO TO 270

290 CONTINUE

TOTAL=TOTAL+DELT  
IF(TOTAL.GE.60)DELTA=20\*60  
WRITE(7,32)A(1),A(6),A(37),A(42),A(145),A(150),  
+ A(6)-A(1),TOTAL  
32 FORMAT(' ',8F9.2)

READ(2,\*)KD,KD,KD

IF(A(1).LT.(1000-1))GO TO 10  
STOP  
END

```

C*****
C
C   PROGRAM LISTING   +++   THPING1   +++
C   THIS PROGRAM CALCULATES THE UNSTEADY TEMP. & STRESS
C   DIST. ALONG THE SECTION AB IN THE INGOT USING
C   FINITE DIFFERENCE METHOD
C
C*****

```

```

DIMENSION TO(14),TN(14)
REAL K(2000),M,N,CP(2000),ALPHA(2000)

```

```

YST(T)=69000*6498.76-((34500*6498.76)*(T-298)/1200.0)
YMOD(T)=206482.8E6-((103421.4E6)*(T-298)/1200.0)

```

```

OPEN(UNIT=1,FILE='CONDC.DAT',TYPE='OLD')
OPEN(UNIT=2,FILE='SPHEAT.DAT',TYPE='OLD')
OPEN(UNIT=3,FILE='COEFF.DAT',TYPE='OLD')
OPEN(UNIT=9,FILE='FDIFF2.DAT',TYPE='NEW')
OPEN(UNIT=10,FILE='FDIFF1.DAT',TYPE='NEW')

```

```

READ(1,*)(K(I),I=1,2000)
READ(2,*)(CP(I),I=1,2000)
READ(3,*)(ALPHA(I),I=1,2000)

```

```

DELT=10
RHO=7840.0
TIME=0.0
TF=1000.0
DR=0.086667*2.54*12/100.0

```

```

DO 10 I=1,14
TO(I)=298.0

```

```

CONTINUE
ITEMP=IFIX(TO(1)-273)
ALP=K(ITEMP)/(RHO*CP(ITEMP))
M=DR*DR/(ALP*DELT)
TN(1)=4*TO(2)/M+(1-4/M)*TO(1)
RTOT=0.0

```

```

DO 20 I=2,13
RTOT=RTOT+DR
ITEMP=IFIX(TO(I)-273)
ALP=K(ITEMP)/(RHO*CP(ITEMP))
M=DR*DR/(ALP*DELT)
SUM1=(2+DR/RTOT)*0.5*(TO(I+1)-TO(I))
SUM2=(2-DR/RTOT)*0.5*(TO(I-1)-TO(I))
SUM=(SUM1+SUM2)/M
TN(I)=TO(I)+SUM
CONTINUE

```

20

```

RTOT=RTOT+DR
TF1=TF
TO1=TO(14)
ITEMP=IFIX(TO(14)-273)

```

```

H1=0.7*(TF1**4-TO1**4)/(TF1-TO1)
H1=H1*5.669E-8
H2=5.6782*0.27*(1.8*(TF1-TO1)/2.25)**0.25
H=H1+H2
N=H*DR/K(ITEMP)
ALP=K(ITEMP)/(RHO*CP(ITEMP))
M=DR*DR/(ALP*DELT)
SUM1=(8*RTOT/DR-4)*TO(13)/(M*(4*RTOT/DR-1))
SUM2=8*RTOT*N*TF/(DR*M*(4*RTOT/DR-1))
SUM3=(8*RTOT*N/DR+8*RTOT/DR-4)/(M*(4*RTOT/DR-1))
SUM3=(1-SUM3)*TO(14)
TN(14)=SUM1+SUM2+SUM3

```

```

30 DO 30 I=1,14
   TO(I)=TN(I)

```

```

KCRIT=0.0
TIME=TIME+DELT

```

```

51 DO 50 I=300,3600,300
   IF(TIME.EQ.I)GO TO 51
   GO TO 50
   KCRIT=1
   WRITE(9,*)TN(1),TN(14),TIME
50 CONTINUE

```

```

71 DO 70 I=3600,54000,1800
   IF(TIME.EQ.I)GO TO 71
   GO TO 70
   KCRIT=1
   WRITE(9,*)TN(1),TN(14),ITMIN
70 CONTINUE

```

```

IF(KCRIT.NE.1)GO TO 60

```

```

TOTAL1=0.0
RT=0.0
DO 100 I=1,13
  RT=RT+DR
  RT1=RT-DR
  TAV=0.5*(TN(I)+TN(I+1))
  ITAV=0.5*(TN(I)+TN(I+1))-273
  FAC1=ALPHA(ITAV)*YMOD(TAV)*TAV/(0.7*2)
  TOTAL1=TOTAL1+FAC1*(RT*RT-RT1*RT1)
100 CONTINUE

```

```

TOTAL1=TOTAL1/(0.3429*0.3429)

```

```

DMAX=0.0
SMAX=0.0

```

```

SMIN=0.0
RT=0.0
TOTAL2=0.0
TOTAL3=0.0
DO 101 I=1,13
RT=RT+DR
RT1=RT-DR
S1=0.0
S2=10E30
TAV=0.5*(TN(I)+TN(I+1))
ITAV=0.5*(TN(I)+TN(I+1))-273
FAC1=ALPHA*(TAV)*YMOD(TAV)*TAV/((0.7*2)
TOTAL2=TOTAL2+FAC1*(RT*RT-RT1*RT1)
TOTAL3=FAC1*2
TOTAL4=TOTAL2/(RT*RT)
RS=TOTAL1-TOTAL4
CS=TOTAL1+TOTAL4-TOTAL3
AS=TOTAL1*2-TOTAL3
DE=SQRT(((RS-CS)**2)+((CS-AS)**2)+((AS-RS)**2))
DE=DE/SQRT(2.0)
DE=DE/YST(TAV)
IF(ABS(RS).GT.ABS(S1))S1=RS
IF(ABS(RS).LT.ABS(S2))S2=RS
IF(ABS(CS).GT.ABS(S1))S1=CS
IF(ABS(CS).LT.ABS(S2))S2=CS
IF(ABS(AS).GT.ABS(S1))S1=AS
IF(ABS(AS).LT.ABS(S2))S2=AS

S3=S1-S2
S3=S3/YST(TAV)
S1=S1/YST(TAV)
IF(ABS(S1).LT.ABS(SMAX))GO TO 110
SMAX=S1
KN1=I
110 IF(ABS(S3).LT.ABS(SMIN))GO TO 111
SMIN=S3
KN2=I
111 IF(ABS(DE).LT.ABS(DMAX))GO TO 101
DMAX=DE
KN3=I
101 CONTINUE

WRITE(10,99)DMAX,KN3,SMAX,KN1,SMIN,KN2,ITMIN
99  FORMAT(' ',3(F10.5,I4),I5)
IF(TN(1).GE.(TF-1))GO TO 40
GO TO 60
40 CONTINUE
END

```

```

C*****
C*
C*   PROGRAM LISTING   +++   BCOND   +++
C*   THIS PROGRAM GENERATES THE DATA FOR SUBROUTINE BOUNDARY
C*   IN THE PROGRAM STRESS.
C*
C*****

```

```

DIMENSION NS(3),D(6)
OPEN(UNIT=2,FILE='OUTPUT1.DAT',TYPE='OLD')
OPEN(UNIT=3,FILE='OUTPUT3.DAT',TYPE='NEW')
WRITE(3,*)' -1',' -1'
K1=6
K2=25
C --- K1 -- NO. OF NODES IN THE R-DIRECTION
C --- K2 -- NO. OF NODES IN THE Z-DIRECTION

READ(2,*)NO,NEL,KD
DO 10 IK=1,NEL
READ(2,*)KD,NS,D,KB
IF(.NOT.(NS(1).EQ.1 .AND. NS(2).EQ.2))GO TO, 20

KV1=NS(1)*2-1
KV2=NS(1)*2
KV3=NS(2)*2
VV=0.0
WRITE(3,*)KV1,VV
WRITE(3,*)KV2,VV
WRITE(3,*)KV3,VV
20 DO 30 I=3,K1
IF(NS(2).NE.I)GO TO 30
KV=NS(2)*2
VV=0.0
WRITE(3,*)KV,VV
30 CONTINUE
DO 40 I=K1+1,NO,K1
IF(.NOT.(NS(1).EQ.I.AND.NS(2).EQ.(I+1)))GO TO 40
KV=NS(1)*2-1
VV=0.0
WRITE(3,*)KV,VV
40 CONTINUE
10 CONTINUE
WRITE(3,*)(K1*K2-K1+1)*2-1,VV
WRITE(3,*)' -1',' -1'
END

```



```

C*****
C
C   PROGRAM LISTING   +++   OPTI   +++
C   THIS PROGRAM CALCULATES THE OPTIMUM FURNACE TEMPERATURE
C   PATH FOR INGOT HEATING.
C
C   THIS PROGRAM USES THE SUBROUTINES BOUND,DECOMP,SOLVE,STRESS,
C   ZPOLAR & OPTIVAR PACKAGE
C*****

```

```

DIMENSION X(1),XSTRT(1),RMAX(1),RMIN(1),PHI(2),PSI(1),W(30)
COMMON/DAVID/IDATA,IPRINT,F,G,MAXM,TOL,ZERO,R,REDUCE
COMMON/SUBS/RMIN,RMAX
COMMON/SUBS1/ROLD

```

```
OPEN(UNIT=1,FILE='STRESS5.DAT',TYPE='OLD')
```

```
READ(1,*)ROLD,DUM,DUM,DUM,DUM,DUM,DUM,DUM
```

```

N=1
NCONS=2
NEQUS=0
NPENAL=2

```

```

RMAX(1)=ROLD+300
RMIN(1)=ROLD-200
XSTRT(1)=ROLD-40

```

```

IPRINT=-1
IDATA=0
MAXM=200
F=0.05
G=0.05
ZERO=0.1
TOL=0.1
CALL DAVID(N,NCONS,NEQUS,NPENAL,RMAX,RMIN,XSTRT,X,U,PHI,PSI,
+
100 NVIOL,W)
CONTINUE
STOP
END

```

```

C*****
C
C   SUBTOUTINE EQUAL
C
C*****

```

```

SUBROUTINE EQUAL(X,PSI,NEQUS)
DIMENSION X(1),PSI(1)
RETURN

```

END

```
C*****  
C  
C   SUBROUTINE CONST  
C  
C*****
```

```
      SUBROUTINE CONST(X,NCONS,PHI)  
      DIMENSION X(1),PHI(1)  
      COMMON/SUBS/RMI,RMA  
      PHI(1)=RMA-X(1)  
      PHI(2)=X(1)-RMI  
      RETURN  
      END
```

```

C*****
C
C LISTING OF THE SUBROUTINE   +++ UREAL +++
C THIS PROGRAM COMPUTES THE UNSTEADY NONLINEAR TEMPERATURE &
C STRESS DISTRIBUTION IN THE INGOT AND FINDS THE VALUE OF THE
C OBJECTIVE FUNCTION TO BE MINIMIZED.
C*****

```

```

SUBROUTINE UREAL(TN,U)
REAL KT, LENG, MNSE, MSSE, KTH(2000), SPHT(2000), MNSE, MSSE
DIMENSION NS(3), ESM1(3,3), EF(3), R(3), Z(3), B(3), C(3)
DIMENSION A(20000), U(2000)
DIMENSION CAP(3,3), ESM2(3,3), PM(3), AA(3), ESM(3,3)
DATA NCL/1/
COMMON/SUBS1/TO

```

```

TOTAL=0.0
PHI=3.142857
DELTA=60.0*5
dell=delta/60.0
EPSI=0.7
SIGM=5.669E-8
PRO=PHI*EPSI*SIGM
RHO=7840.0

```

```

OPEN(UNIT=2, FILE='OUTPUT1.DAT', TYPE='OLD')
OPEN(UNIT=3, FILE='CONDOC.DAT', TYPE='OLD')
OPEN(UNIT=6, FILE='SPHEAT.DAT', TYPE='OLD')
OPEN(UNIT=8, FILE='TEMOLD.DAT', TYPE='OLD')
OPEN(UNIT=7, FILE='TEMP4.DAT', TYPE='NEW')
OPEN(UNIT=9, FILE='TEMP5.DAT', TYPE='NEW')
OPEN(UNIT=10, FILE='STRESS4.DAT', TYPE='NEW')

```

```

READ(2,*)NP, NE, NBW
JGF=NP
JGSM=JGF*2
JEND=JGSM+NP*NBW

```

```

READ(3,*)(KTH(I), I=1, 2000)
READ(6,*)(SPHT(I), I=1, 2000)
READ(8,*)(A(I), I=1, JGF)

```

```

100 DO 100 I=1, JEND
A(I)=0.0

```

```

DO 120 I=JGF+1, JEND
A(I)=0.0
120 CONTINUE

```

```

DO 130 KK=1, NE
READ(2,*) NEL, NS, R(1), Z(1), R(2), Z(2), R(3), Z(3), ISIDE
RAVER=(R(1)+R(2)+R(3))/3.0

```

EF4=(RAVER\*PRO\*LENG/210.0)\*(EF41+EF42)

EF(J)=EF(J)-EF3+EF1  
 EF(K)=EF(K)-EF4+EF2

ESH(J,J)=ESH(J,J)+(RAVER\*HL\*PHI\*(3.\*R(J)+R(K)))/6.0  
 ESM(J,K)=ESH(J,K)+(RAVER\*HL\*PHI\*(R(J)+R(K)))/6.0  
 ESM(K,J)=ESH(J,K)  
 ESM(K,K)=ESH(K,K)+(RAVER\*HL\*PHI\*(R(J)+3.\*R(K)))/6.0

160 CONTINUE  
 CAP(1,1)=DP\*(12.\*R(1)\*\*2.+2.\*R(2)\*\*2.+2.\*R(3)\*\*2.+6.\*R(1)\*R(2)  
 +6.\*R(1)\*R(3)+2.\*R(2)\*R(3))  
 CAP(1,2)=DP\*(3.\*R(1)\*\*2.+3.\*R(2)\*\*2.+R(3)\*\*2.+4.\*R(1)\*R(2)+2.\*  
 +R(1)\*R(3)+2.\*R(2)\*R(3))  
 CAP(2,1)=CAP(1,2)  
 CAP(1,3)=DP\*(3.\*R(1)\*\*2.+R(2)\*\*2.+3.\*R(3)\*\*2.+2.\*R(1)\*R(2)+4.\*  
 +R(1)\*R(3)+2.\*R(2)\*R(3))  
 CAP(3,1)=CAP(1,3)  
 CAP(2,2)=DP\*(2.\*R(1)\*\*2.+12.\*R(2)\*\*2.+2.\*R(3)\*\*2.+6.\*R(1)\*R(2)  
 +2.\*R(1)\*R(3)+6.\*R(2)\*R(3))  
 CAP(2,3)=DP\*(R(1)\*\*2.+3.\*R(2)\*\*2.+3.\*R(3)\*\*2.+2.\*R(1)\*R(2)+2.\*  
 +R(1)\*R(3)+4.\*R(2)\*R(3))  
 CAP(3,2)=CAP(2,3)  
 CAP(3,3)=DP\*(2.\*R(1)\*\*2.+2.\*R(2)\*\*2.+12.\*R(3)\*\*2.+2.\*R(1)\*R(2)  
 +6.\*R(1)\*R(3)+6.\*R(2)\*R(3))

DO 170 I=1,3  
 DO 170 J=1,3  
 ESM1(I,J)=(2.\*CAP(L,J)/DELTA)-ESH(I,J)  
 170 CONTINUE

DO 180 I=1,3  
 DO 180 J=1,3  
 PM(I)=PM(I)+(ESM1(I,J)\*AA(J))  
 180 CONTINUE

DO 210 I=1,3  
 EF(I)=PM(I)+EF(I)  
 210 CONTINUE

DO 130 I=1,3  
 II=NB(I)  
 J5=NP+II  
 A(J5)=A(J5)+EF(I)  
 130 CONTINUE

REWIND 2

DO 300 I=1,JGSM  
 D(I)=A(I)

DO 301 I=1,JGF  
 A(I)=0.5\*(A(I)+D(I))

301

D(I)=A(I)

READ(2,\*)KD,KD,KD

DO 430 KK=1,NE,

READ(2,\*)NEL,NS,R(1),Z(1),R(2),Z(2),R(3),Z(3),ISIDE

RAVER=(R(1)+R(2)+R(3))/3.0

B(1)=Z(2)-Z(3)

B(2)=Z(3)-Z(1)

B(3)=Z(1)-Z(2)

C(1)=R(3)-R(2)

C(2)=R(1)-R(3)

C(3)=R(2)-R(1)

AR4=(R(2)\*Z(3)+R(3)\*Z(1)+R(1)\*Z(2)-R(2)\*Z(1)-R(3)\*Z(2)-R(1)\*Z(3))\*2.0

ITEMP=IFIX(((A(NS(1))+A(NS(2))+A(NS(3)))/3.0)-273.0)

KT=KTH(ITEMP)

SPEHT=SPHT(ITEMP)

RLAMDA=RHO\*SPEHT

DP=PHI\*RLAMDA\*AR4/360.0

DO 450 I=1,3

EF(I)=0.0

DO 450 J=1,3

ESH(I,J)=((KT\*B(I))\*B(J)+KT\*C(I)\*C(J))\*RAVER\*RAVER\*2.\*PHI/AR4

450

CONTINUE

IF(ISIDE .LE. 0) GO TO 460

J=ISIDE

K=J+1

LENG=SQRT((R(K)-R(J))\*\*2.+(Z(K)-Z(J))\*\*2.)

TEMP1=ITEMP+223

TEMP2=1.8\*(TN-TEMP1)

H=ABS(TEMP2)/2.25

H=H\*\*(1./4.)

H=0.27\*H

H=5.6782\*H

HL=H\*LENG

EF(J)=EF(J)+(RAVER\*HL\*PHI\*TN\*(2.\*R(J)+R(K)))/3.0

EF(K)=EF(K)+(RAVER\*HL\*PHI\*TN\*(R(J)+2.\*R(K)))/3.0

M=NS(J)

N=NS(K)

EF1=(PRO\*LENG\*RAVER\*(2.\*R(J)+R(K)))/3.0\*(TN\*\*4)

EF2=(PRO\*LENG\*RAVER\*(R(J)+2.\*R(K)))/3.0\*(TN\*\*4)

EF31=((60\*A(M)\*\*4)+(40\*A(N)\*A(M)\*\*3)+(24\*A(M)\*A(M)\*  
 + A(N)\*A(N))+(12\*A(M)\*A(N)\*\*3)+(4\*A(N)\*\*4))\*R(J)  
 EF32=((10\*A(M)\*\*4)+(16\*A(N)\*A(M)\*\*3)+(18\*A(M)\*A(M)\*A(N)\*\*2)+  
 + (16\*A(M)\*A(N)\*\*3)+(10\*A(N)\*\*4))\*R(K)  
 EF3=(RAVER\*PRO\*LENG/210.0)\*(EF31+EF32)

```

DO 140 I=1,3
AA(I)=A(NS(I))
CONTINUE

140 B(1)=Z(2)-Z(3)
      B(2)=Z(3)-Z(1)
      B(3)=Z(1)-Z(2)
      C(1)=R(3)-R(2)
      C(2)=R(1)-R(3)
      C(3)=R(2)-R(1)
      AR4=(R(2)*Z(3)+R(3)*Z(1)+R(1)*Z(2)-R(2)*Z(1)-R(3)*Z(2)
      -R(1)*Z(3)) *2.0

ITEMP=IFIX(((A(NS(1))+A(NS(2))+A(NS(3)))/3.0)-273.0)
KT=KTH(ITEMP)
SPEHT=SPHT(ITEMP)
RLAMDA=RHO*SPEHT
DP=PHI*RLAMDA*AR4/360.0
DO 150 I=1,3
EF(I)=0.0
PM(I)=0.0
DO 150 J=1,3
ESM(I,J)=((KT*B(I)*B(J)+KT*C(I)*C(J))*RAVER*RAVER*2.*PHI)/AR4
CONTINUE

150 IF(ISIDE .LE. 0) GO TO 160
J=ISIDE
K=J+1
LENG=SQRT((R(K)-R(J))**2.+(Z(K)-Z(J))**2.)
TEMP1=ITEMP+273
TEMP2=1.8*(T0-TEMP1)
H=ABS(TEMP2)/2.25
H=H*(1./4.)
H=0.27*H
H=5.6782*H

HL=H*LENG
EF(J)=EF(J)+(RAVER*HL*PHI*TO*(2.*R(J)+R(K)))/3.0
EF(K)=EF(K)+(RAVER*HL*PHI*TO*(R(J)+2.*R(K)))/3.0
M=NS(J)
N=NS(K)

EF1=(PRO*LENG*RAVER*(2*R(J)+R(K))/3.0)*(TO**4)
EF2=(PRO*LENG*RAVER*(R(J)+2*R(K))/3.0)*(TO**4)

EF31=((60*A(M)**4)+(40*A(N)*A(M)**3)+(24*A(M)*A(M)*
+ A(N)*A(N))+(12*A(M)*A(N)**3)+(4*A(N)**4))*R(J)
EF32=((10*A(M)**4)+(16*A(N)*A(M)**3)+(18*A(M)*A(M)*A(N)**2)+
+ (16*A(M)*A(N)**3)+(10*A(N)**4))*R(K)
EF3=(RAVER*PRO*LENG/210.0)*(EF31+EF32)

EF41=((60*A(N)**4)+(40*A(M)*A(N)**3)+(24*A(M)*A(M)*
+ A(N)*A(N))+(12*A(N)*A(M)**3)+(4*A(M)**4))*R(K)
EF42=((10*A(N)**4)+(16*A(M)*A(N)**3)+(18*A(M)*A(M)*A(N)**2)+
+ (16*A(N)*A(M)**3)+(10*A(N)**4))*R(J)

```

```

EF41=((60*A(N)**4)+(40*A(M)*A(N)**3)+(24*A(M)*A(N)*
+ A(N)*A(N))+(12*A(N)*A(N)**3)+(4*A(M)**4))*R(K)
EF42=((10*A(N)**4)+(16*A(M)*A(N)**3)+(18*A(M)*A(M)*A(N)**2)+
+ (16*A(N)*A(M)**3)+(10*A(M)**4))*R(J)
EF4=(RAVER*PRO*LENG/210.0)*(EF41+EF42)

```

```

EF(J)=EF(J)-EF3+EF1
EF(K)=EF(K)-EF4+EF2

```

```

ESM(I,J)=ESM(J,J)+(RAVER*HL*PHI*(3.*R(J)+R(K)))/6.0
ESM(I,K)=ESM(J,K)+(RAVER*HL*PHI*(R(J)+R(K)))/6.0
ESM(K,J)=ESM(J,K)
ESM(K,K)=ESM(K,K)+(RAVER*HL*PHI*(R(J)+3.*R(K)))/6.0

```

460

CONTINUE

```

CAP(1,1)=DP*(12.*R(1)**2.+2.*R(2)**2.+2.*R(3)**2.+6.*R(1)*R(2)
+ 6.*R(1)*R(3)+2.*R(2)*R(3))
CAP(1,2)=DP*(3.*R(1)**2.+3.*R(2)**2.+R(3)**2.+4.*R(1)*R(2)+2.*
+ R(1)*R(3)+2.*R(2)*R(3))
CAP(2,1)=CAP(1,2)
CAP(1,3)=DP*(3.*R(1)**2.+R(2)**2.+3.*R(3)**2.+2.*R(1)*R(2)+4.*
+ R(1)*R(3)+2.*R(2)*R(3))
CAP(3,1)=CAP(1,3)
CAP(2,2)=DP*(2.*R(1)**2.+12.*R(2)**2.+2.*R(3)**2.+6.*R(1)*R(2)
+ 2.*R(1)*R(3)+6.*R(2)*R(3))
CAP(2,3)=DP*(R(1)**2.+3.*R(2)**2.+3.*R(3)**2.+2.*R(1)*R(2)+2.*
+ R(1)*R(3)+4.*R(2)*R(3))
CAP(3,2)=CAP(2,3)
CAP(3,3)=DP*(2.*R(1)**2.+2.*R(2)**2.+12.*R(3)**2.+2.*R(1)*R(2)
+ 6.*R(1)*R(3)+6.*R(2)*R(3))

```

DO 470 I=1,3

DO 470 J=1,3

ESM2(I,J)=(2.\*CAP(I,J)/DELTA)+ESM(I,J)

470

CONTINUE

DO 430 I=1,3

II=NS(I)

J5=NP+II

A(J5)=A(J5)+EF(I)

DO 190 J=1,3

JJ=NS(J)

JJ=JJ-II+1

IF(JJ)190,190,200

200

J5=JGSM+(JJ-1)\*NP+II

A(J5)=A(J5)+ESM2(I,J)

190

CONTINUE

430

CONTINUE

REWIND 2

CALL DECOMP(A(JGSM+1),NP,NBW)

CALL SOLVE(A(JGSM+1),A(JGF+1),A(1),NP,NBW,NCL)

DO 240 I=1,JGF

```
IF(ABS(D(I)-A(I)).GE.1.0)GO TO 250
240 CONTINUE

GO TO 290

250 CONTINUE

DO 260 I=JGF+1,JEND
260 A(I)=0.0

DO 280 I=1,JGF
280 A(JGF+I)=D(JGF+I)
CONTINUE

GO TO 270

290 CONTINUE

CALL STRESS(A(1),DEN,NO1,MNSE,NO2,MSSE)
U=(ABS(DEN)-0.9)
IF(ABS(DEN)-0.9).GT.0.05)GO TO 490
WRITE(7,32)A(1),A(6),A(37),A(42),A(145),A(150),
A(6)-A(1)
32 * FORMAT(' ',7F9.2)
WRITE(9,*)(A(I),I=1,JGF)
WRITE(10,*)TN,DEN,NO1,MNSE,NO2,MSSE,NO3

490 CONTINUE
RETURN
END
```



```

C*****
C
C LISTING OF THE SUBROUTINE *** STRESS ***
C THIS SUBROUTINE COMPUTES THE THERMO - ELASTIC STRESSES OF THE
C CYLINDRICAL INGOT
C THIS SUBROUTINE USES THE IMSL ZPOLAR.
C
C*****

```

```

SUBROUTINE STRESS(A,DEN,KE1,MNSE,KE2,MSSE,KE3)
COMPLEX ROOT(3)
DIMENSION NS(3),R(3),Z(3),B(3),C(3),AA(3),A(1000)
DIMENSION ROOT1(4),DENER(1000),ALPHA(2000)
DIMENSION NSS(6),ESMS(6,6),EPS(6),BS(4,6),CS(6,4),DS(4,4)
DIMENSION STRA(4),STRE(4),ETS(4),US(6),AS(1000),SSTRE(1000)
DIMENSION RSTRE(1000),ASTRE(1000),CSTRE(1000),ETS1(4,1000)
DIMENSION S1(1000),S2(1000)
REAL MNSE,MSSE

```

```

YST(T)=69000*6498.76-((34500*6498.76)*(T-298)/1200.0)
YMOD(T)=206842.8E6-((103421.4E6)*(T-298)/1200.0)

```

```

DATA NCL/1/
PHI=3.142857
PR=0.3

```

```

TINIT=298.0
ICRIT=0

```

```

OPEN(UNIT=8,FILE='OUTPUT2.DAT',TYPE='OLD')
OPEN(UNIT=9,FILE='OUTPUT3.DAT',TYPE='OLD')
OPEN(UNIT=10,FILE='COEFF.DAT',TYPE='OLD')

```

```

READ(10,*)(ALPHA(I),I=1,2000)
READ(8,*)NP,NE,NBW

```

```

REWIND 10

```

```

NPS=NP*2.0
NBWS=NBW*2.0
JGFS=NPS
JGSMS=JGFS+NPS
JENDS=JGSMS+NPS*NBWS

```

```

DO 503 I=1,JENDS
AS(I)=0.0

```

503

```

DO 130 KK=1,NE
537 READ(3,*) NEL,NS,R(1),Z(1),R(2),Z(2),R(3),Z(3),ISIDE
RAVER=(R(1)+R(2)+R(3))/3.0
ZAVER=(Z(1)+Z(2)+Z(3))/3.0
DO 140 I=1,3
AA(I)=A(NS(I))
140 CONTINUE

```

140

```

TAVER=(AA(1)+AA(2)+AA(3))/3.0
YM=YMOD(TAVER)
YSTRE=YST(TAVER)
ITEMP=IFIX(TAVER-273)

```

```

ALP=ALPHA(ITEMP)
DTEMP=TAVER-TINIT

```

```

RAT= YM/((1.0+PR)*(1-2*PR))
DS(1,1)=RAT*(1-PR)
DS(1,2)=RAT*PR
DS(1,3)=RAT*PR
DS(1,4)=0.0
DS(2,1)=DS(1,2)
DS(2,2)=RAT*(1-PR)
DS(2,3)=RAT*PR
DS(2,4)=0.0
DS(3,1)=DS(1,3)
DS(3,2)=DS(2,3)
DS(3,3)=RAT*(1-PR)
DS(3,4)=0.0
DS(4,1)=DS(1,4)
DS(4,2)=DS(2,4)
DS(4,3)=DS(3,4)
DS(4,4)=RAT*(1-2*PR)/2.0

```

```

B(1)=Z(2)-Z(3)
B(2)=Z(3)-Z(1)
B(3)=Z(1)-Z(2)
C(1)=R(3)-R(2)
C(2)=R(1)-R(3)
C(3)=R(2)-R(1)
AR2=(R(2)*Z(3)+R(3)*Z(1)+R(1)*Z(2)-R(2)*Z(1)-R(3)*Z(2)
      -R(1)*Z(3))

```

```

DO 501 I=1,3
NSS(2*I-1)=NS(I)*2-1
NSS(2*I)=NS(I)*2

```

501

```

DO 502 I=1,4
DO 502 J=1,6
BS(I,J)=0.0

```

502

```

BS(1,1)=B(1)
BS(1,3)=B(2)
BS(1,5)=B(3)
BS(2,2)=C(1)
BS(2,4)=C(2)
BS(2,6)=C(3)
BS(3,1)=(R(2)*Z(3)-R(3)*Z(2)+B(1)*RAVER+C(1)*ZAVR)/RAVER
BS(3,3)=(R(3)*Z(1)-R(1)*Z(3)+B(2)*RAVER+C(2)*ZAVR)/RAVER
BS(3,5)=(R(1)*Z(2)-R(2)*Z(1)+B(3)*RAVER+C(3)*ZAVR)/RAVER
BS(4,1)=C(1)
BS(4,2)=B(1)
BS(4,3)=C(2)

```

```

BS(4,4)=B(2)
BS(4,5)=C(3)
BS(4,6)=B(3)

```

```

ETS(1)=ALP*DTEMP
ETS(2)=ETS(1)
ETS(3)=ETS(1)
ETS(4)=0.0

```

```

IF(ICRIT.EQ.-1)GO TO 531

```

```

DO 507 I=1,6
DO 507 J=1,4
CS(I,J)=0.0
DO 507 K=1,4
507 CS(I,J)=CS(I,J)+BS(K,I)*DS(K,J)

```

```

DO 508 I=1,6
SUM1=0.0
DO 509 K=1,4
509 SUM1=SUM1+CS(I,K)*ETS(K)
DO 508 J=1,6
SUM=0.0
DO 510 K=1,4
510 SUM=SUM+CS(I,K)*BS(K,J)
ESMS(I,J)=SUM*PHI*RAVER/AR2
508 EPS(I)=SUM1*PHI*RAVER

```

```

DO 511 I=1,6
IIS=NSS(I)
JJS=JGFS+IIS
AS(JJS)=AS(JJS)+EPS(I)
DO 512 J=1,6
JJS=NSS(J)
JJS=JJS+1-IIS
513 IF(JJS)512,512,513
JJS=JGMS+(JJS-1)*NPS+IIS
512 AS(JJS)=AS(JJS)+ESMS(I,J)
511 CONTINUE
CONTINUE

```

```

130 CONTINUE

```

```

CALL BOUND(AS(JGMS+1),AS(JGFS+1),NPS,NBWS,NCL)
CALL DECOMP(AS(JGMS+1),NPS,NBWS)
CALL SOLVE(AS(JGMS+1),AS(JGFS+1),AS(1),NPS,NBWS,NCL)

```

```

REWIND 3
REWIND 11

```

```

ICRIT=1
NUM=1

```

```

READ(3,*) KD,KD
READ(3,*)KD,KD

```

```

GO TO 537

531  KK=NUM
      DO 504 I=1,6,2
        NO1=NSS(I)
        NO2=NSS(I+1)
        US(I)=AS(NO1)
504  US(I+1)=AS(NO2)

      DO 505 I=1,4
        STRA(I)=0.0
        DO 505 K=1,6
505  STRA(I)=STRA(I)+BS(I,K)*US(K)/AR2

      DO 506 I=1,4
        STRE(I)=0.0
        DO 506 K=1,4
506  STRE(I)=STRE(I)+DS(I,K)*(STRA(K)-ETS(K))
        CONTINUE

      RSTRE(KK)=STRE(1)
      ASTRE(KK)=STRE(2)
      CSTRE(KK)=STRE(3)
      SSTRE(KK)=STRE(4)

      DENER(KK)=((0.5*((ASTRE(KK)-RSTRE(KK))**2))+0.5*((RSTRE(KK)
+      -CSTRE(KK))**2))+0.5*((CSTRE(KK)-ASTRE(KK))**2))+
+      3*(SSTRE(KK)**2)**0.5

      ROOT1(1)=1.0
      ROOT1(2)=- (RSTRE(KK)+ASTRE(KK)+CSTRE(KK))
      ROOT1(3)=RSTRE(KK)*ASTRE(KK)+ASTRE(KK)*CSTRE(KK)+RSTRE(KK)
+      *CSTRE(KK) -SSTRE(KK)*SSTRE(KK)
      ROOT1(4)=- (RSTRE(KK)*ASTRE(KK)*CSTRE(KK)-CSTRE(KK)
+      *(SSTRE(KK)**2))

      CALL ZPOLR(ROOT1,3,ROOT,IER)

      DENER(KK)=DENER(KK)/YSTRE
      S1(KK)=ROOT(1)/YSTRE
      S2(KK)=(ROOT(1)-ROOT(3))/YSTRE
      NUM=NUM+1
      IF(NUM.LE.NE)GO TO 537

      REWIND 3

      DEN=0.0
      MNSE=0.0
      MSSE=0.0

      DO 605 I=1,NE
        IF(ABS(DENER(I)).LE.ABS(DEN))GO TO 605
        DEN=DENER(I)
        KE1=I
605  CONTINUE

```

```
DO 606 I=1,NE
IF(ABS(S1(I)).LE.ABS(MNSE))GO TO 606
MNSE=S1(I)
KE2=I
CONTINUE
```

606

```
DO 607 I=1,NE
IF(ABS(S2(I)).LE.ABS(MSSE))GO TO 607
MSSE=S2(I)
KE3=I
CONTINUE
```

607

```
RETURN
END
```

C\*\*\*\*\*

C SUBROUTINE \*\*\* BOUND \*\*\*

C\*\*\*\*\*

```

SUBROUTINE BOUND(GSM,GF,NP,NBW,NCL)
DIMENSION GSM(NP,NBW),GF(NP,NCL),IB(1),BV(1)
DO 216 JM=1,1
ID1=0
INK=0
202 READ(11,*)IB,BV
203 FORMAT(6I3,2X,6F10.5)
ID=0
DO 204 L=1,I
IF(IB(L).LE.0) GO TO 205
ID-ID+1
I-IB(L)
204 GF(I,JM)=BV(L)+GF(I,JM)
GO TO 206
205 INK=1
IF(ID.EQ.0) GO TO 216
206 IF(ID1.EQ.1) GO TO 222
222 IF(INK.EQ.1)GO TO 216
ID1=1
GO TO 202
216 CONTINUE
INK=0
209 READ(11,*)IB,BV
ID=0
DO 221 L=1,1
IF(IB(L).LE.0)GO TO 215
ID-ID+1
I-IB(L)
BC=BV(L)
K=I-1
DO 211 J=2,NBW
M=I+J-1
IF(M.GT.NP)GO TO 210
DO 218 JM=1,NCL
GF(M,JM)=GF(M,JM)-GSM(I,J)*BC
218 GSM(I,J)=0.0
IF(K.LE.0)GO TO 211
DO 219 JM=1,NCL
GF(K,JM)=GF(K,JM)-GSM(K,J)*BC
219 GSM(K,J)=0.0
K=K-1
211 CONTINUE
DO 220 JM=1,NCL
220 GF(I,JM)=GSM(I,1)*BC
221 CONTINUE
GO TO 214
INK=1
215 IF(ID.EQ.0)RETURN

```

```

214   IF(INK.EQ.1)RETURN
      GO TO 209
      END

```

```

C*****

```

```

C      SUBROUTINE      ***  DECOMP  ***

```

```

C*****

```

```

      SUBROUTINE DECOMP(GSM,NP,NBW)
      DIMENSION GSM(NP,NBW)
      IO=61
      NP1=NP-1
      DO 226 I=1,NP1
      MJ=I+NBW-1
      IF(MJ.GT.NP) MJ=NP
      NJ=I+1
      MK=NBW
      IF((NP-I+1).LT.NBW) MK=NP-I+1
      ND=0
      DO 225 J=NJ,MJ
      MK=MK-1
      ND=ND+1
      NL=ND+1
      DO 225 K=1,MK
      NK=ND+K
225   GSM(J,K)=GSM(J,K)-GSM(I,NL)*GSM(I,NK)/GSM(I,1)
226   CONTINUE
      RETURN
      END

```

```

C*****

```

```

C      SUBROUTINE      ***  SOLVE  ***

```

```

C*****

```

```

      SUBROUTINE SOLVE(GSM,GF,X,NP,NBW,NCL)
      DIMENSION GSM(NP,NBW),GF(NP,NCL),X(NP,NCL)
      IO=61
      NP1=NP-1
      DO 265 KK=1,NCL
      JM=KK
      DO 250 I=1,NP1
      MJ=I+NBW-1
      IF(MJ.GT.NP) MJ=NP
      NJ=I+1

```

```
L=1
DO 250 J=NJ,MJ
L=L+1
250 GF(J, KK)=GF(J, KK)-GSM(I, L)*GF(I, KK)/GSM(I, 1)
X(NP, KK)=GF(NP, KK)/GSM(NP, 1)
DO 252 K=1, NP1
I=NP-K
MJ=NBW
IF((I+NBW-1).GT.NP) MJ=NP-I+1
SUM=0.0
DO 251 J=2, MJ
N=I+J-1
251 SUM=SUM+GSM(I, J)*X(N, KK)
252 X(I, KK)=(GF(I, KK)-SUM)/GSM(I, 1)
265 CONTINUE
RETURN
END
```









